

AD-A179 226

EXPERIMENTAL AND THEORETICAL STUDIES OF LASER COOLING
AND EMITTANCE CONTR. (U) HUGHES RESEARCH LABS MALIBU CA
J F LAN ET AL 31 JAN 87 MAC-REF-E9915 AFOSR-TR-87-0339

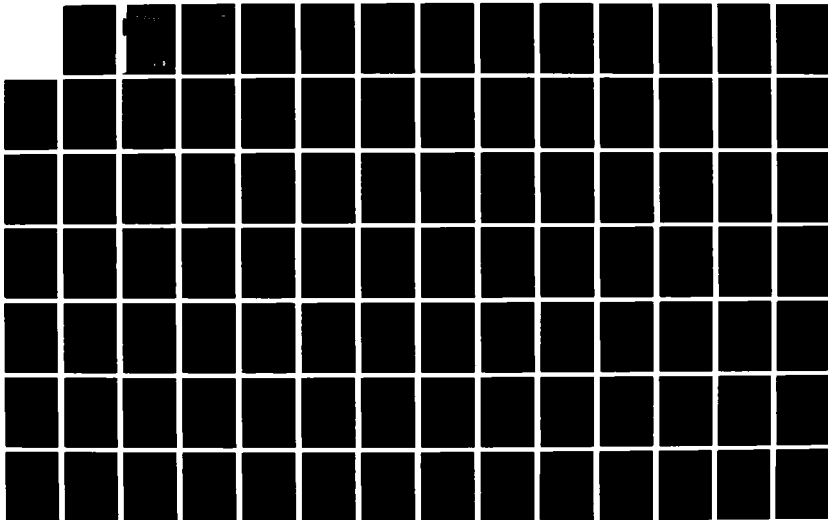
1/2

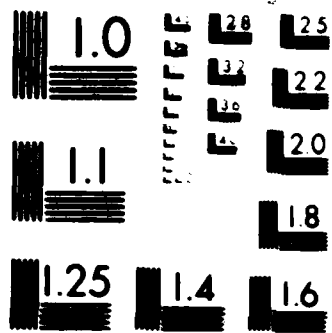
UNCLASSIFIED

F49620-02-C-0004

F/G 20/0

NL





XEROCOPY RESOLUTION TEST CHART

DTIC FILE COPY

2

HAC Ref. No. E9915

EXPERIMENTAL AND THEORETICAL STUDIES OF LASER COOLING AND EMITTANCE CONTROL OF NEUTRAL BEAMS

AFOSR-TR-87-0338

J.F. Lam, R.A. McFarlane, A.J. Palmer, D.G. Steel, and R.S. Turley

Hughes Research Laboratories
3011 Malibu Canyon Road
Malibu, CA 90265

Approved for public release;
distribution is unlimited.

JANUARY 1987

F49620-82-C-0004

Final Report

1 November 1981 through 31 January 1987

Air Force Office of Scientific Research (AFSC)
Bolling AFB, DC 20332-6448

AIR FORCE OFFICE OF SCIENTIFIC RESEARCH (AFSC)
BOLLING AIR FORCE BASE, DC 20332-6448
THIS TECHNICAL REPORT (TR) HAS BEEN REVIEWED AND IS
APPROVED FOR PUBLIC RELEASE AS FAR AS AFOSR-12,
DISTRIBUTION IS UNLIMITED.
MATTHEW T. KOPPEL
Chief, Technical Information Division

DTIC
ELECTE
APR 17 1987
S D

E

87 4 15 148

AD-A179 226

ADA179226

REPORT DOCUMENTATION PAGE

Form Approved
OASD No. 0704-0100

1a REPORT SECURITY CLASSIFICATION Unclassified		1b RESTRICTIVE MARKINGS	
2a SECURITY CLASSIFICATION AUTHORITY		3 DISTRIBUTION/AVAILABILITY OF REPORT Approved for public release distribution unlimited	
2b DECLASSIFICATION/DOWNGRADING SCHEDULE		5 MONITORING ORGANIZATION REPORT NUMBER(S) AFOSR-TR 87-0334	
6a NAME OF PERFORMING ORGANIZATION Hughes Research Laboratories	6b OFFICE SYMBOL (if applicable)	7a NAME OF MONITORING ORGANIZATION AFOSR	
6c ADDRESS (City, State, and ZIP Code) 3011 Malibu Canyon Road Malibu, CA 90265		7b ADDRESS (City, State, and ZIP Code) Bolling AFB, DC 20332-6448	
8a NAME OF FUNDING/SPONSORING ORGANIZATION AIR FORCE OFFICE OF SCIENTIFIC RESEARCH (AFSC)	8b OFFICE SYMBOL (if applicable) N1	9 PROCUREMENT INSTRUMENT IDENTIFICATION NUMBER F49620-82-C-0004	
8c ADDRESS (City, State, and ZIP Code) Bolling AFB, DC 20332-6448		10 SOURCE OF FUNDING NUMBERS PROGRAM ELEMENT NO 611024 PROJECT NO 2501 TASK NO 117 WORK UNIT ACCESSION NO	
11 TITLE (Include Security Classification) EXPERIMENTAL AND THEORETICAL STUDIES OF LASER COOLING AND EMITTANCE CONTROL OF NEUTRAL BEAMS (U)			
12 PERSONAL AUTHOR(S) J.F. Lam, R.A. McFarlane, A.J. Palmer, D.G. Steel, and R.S. Turley			
13a TYPE OF REPORT Final Report	13b TIME COVERED FROM 1 NOV 81 TO 31 JAN 87	14 DATE OF REPORT (Year, Month, Day) 1987 JANUARY 29	15 PAGE COUNT 64
16 SUPPLEMENTARY NOTATION			
17 COSATI CODES FIELD GROUP SUB-GROUP		18 SUBJECT TERMS (Continue on reverse if necessary and identify by block number)	
19 ABSTRACT (Continue on reverse if necessary and identify by block number) <p>We report on experimental and theoretical studies of issues relevant to laser cooling and emittance control of neutral beams. Experimental accomplishments include development of a technique for state specific velocity selection in atomic beams, observation of the Optical Kapitza Dirac Effect, construction of sodium and atomic hydrogen beam facilities, and initial development of a tunable, transform limited, VUV source. Theoretical accomplishments include development of a theory of π pulse cooling, a theory of two photon ionization in atomic hydrogen resonant with the Lyman-α transition, and an incorporation of the effects of intense fields in the theory of the Optical Kapitza Dirac Effect.</p>			
20 DISTRIBUTION/AVAILABILITY OF ABSTRACT <input type="checkbox"/> UNCLASSIFIED/UNLIMITED <input checked="" type="checkbox"/> SAME AS RPT <input type="checkbox"/> DTIC USERS		21 ABSTRACT SECURITY CLASSIFICATION Unclassified	
22a NAME OF RESPONSIBLE INDIVIDUAL Bruce L Smith		22b TELEPHONE (Include Area Code) 107	22c OFFICE SYMBOL N1

TABLE OF CONTENTS

SECTION	PAGE
1 INTRODUCTION.....	7
2 REVIEW OF THE PHYSICS OF ATOMIC BEAM-LASER INTERACTION.....	9
3 OPTICAL KAPITZA-DIRAC EFFECT.....	21
A. Introduction.....	21
B. Theoretical Studies.....	23
C. Experimental Studies.....	34
4 ATOMIC HYDROGEN TWO-PHOTON IONIZATION.....	47
A. Introduction.....	47
B. Theoretical Studies.....	47
C. Experimental Studies.....	57
5 π -PULSE COOLING.....	
6 SUMMARY.....	
7 PUBLICATIONS.....	
REFERENCES.....	
APPENDICES	
A. RADIATION COOLING WITH π PULSES.....	A-1
B. A THEORY OF RESONANT 2-PHOTON INDUCED IONIZATION OF HYDROGENIC SYSTEMS.....	B-1
C. VELOCITY-SPECIFIC ATOMIC-STATE SELECTION IN AN ATOMIC BEAM BY CONTINUOUS-WAVE OPTICAL PUMPING.....	C-1
D. H ⁻ PHOTONEUTRALIZATION.....	D-1



Accession For.....	
NTIS GRA&I	<input checked="" type="checkbox"/>
DTIC TAB	<input type="checkbox"/>
Unannounced	<input type="checkbox"/>
Justification.....	
By.....	
Distribution/.....	
Availability Codes	
Dist	Avail and/or Special
A-1	

LIST OF ILLUSTRATIONS

FIGURE		PAGE
1	Two-level atom eigenstates and energy levels....	10
2	Collisional cooling scheme.....	13
3	Spontaneous cooling scheme.....	14
4	Position-dependence of "dressed" atom energies and states in a standing wave.....	18
5	π -pulse cooling scheme.....	20
6	Optical Kapitza-Dirac Effect: theory.....	27
7	The bare atom plus field states.....	28
8	The dressed atom states.....	28
9	The infinite ladder of dressed states.....	29
10	The bare atom plus field states in a bidirectional photon field.....	31
11	The dressed atom states for a bidirectional photon field.....	32
12	Optical Kapitza-Dirac Effect: experimental block diagram.....	35
13	Sodium oven block diagram.....	35
14	Sodium velocity selection scheme.....	37
15	Energy-level diagram for the sodium D_2 line of atomic sodium at 589 nm, showing the hyperfine splitting.....	38
16	Optical pumping mechanism between the $F=2$ ground state and $F=3$ excited state in the D_2 transition in atomic sodium.....	40
17	OKDE interaction region.....	41
18	Spatial beam profile monitor.....	43
19	Experimental data showing the effect of the internal standing wave on the spatial profile of the atomic beam.....	44

FIGURE		PAGE
20	Model used in two-photon ionization calculations.....	49
21	Effect of intensity on photo-ionization.....	54
22	Effect of detuning of photo-ionization.....	55
23	Effect of detuning on excited state population.....	56
24	Experimental setup for generation of VUV Lyman- α radiation.....	59
25	Mercury cell for VUV generation.....	61
26	Four-wave mixing process used for generation of VUV Lyman- α radiation in mercury.....	62
27	Nitric oxide ionization detector.....	64
28	Hydrogen atomic beam apparatus.....	65
29	π -pulse cooling process.....	

SECTION 1

INTRODUCTION

Laser cooling of neutral particle beams provides a promising mechanism for reducing the divergence of the relativistic atomic beams presently being considered for inclusion in space-based weapons systems. The nature of the cooling process is such that the emittance of the resulting beam is not subject to the constraints of Liouville's theorem, as are magnetostatic or electrostatic focusing systems. In static focusing systems, the emittance of the beam, which is proportional to the product of the beam size and the beam divergence, is a conserved quantity. Thus, the only way to reduce beam divergence is at the expense of beam size. Laser cooling permits beam divergence reduction without increasing beam size. Smaller beams permit smaller optics in the accelerator, thus reducing the size, weight, and cost of eventual weapons systems.

Interest in laser cooling technologies has also recently been expressed in the related area of atomic trapping. Neutral particles can be trapped in an electromagnetic field and confined there for extended periods of time. Applications of such trapped particles include precision atomic spectroscopy and containment and study of anti-matter. Atomic spectroscopy has DoD applications in precise atomic clocks and frequency standards. Anti-matter containment is important in concepts currently being considered by the Air Force for use in exotic fuels and weapons.¹

Under this contract, we studied three areas relevant to the cooling and trapping of neutral atoms in electromagnetic fields. The first of these areas was the Optical Kapitza-Dirac Effect (often referred to as the Optical Stern-Gerlach Experiment) which concerns the result of the interaction of an atomic beam with a resonant or nearly resonant standing wave. The onset of this effect provides one of the fundamental limits in one of our

proposed cooling schemes. In addition, the effect provides an interesting manifestation of the fundamental interaction between atoms and light.

In the second area of study, we measured the two-photon ionization cross section of atomic hydrogen at 1216 \AA , the Lyman-alpha (L_α) resonant transition from the ground state ($1s$) to the first excited state ($2p$). This two photon cross section will limit the maximum cooling rates possible for a beam of hydrogen atoms. If the laser beam is too intense, a significant proportion of the neutral atoms will be ionized during the cooling process.

Our third area of study under this contract the development of the concept of π -Pulse Cooling. Under appropriate circumstances, π -pulse provides a means for faster cooling than is possible with the conventional steady-state radiation method.

Section 2 of the report is a review of the physics of the interaction of laser radiation with neutral atoms, as applied to the studies done in this program. The section emphasis is on how radiation forces can be used to cool and trap neutral atoms. The following three sections discuss our research in the areas of the Optical Kapitza-Dirac Effect (OKDE), hydrogen resonant two-photon ionization, and π -Pulse Cooling. Section 6 summarizes our research results and puts them in the perspective of current research efforts in laser cooling and trapping. Implications of laser cooling and trapping for current and future DoD projects is mentioned and we also make some suggestions for further research in this area. The final section is a list of publications stemming in whole or in part from this contract. For the reader's convenience, we have included the full text of each publication.

SECTION 2

REVIEW OF THE PHYSICS OF ATOMIC BEAM-LASER INTERACTION

When an atom interacts with an external electromagnetic field, the center of mass motion of the atom is modified by the recoil of the atom when absorbing or emitting photons. Under appropriate conditions, the collective atomic recoil serves to reduce the momentum spread of an atomic sample (laser cooling) or to produce a diffraction pattern from a beam of atoms (the Optical Kapitza-Dirac Effect).

In this section, we will review some physics necessary for understanding the most prominent features of these two effects. In addition, we will present several techniques that could be used to cool an atomic sample. The theory of the Optical Kapitza-Dirac Effect will be developed in Section 3. Details of the specific theoretical and experimental developments achieved with the support of this contract will be discussed in Sections 3, 4, and 5.

The Hamiltonian for the interaction of an atom with a laser field can be written in the form

$$H = H_0 + H_I + H_F + H_{CM} \quad (2.1)$$

H_0 is the Hamiltonian for the internal atomic degrees of freedom. For the purposes of the following discussion, we will assume that the unperturbed atom can be accurately modeled as consisting of two levels, a ground state, $|a\rangle$, and an excited state $|b\rangle$ (see Figure 1). H_I represents the coupling between the electromagnetic fields and the atom. In the cases we will consider here, the dominant contribution to H_I is given by $H_I = -\mu \cdot E$, where μ is the atomic dipole moment and E is the electric field. H_F is the free-field Hamiltonian for the electromagnetic field. H_{CM} represents the center of mass motion of the atom, where $H_{CM} = p^2/2m$.



Figure 1 Two level atom eigenstates and energy levels.

In the low intensity limit, the eigenstates of the atomic and electromagnetic fields are decoupled, and the internal and external atomic states are independent of the intensity of the electromagnetic field. In the high intensity limit, the electromagnetic field serves to mix the unperturbed atomic eigenstates. This mixing can be most easily handled by replacing the "pure" atomic states with "dressed states" (eigenstates of the atom plus laser field system), which will be denoted as $|+,n\rangle$ or $|-,n\rangle$, where n is the photon number of the state.

The dressed states occur in doublets, each state consisting of a mixture of the two states $|a,n+1\rangle$ and $|b,n\rangle$. Let δ be the detuning--the difference between the laser frequency ω_L and the transition energy $E_b - E_a$. We will denote the Rabi flopping frequency as ω_R , where

$$\omega_R = \mu \cdot \mathbf{E} / \hbar \quad (2.2)$$

The quantity μ is the dipole interaction matrix element $e\langle b|r|a\rangle$ and \mathbf{E} is the electric field vector. If the phase of the dipole interaction matrix element is chosen to be real, the amount of mixing of the two states is governed by the intensity dependant expressions⁴

$$\begin{aligned} |+,n\rangle &= \cos(\theta) |a,n+1\rangle + \sin(\theta) |b,n\rangle \\ |-,n\rangle &= -\sin(\theta) |a,n+1\rangle + \cos(\theta) |b,n\rangle, \end{aligned} \quad (2.3)$$

where the mixing angle θ is defined by $\tan(\theta) = (\Omega / \delta) / \omega_R$ and Ω is defined to be $(\delta^2 + \omega_R^2)^{1/2}$.⁵ The energies of the two eigenstates are

$$\begin{aligned} \frac{E^+}{\hbar} &= (n+1)\omega_L - \frac{\delta}{2} \pm \frac{\Omega}{2} \\ \frac{E^-}{\hbar} &= (n+1)\omega_L - \frac{\delta}{2} \mp \frac{\Omega}{2} \end{aligned} \quad (2.4)$$

A number of schemes have been used to cool a gas by taking advantage of the exchange of momenta between photons and the constituent atoms of the gas. Four general schemes have been proposed, which we will designate as collisional, spontaneous, stimulated, and π -pulse. Realizations of each of these schemes will be discussed below.

1. Collisional Cooling

An example of a collisional cooling scheme is shown in Figure 2. A laser is tuned to the red side of an atomic resonance, exciting the atom from $|a\rangle$ to $|b\rangle$. The atom spontaneously decays from $|b\rangle$ to $|a\rangle$, losing an energy $E_b - E_a$, slightly more than the energy of the exciting laser. The extra energy is lost in collisions with other atoms in the gas. This technique is the least efficient of the laser cooling prospects we will discuss. The change of momentum per absorbed photon is typically only a fraction of the photon momentum.

2. Spontaneous Cooling

A much more efficient technique for cooling atoms is what we call spontaneous cooling. A group at the National Bureau of Standards was able to use this technique to cool a thermal beam of sodium atoms down to a temperature of 100 mK.² Figure 3 is an illustration of the technique we originally envisioned for transverse cooling of a relativistic atomic beam by spontaneous cooling. In this technique, two laser beams are incident on either side of the atomic beam to be cooled. The frequency ω of the light seen in the rest frame of each atom will be Doppler shifted to a new frequency ω' which depends on the velocity of the atom. If β is the speed of the atom in units of the speed of light, and $\gamma = 1/\beta^2 - 1$, the frequency ω' is given by

$$\omega' = \gamma(1 - \beta \cos \theta) \omega$$

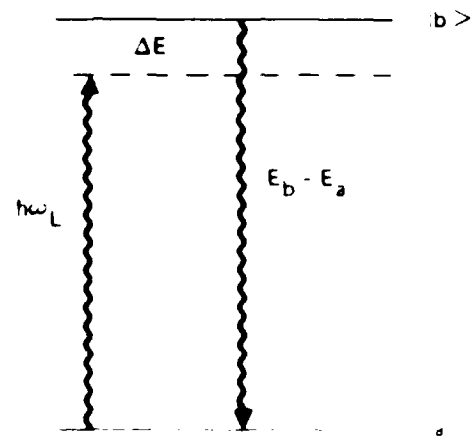


Figure 2 Collisional cooling scheme. The atom absorbs energy $h\omega_L$ and emits energy $E_b - E_a$. The energy difference ΔE is carried away by a collision partner.

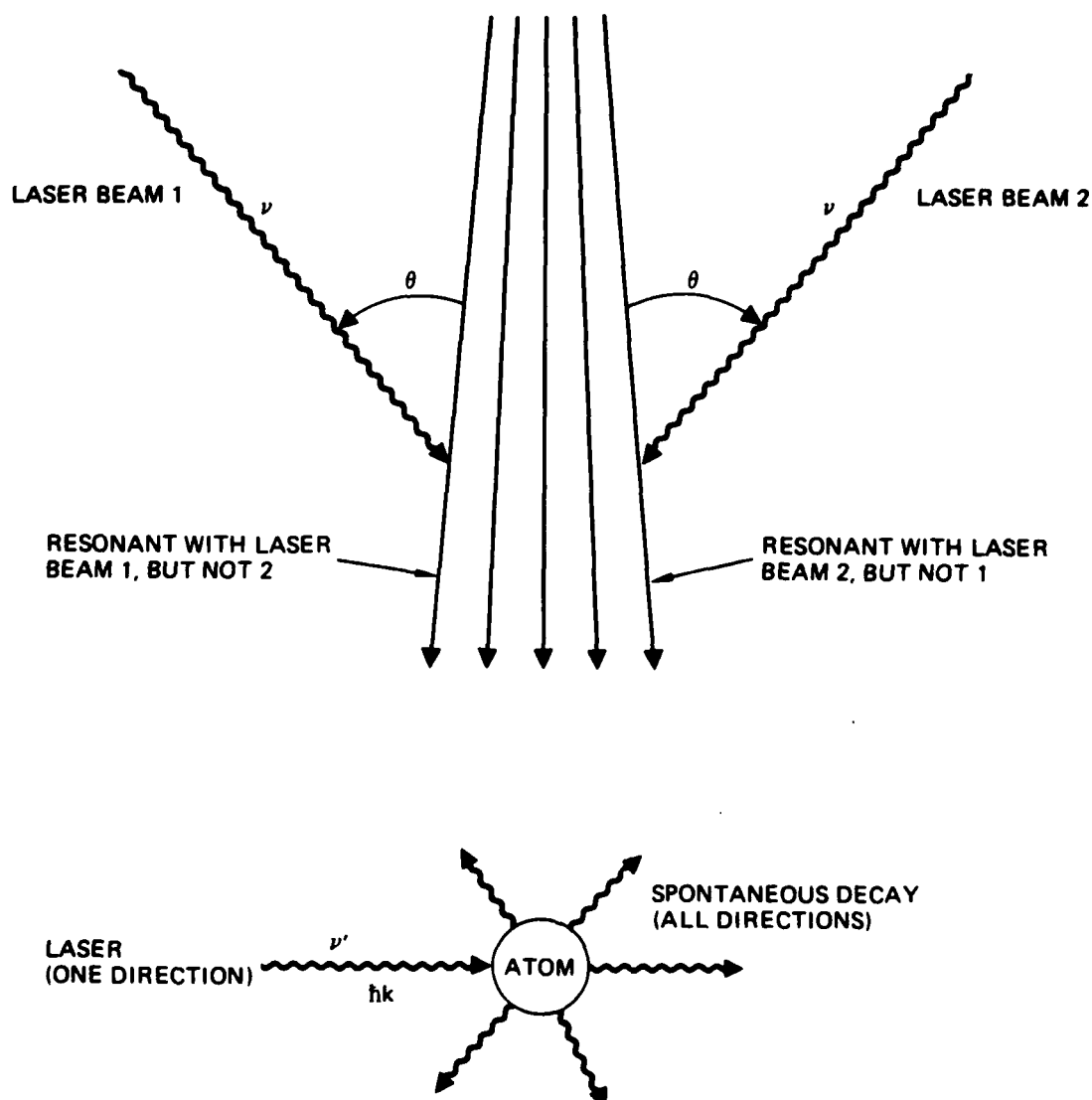


Figure 3. Spontaneous cooling scheme. Atoms moving towards laser beam 1 are resonant with it, but non-resonant with laser beam 2. They are "pushed" away from laser 1 by the recoil of the absorbed photon from laser 1. Since the atom scatters the absorbed photon into 4π , the net effect of the fluorescence is 0. Atoms moving toward laser beam 2 are likewise moved toward a central trajectory.

As indicated in Figure 3, θ is the angle between the laser beam and the atomic velocity vector. In the non-relativistic limit of velocities much slower than the speed of light, this expression reduces to

$$\nu' - \nu = -\mathbf{k} \cdot \mathbf{v} / 2\pi, \quad (2.6)$$

where \mathbf{k} is the wave vector of the laser beam.

Spontaneous cooling techniques take advantage of this inhomogeneous Doppler shift to cool the atoms in the beam. For simplicity, imagine a beam in which all of the atoms have a uniform speed, but slightly different trajectories. The $\cos(\theta)$ term of Eq. (2.5) will cause the resonant frequency of each atom to have an angle-dependent frequency shift. Thus the laser will only be resonant with atoms within a narrow angular range. These atoms will pick up one unit of photon momentum, $\hbar\mathbf{k}$, as they absorb a photon from the laser beam. An equal amount of momentum is lost when the photon is reradiated as the atom relaxes to the ground state. However, the photons absorbed from the laser are all in the same direction and their effect is cumulative. The photons radiated by the excited atoms are radiated into a 4π solid angle. The effects of the radiated photons average out to zero.

In the setup illustrated in Figure 3, atoms moving away from the central trajectories of the atomic beam will be "pushed" away from the lasers they are moving toward. Atoms moving on the central trajectory or away from a particular cooling laser will not be non-resonant with the laser light and therefore unaffected. As the cooling process continues, the distribution of atomic resonance frequencies will shift toward the frequency of the atoms with the central trajectory. To further cool the distribution, the laser frequency needs to be shifted to remain resonant with atoms on the periphery of the velocity distributions. Alternatively, an external electric or magnetic

field or both, could be applied to slightly shift the atomic resonance via the Stark or Zeeman effects as the distribution is cooled.

The fact that all real beams have a non-zero spread in atomic velocities slightly complicates the process of spontaneous cooling, because the frequency shift of the atoms depends on their speeds as well as on their trajectories. For example, consider a beam of 250-MeV hydrogen atoms with a gaussian momentum spread $\sigma_p = p \times 10^{-4}$, which is being cooled by means of the L_α transition at 1216 Å. Assume that the angular divergence of the beam is one mrad. If the cooling laser is oriented 75° with respect to the atomic beam, the velocity variations in the beam result in a variation of 60 GHz in the required resonant laser frequency. The trajectory variations in the beam will require only a 1.6-GHz frequency spread. In short, there is a problem in that the frequency shifts caused by the divergence could be masked by those caused by longitudinal momentum spread.

Fortunately, this problem can be solved by an appropriate orientation of the cooling lasers. If the angle between the beams is chosen to be the so called "magic angle" θ_m , given by

$$\theta_m = \arccos(\beta) \quad , \quad (2.7)$$

the effects of speed variations on the frequency spread in the atoms will be minimized. In the example above, the velocity variations in the beam will then result in a variation of only 8.6 MHz in the laser frequency. The trajectory variations will demand a variation of 2.5 GHz. With a non-relativistic beam, the magic angle reduces to 90°, as would be expected from Eq. (2.7).

2. Stimulated Cooling

A disadvantage of the spontaneous cooling mechanism outlined above is that the minimum cooling time is limited to

$$\tau = 2\gamma\hbar k/v_{\text{perp}} \quad , \quad (2.8)$$

where γ is the spontaneous decay lifetime, k is the photon wave vector, and v_{perp} is the maximum transverse velocity component of the atomic beam. With an intense laser beam, it is possible for the stimulated decay rate of the atoms to greatly exceed the spontaneous decay rate. Aspect et al.³ have demonstrated such a cooling scheme⁴, utilizing stimulated emission that reduced the cooling time by an order of magnitude over that achieved by the spontaneous process. Their non-relativistic approach consists of passing the atoms through a standing wave that is tuned to the high energy side of an atomic resonance frequency. The standing wave provides a periodic spatial intensity distribution that induces a spatial periodicity in the energies of the atomic states, as illustrated in Figure 4. The admixture of unperturbed atomic states in the dressed $|+\rangle$ and $|-\rangle$ states also shows a position dependence.

Consider an atom with a velocity that has a small transverse component along the periodicity direction of a standing wave. If the atom begins in the $|+,n\rangle$ state at a node of the standing wave, $\cos(\theta)=1$ and the atom is in a pure $|a,n+1\rangle$ state, and at the node of a transverse potential well. As the atom adiabatically moves to an anti-node in the distribution, some of the $|b,n\rangle$ state is mixed into the configuration. Spontaneous decay to a $|+,n-1\rangle$ or a $|-,n-1\rangle$ becomes possible. Upon decay to a $|-,n-1\rangle$ state, the atom will again find itself at the bottom of a transverse potential well that it will climb again. The energy required to climb the potential well creates a drag force, which serves to damp out the transverse velocity component of the beam.

This technique shows promise for greatly enhanced cooling rates without saturation. Further research should be pursued how this method could be applied to cooling a relativistic beam.

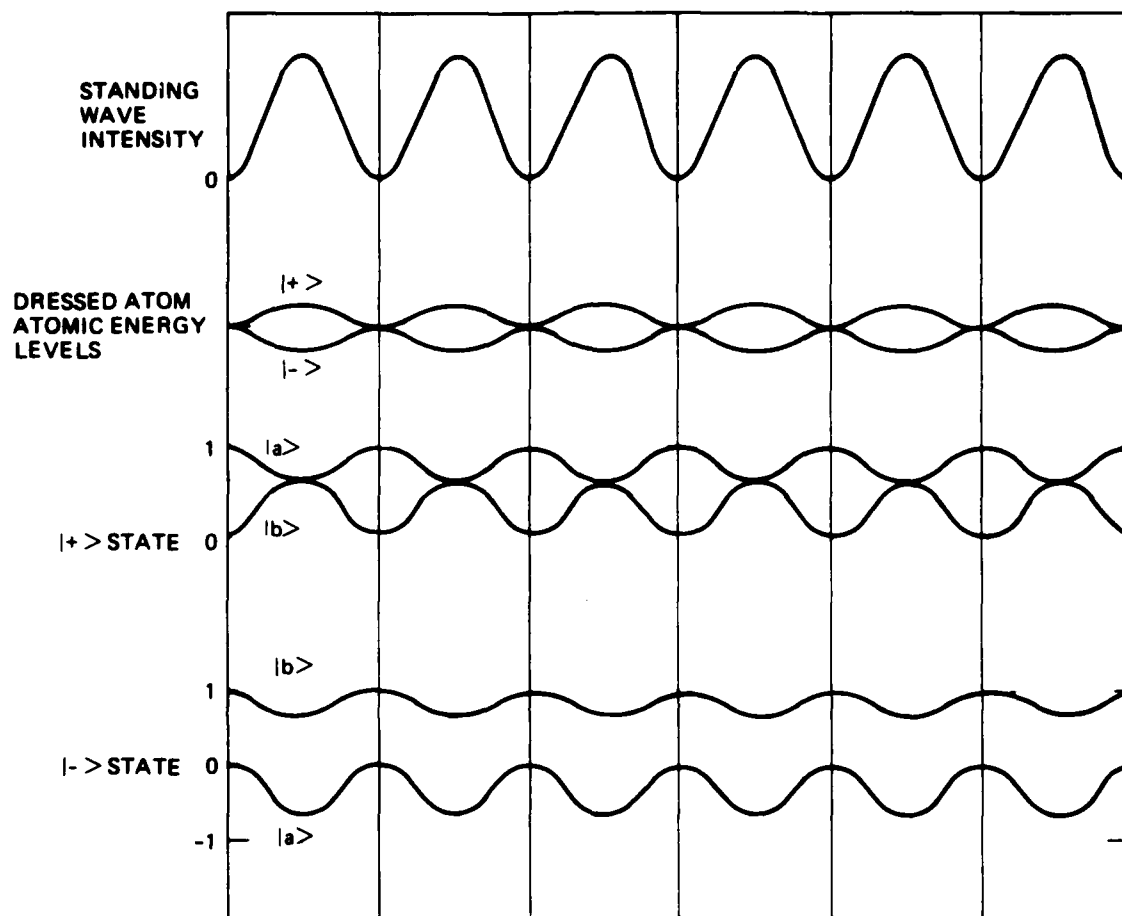


Figure 4. Position-dependence of "dressed" atom energies and states in a standing wave.

3. π -Pulse Cooling

Another way to improve on the cooling rate limit of spontaneous cooling is to stimulate radiative decay rather than wait for the excited state to decay spontaneously. By appropriate selection of the duration and intensity of the cooling pulses, it is possible to obtain a unit probability of a transition from the ground state to the excited state, or vice versa. Such a pulse is called a π -pulse. Cooling an atomic beam with this technique is illustrated in Figure 5. The atom is originally in the ground state when it is hit with the first π pulse. This pulse gives the atom a unit probability of being in the excited state, and transfers one unit of photon momentum to the atom. A second π -pulse is then applied from the opposite side of the beam to stimulate the atom back down to the ground state. The atomic recoil from the second pulse is in the same direction as the momentum picked up from the first pulse. If the Doppler effect is used to act selectively on only those atoms moving towards the source of the first pulse, this process is very similar to the spontaneous cooling scheme. The π -pulse cooling rate will be given by the stimulated decay rate, which is much faster than the limiting spontaneous decay rate of the spontaneous cooling process.

Further details of this process can be found in Section 5 and in the Palmer and Lam paper included in the Publications section.

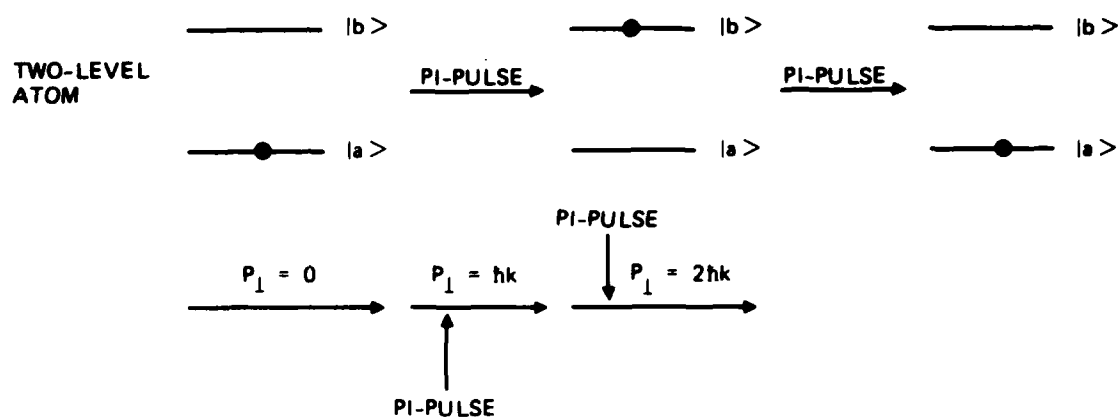


Figure 5. π -pulse cooling scheme. Atoms are hit with a π -pulse while in the ground state, giving them one unit of photon momentum. The atoms are then stimulated back to the ground state from the opposite side, giving them another unit of photon momentum in the same direction.

SECTION 3

OPTICAL KAPITZA-DIRAC EFFECT

A. INTRODUCTION

The Optical Kapitza-Dirac Effect occurs when a beam of atoms passes through a standing wave region of resonant or near resonant radiation. A physical picture of many of the aspects of this effect can be obtained by considering the energy levels of the dressed atomic states in a spatially modulated laser field. If the atoms enter the interaction region adiabatically from the ground state, they will stay in the $|+\rangle$ state during the interaction (in the absence of spontaneous decay). The gradient of the field intensity results in a position-dependent force being exerted on each atom. An initially well-collimated beam will acquire a transverse velocity distribution as illustrated in the smooth curve of Figure 6. A full quantum-mechanical treatment of the effect results in a curve consisting of discrete lines, as shown in the second curve of the figure. The discrete spectrum results from the fact that momentum transfer to the atom is always in the direction of the laser beam, and occurs in discrete units of the photon momentum.

A semi-classical calculation of this effect was done first by Cook and Bernhardt.⁵ Later refinements by Bernhardt and Shore,⁶ Arimondo et al.,⁷ and by Tanguy et al.^{8,9} involved quantizing the radiation field, detuning from resonance, considering the effect of spontaneous emission, developing a Gaussian laser beam profile, and misaligning the laser and atomic beams.

Concurrent work on this effect has been done by Pritchard's group at M.I.T., in which they obtained similar results to those reported here.¹⁰

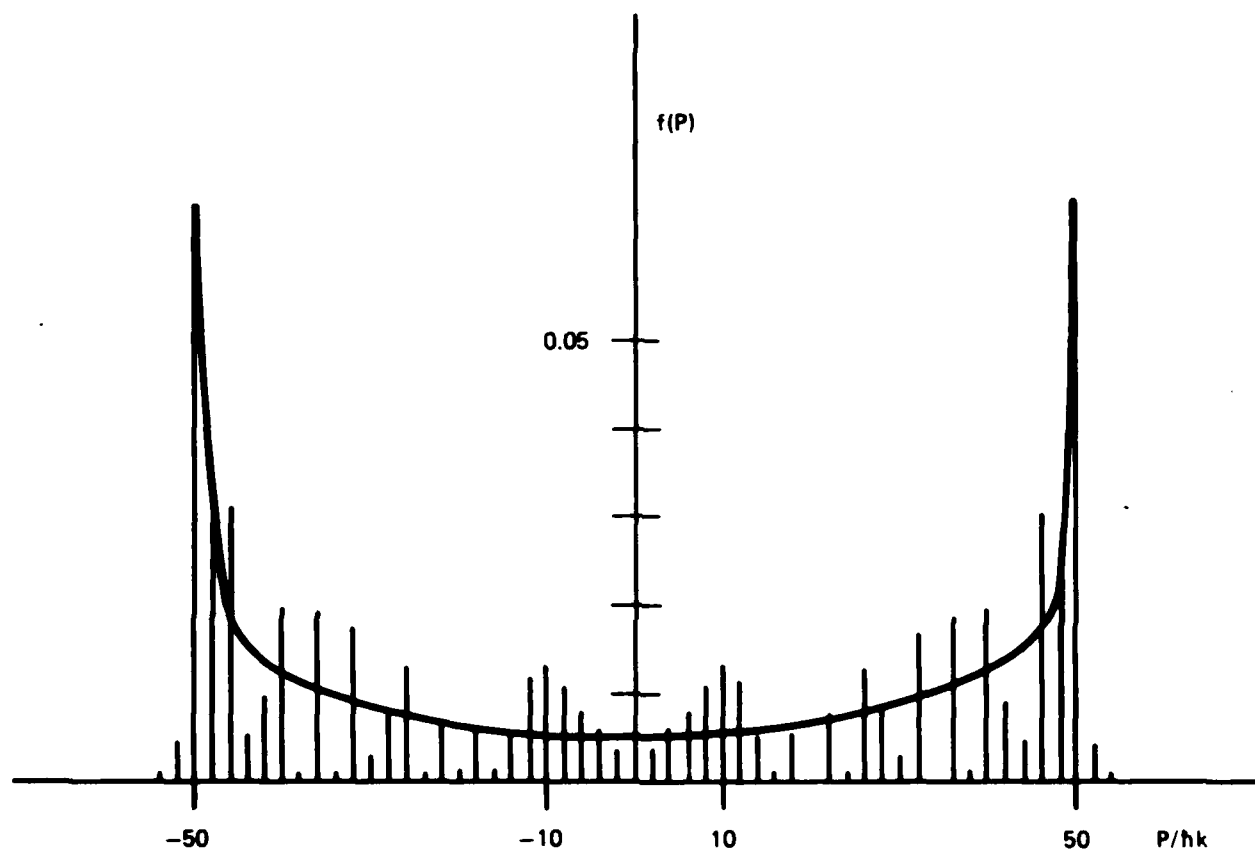


Figure 6. Optical Kapitza-Dirac Effect: theory. The momentum distribution function for $\Omega\tau = 50$ (after Ref. 7). The discrete lines represent the quantized nature of momentum transfer. Every other line is omitted. The smooth curve represents the quasiclassical calculation.

B. THEORETICAL STUDIES

The current understanding of spontaneous radiative cooling is that the optimum intensity for cooling is equal to the saturation intensity of the atomic transition. This conclusion raises the important question of how is the atom's translational motion perturbed by such a strong laser field. Past studies of atom-laser interactions point to the fact that in the regime where the laser intensity is equal to or greater than the saturation intensity of the atom, the atomic structure is significantly modified, and it is not possible to treat the atom and the radiation field as separate entities. Therefore, we must approach the problem from the quantum electrodynamics (QED) point of view. The essence of this approach is solving the entire problem of the atom plus field exactly (i.e., finding the eigenstates of the total Hamiltonian). We then use the exact eigenstates to construct experimental observables. For atomic motion, the observable is the momentum distribution of the atoms in the presence of the radiation field.

This technique, called the dressed atom approach, was pioneered by Cohen-Tannoudji in his studies of resonance fluorescence in intense fields.¹¹ The term "dressed" atom has an intuitive appeal because the eigenstate of the total Hamiltonian contains the photon number states, which can be interpreted as the "cloth" for the "bare" atomic states. In QED terminology, the physical properties of the atom have been renormalized by the presence of the photon field.

This section develops the dressed atom solutions in several stages. First, we will discuss the bare atom plus photon states. Then we will introduce the concept of electric dipole coupling for generating the dressed states for a unidirectional photon field. We will then generalize the dressed states to bidirectional photon fields (i.e., the standing wave problem).

Consider the two-level system, shown in Figure 1, where $|a\rangle$ and $|b\rangle$ are the ground and excited states respectively. The Hamiltonian of the bare atom plus photon field is given by

$$H_0 = p^2/2M + \sum \hbar\omega_a b_a^\dagger b_a + \sum \hbar\omega_k (a_k^\dagger a_k + 1/2) , \quad (3.1)$$

where $p^2/2M$ is the kinetic energy of the center of mass of the atom, $\hbar\omega_a$ is the energy of the atomic state $|a\rangle$, and b_a and b_a^\dagger are the respective lowering and raising operators respectively. In terms of the Dirac Ket and Bra notation, $b_a^\dagger b_a = |a\rangle\langle a|$. The term $\hbar\omega_k$ denotes the energy of the photon having wavevector k ; a_k and a_k^\dagger are the annihilation and creation operators, respectively, for the photon field. The sum over k is over all values of k and polarization states of the photon field. The eigenstates of H_0 are given by

$$|p, a, n_k\rangle = |p\rangle \times |a\rangle \times |n_k\rangle , \quad (3.2)$$

where $|p\rangle$ is the eigenstate of $p^2/2M$, and $|n_k\rangle$ is the eigenstate of $|n_k\rangle$. The product sign indicates all possible product combinations. The direct products of "bare" states in Eq. (3.2) are a result of the fact that the Hamiltonian does not contain the coupling between the atomic and photon fields.

To generate the dressed states, we start with the Hamiltonian for an atom interacting with a single-mode photon field,

$$H_1 = p^2/2M + \sum \hbar\omega_a b_a^\dagger b_a + V(t) , \quad (3.3)$$

where the electric dipole coupling to the radiation field is given by

$$V(t) = (1/2) \mu \cdot E_0 b_b^\dagger b_a a \exp(ik \cdot R - \omega t) - (1/2) \mu \cdot E_0 b_a^\dagger b_b a^\dagger \exp(-ik \cdot R + \omega t) , \quad (3.4)$$

and where $E_0 = i(\hbar\omega/2\epsilon_0 v)^{1/2}$ is the amplitude of the photon field. In the derivation of Eq. (3.4) we have invoked the rotating wave approximation. It should be noted that the Hamiltonian H_1 describes the atomic system only. The total Hamiltonian is generated by means of a unitary transformation, which does not change the physical description of the observables.

The Hamiltonian H_1 satisfies the Schroedinger equation

$$i\hbar \partial |\Psi\rangle / \partial t = H_1 |\Psi\rangle , \quad (3.5)$$

which is time dependent since $V(t)$ depends on time through the phase ωt . In the Schroedinger picture, the eigenstates of an operator must be time independent. Hence it is desirable to work in a reference frame where V is time independent. Let us introduce a unitary transformation, $U = \exp(iH_f t)$, where $H_f = \hbar\omega(a^\dagger a + 1/2)$, so that

$$|\Psi\rangle = U |\Phi\rangle , \quad (3.6)$$

where $|\Phi\rangle$ is the state vector in the new frame of reference. Carrying out the transformation for the Schroedinger equation [Eq. (3.5)], we find that $|\Phi\rangle$ satisfies

$$i\hbar \partial |\Phi\rangle / \partial t = H_2 |\Phi\rangle , \quad (3.6)$$

with

$$\begin{aligned} H_2 = H^s_0 - (1/2)\mu E_0 b_b^\dagger b_s a \exp(ik \cdot R) \\ - (1/2)\mu E_0 b_s^\dagger b_b a^\dagger \exp(-ik \cdot R) , \end{aligned} \quad (3.7)$$

where the superscript s denotes a single mode radiation field in Eq. (3.1).

The eigenstates of H_2 can be found by solving the eigenvalue problem,

$$H_2 | \pm \rangle = \Lambda | \pm \rangle , \quad (3.8)$$

where

$$|\Phi\rangle = \exp(-i\Lambda t) | \pm \rangle . \quad (3.9)$$

They are given by

$$|+,n\rangle = \sin\theta |p',b,n-1\rangle + \cos\theta |p,a,n\rangle \quad (3.10)$$

$$|-,n\rangle = -\cos\theta |p',b,n-1\rangle + \sin\theta |p,a,n\rangle , \quad (3.11)$$

with

$$\sin\theta = \langle b|H_2|a\rangle/N \quad (3.12)$$

$$\cos\theta = (E - \Lambda_+)/N \quad (3.13)$$

$$N = \{ (E - \Lambda_+)^2 + |\langle b|H_2|a\rangle|^2 \}^{1/2} \quad (3.14)$$

$$\langle b|H_2|a\rangle = -(1/2)\mu E_0 (n)^{1/2} \langle p'|\exp(ik\cdot R)|p\rangle \quad (3.15)$$

$$E = (p')^2/2M + \hbar\omega_b + \hbar\omega(n - 1/2) \quad (3.16)$$

$$\Lambda_+ = (E+G)/2 + \{ (\hbar\delta)^2 + 4C \}^{1/2}/2 \quad (3.17)$$

$$G = p^2/2M + \hbar\omega_b + \hbar\omega(n + 1/2) \quad (3.18)$$

$$C = (1/4)|\mu E_0|^2 n |\langle p'|\exp(ik\cdot R)|p\rangle|^2 \quad (3.19)$$

$$\delta = \{ (p')^2 - p^2 \} / 2M\hbar + \Delta , \quad (3.20)$$

with $p' = p + \hbar k$ by conservation of linear momentum

Figure 7 shows the energy levels of the bare atom plus field. Figure 8 shows the energy levels of the dressed atom. The energy separation of the dressed states, $|+\rangle$ and $|-\rangle$, is given by $\hbar\Omega = \hbar(\delta^2 + 4C)^{1/2}$, the generalized Rabi frequency. It should be noted too that the atom can absorb from, and emit to, the photon field many times. Hence the dressed atom consists of an infinite ladder of pair states as shown in Figure 9. The dressed states [Eqs. (3.10) and (3.11)] are the main results of this section.

We can write the eigenstate equation for a bidirectional photon field analogously to the calculations for a dressed atom in a unidirectional photon field as

$$H_3 |D_i\rangle = \Lambda_i |D_i\rangle, \quad (3.21)$$

where the Hamiltonian H_3 is given by

$$H_3 = H_0^{s,w} - (1/2)\mu E_0 b_b^\dagger b_s \{a_k e^{ik \cdot R} + a_{-k} e^{-ik \cdot R}\} \\ - (1/2)\mu E_0 b_s^\dagger b_b \{a_k^\dagger e^{ik \cdot R} + a_{-k}^\dagger e^{-ik \cdot R}\}, \quad (3.22)$$

and where the subscripts k and $-k$ denote the bidirectional wavevectors. The Hamiltonian $H_0^{s,w}$ is given by

$$H_0^{s,w} = p^2/2M + \sum \hbar\omega_\alpha b_\alpha^\dagger b_\alpha + \hbar\omega (a_k^\dagger a_k + 1/2) \\ + \hbar\omega (a_{-k}^\dagger a_{-k} + 1/2). \quad (3.23)$$

A direct computation of Eq. (3.21) gives the following expression for the bidirectional dressed eigenstates:

$$|D_i, n_k, n_{-k}\rangle = \sin\phi_i \sin\theta_i |p^s, b, n_k, n_{-k}-1\rangle \\ + \cos\phi_i \sin\theta_i |p^s, b, n_k-1, n_{-k}\rangle \\ + \cos\theta_i |p, a, n_k, n_{-k}\rangle, \quad (3.24)$$

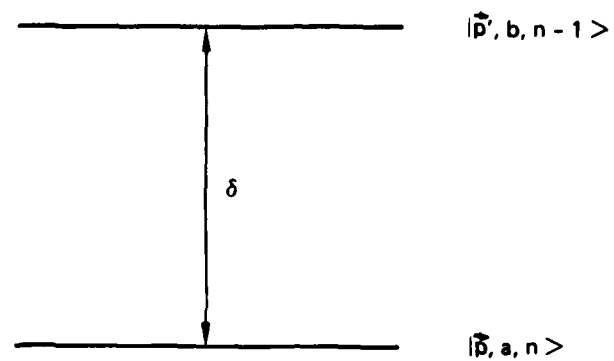


Figure 7. The bare atom plus field states.

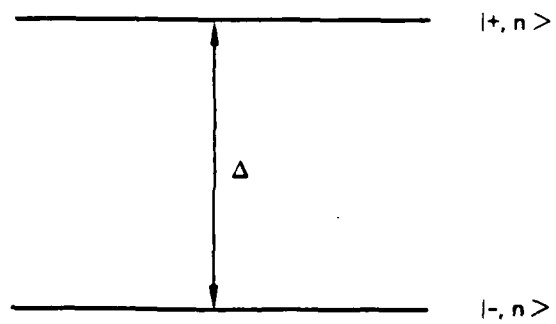


Figure 8. The dressed atom states.

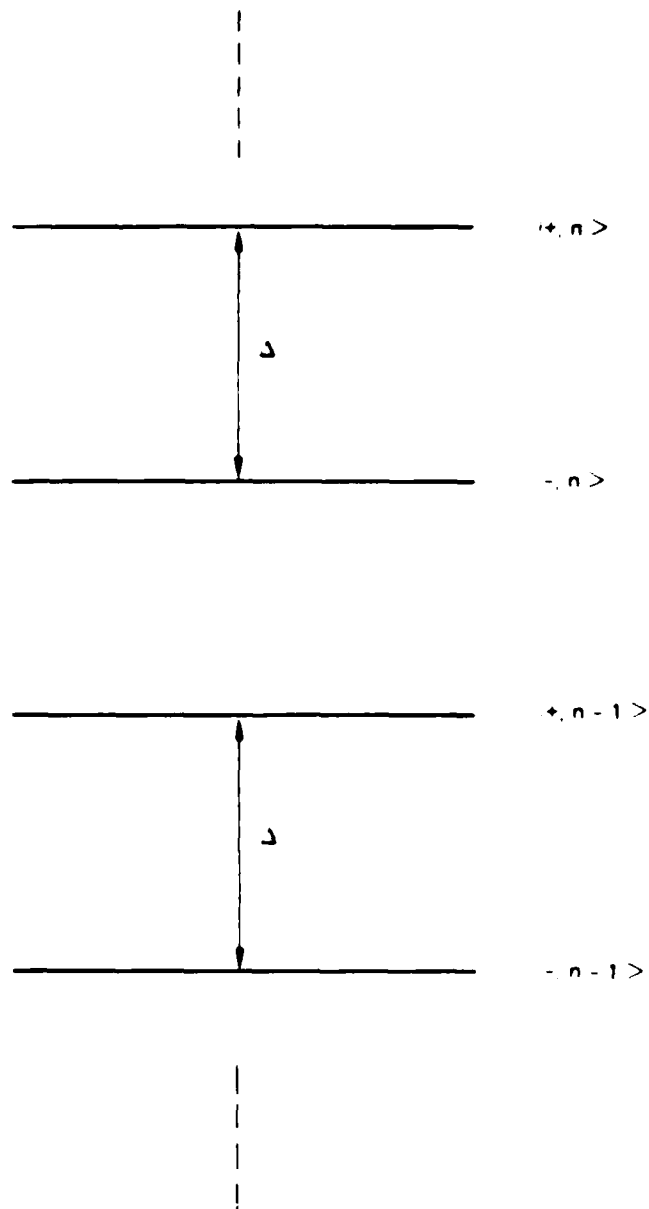


Figure 9. The infinite ladder of dressed states.

where

$$\cos\theta_i = 1/N_i \quad (3.25)$$

$$\cos\theta_i \sin\theta_i = \langle b | H_3' | a \rangle / \{ (F - \Lambda_i) N_i \} \quad (3.26)$$

$$\sin\theta_i \sin\theta_i = \langle b | H_3'' | a \rangle / \{ (E - \Lambda_i) N_i \} \quad (3.27)$$

$$N_i = \{ 1 + |\langle b | H_3' | a \rangle|^2 / (F - \Lambda_i)^2 + |\langle b | H_3'' | a \rangle|^2 / (E - \Lambda_i)^2 \} \quad (3.28)$$

$$E = (p'')^2 / 2M + \hbar\omega_b + \hbar\omega (n_k + n_{-k}) \quad (3.29)$$

$$F = (p')^2 / 2M + \hbar\omega_b + \hbar\omega (n_k + n_{-k}) \quad (3.30)$$

$$G = p^2 / 2M + \hbar\omega_b + \hbar\omega (n_k + n_{-k}) \quad (3.31)$$

$$\langle b | H_3' | a \rangle = (1/2)\mu E_0 b_b^* b_a \{ (n_k)^{1/2} \langle p' | e^{ik \cdot R} | p \rangle + (n_{-k})^{1/2} \langle p' | e^{-ik \cdot R} | p \rangle \} \quad (3.32)$$

Here the expression with the superscript " is obtained from those with superscript ' by the interchange of the corresponding momentum. The dressed state energies Λ_i are roots of the cubic equation,

$$(E - \Lambda)(F - \Lambda)(G - \Lambda) - |\langle b | H_3' | a \rangle|^2 (E - \Lambda) - |\langle b | H_3'' | a \rangle|^2 (F - \Lambda) = 0 \quad (3.33)$$

Figure 10 shows the eigenstates of the bare atom plus the bidirectional field. The frequencies δ' and δ'' have expressions identical to those defined for δ . The superscripts ' and " stand for the momentum $p' = p + \hbar k$ and $p'' = p - \hbar k$, respectively. Figure 11 shows a set of triplet dressed states. The frequency separation can be found by solving the cubic Eq. (3.33).

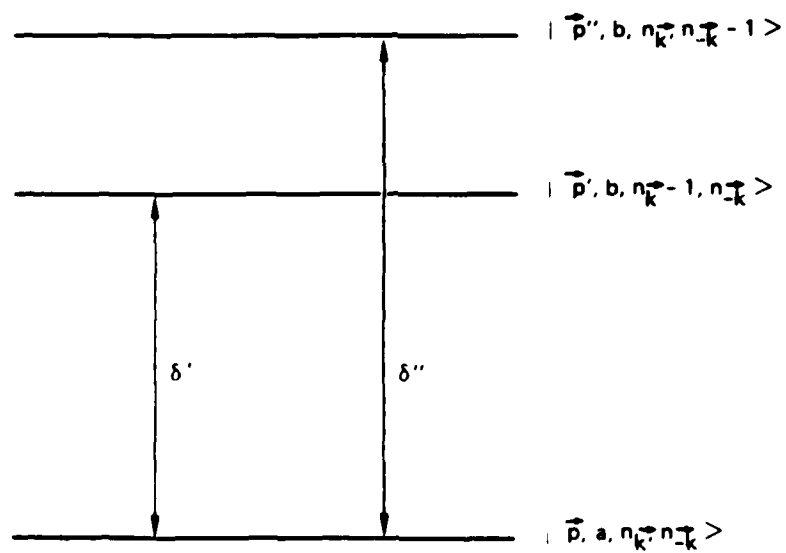


Figure 10. The bare atom plus field states in a bidirectional photon field.

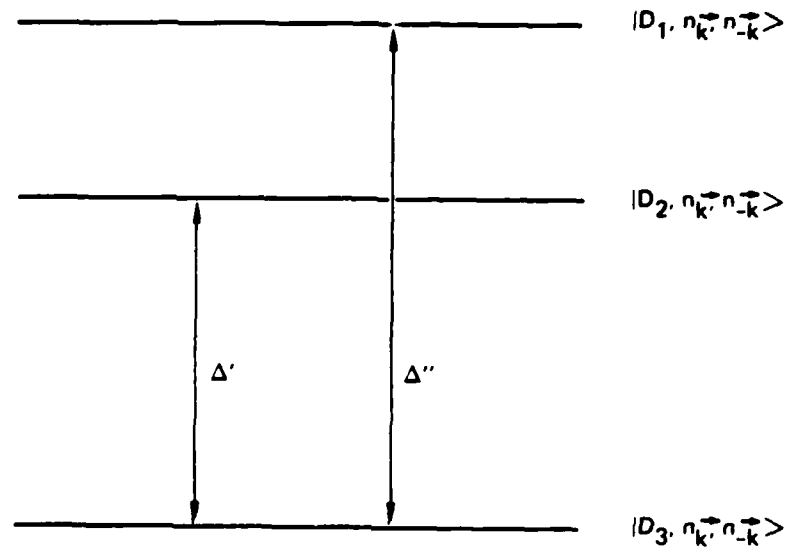


Figure 11. The dressed atom states for a bidirectional photon field.

Eqs. (3.24) constitute the main result of this section. A word of caution is necessary about the regime of validity of our solutions. The dressed atom solutions are valid provided that the laser field is tuned off resonance by more than a natural linewidth. Otherwise, there will be interference effects arising from the standing wave, leading to a far more complicated solution of the problem.

In summary, we have presented an exact description of the dynamics of two-level atoms in the presence of photon fields. The generalization of the stationary "dressed" atom approach to moving atoms shows that the dressed energies and states depend on the linear momenta of the atoms and photons. For a unidirectional photon field, the dressed states are given as a linear coherent superposition of two bare atom plus photon field states: the ground state of the atom moving with momentum p and having n photons present, and the excited state of the atom moving with momentum $p' = p + \hbar k$ and having $n - 1$ photons present. The frequency separation between the two dressed states is given by the momentum-dependent Rabi frequency.

In bidirectional photon fields, the dressed states are linear superpositions of the three bare atom plus bidirectional photon field states: the ground state of the atom moving with momentum p and having n_k and n_{-k} photons present; the excited state of the atom moving with momentum $p' = p + \hbar k$ and having $n_k - 1$ and n_{-k} photons present; and the excited state of the atom moving with momentum $p' = p - \hbar k$ and having n_k and $n_{-k} - 1$ photons present. The frequency separation among the three dressed states is determined by the solution of Eq. (3.33).

These solutions constitute the starting point for the calculation of the momentum distribution of the atoms in the presence of a resonant photon field. An inspection of the dressed state coefficients shows that for a bidirectional field,

an initially symmetric single peak momentum distribution function yields a symmetric splitting around the initial maximum, giving rise to the Optical Kapitza-Dirac Effect. Hence the dressed atom picture appears to provide a self-consistent approach toward the understanding of the effects of radiation forces on atoms.

C. EXPERIMENTAL STUDIES

We experimentally tested the predictions of the Optical Kapitza-Dirac Effect (OKDE) theory using the apparatus whose block diagram is shown in Figure 12. Sodium atoms originate in an oven and are collimated by the snout and a pair of slits. The atoms then pass through a fluorescence monitor that is used to monitor the beam density and the laser frequency. In the succeeding interaction region, the atoms are prepared so that the only atoms present in the $F=2$ ground state lie within a very narrow velocity group. These atoms are then pumped into the $m_f=2$ state to experimentally prepare a "two state" system. The atoms next enter the standing wave region where the OKDE interaction takes place. The spatial profile of the beam, measured 1.5 m downstream from the OKDE interaction region, permits a measure of the OKDE momentum spread. We will discuss each of the various components of the experiment separately, followed by our experimental results.

A diagram of the sodium oven is shown in Figure 13. The oven consists of a 2.0 cm diameter cylinder with a 1-cm-long cylindrical snout. The snout has an inner diameter of 0.03 cm. A 5.0- μm wide translatable vertical slit is located 12.5 cm from the center of the oven to provide initial beam steering and collimation, and is followed by a variable-width slit 127.5 cm from the oven center, and a fixed 25- μm slit just before the standing wave region (165.5 cm from the oven center). With careful alignment of the slits, we were able to achieve a beam width of 175 μm at the spatial beam profile monitor located at the analysis point 123 cm from the standing wave interaction region.

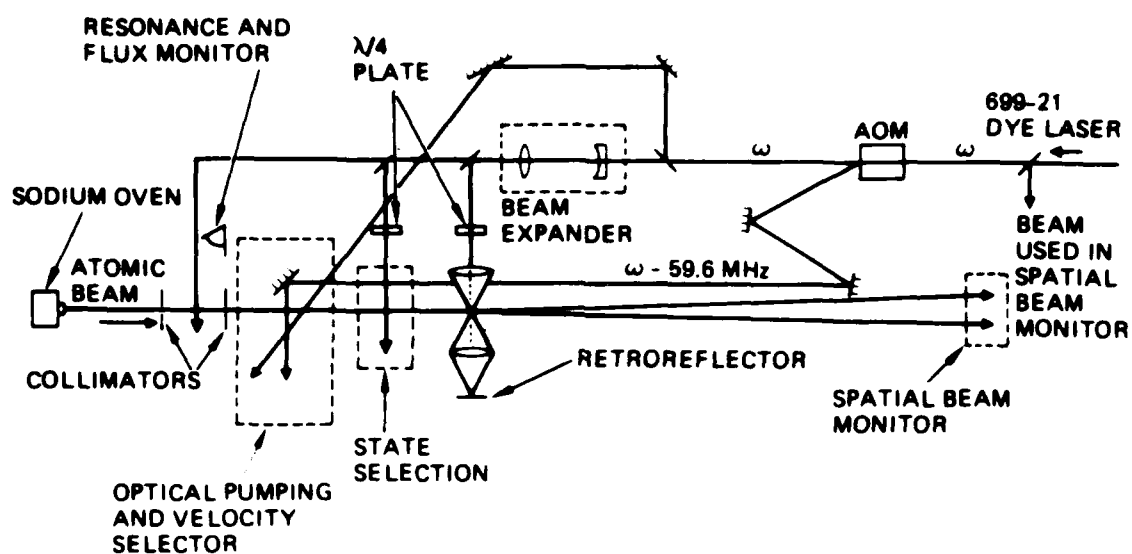


Figure 12. Optical Kapitza-Dirac Effect: experimental block diagram.

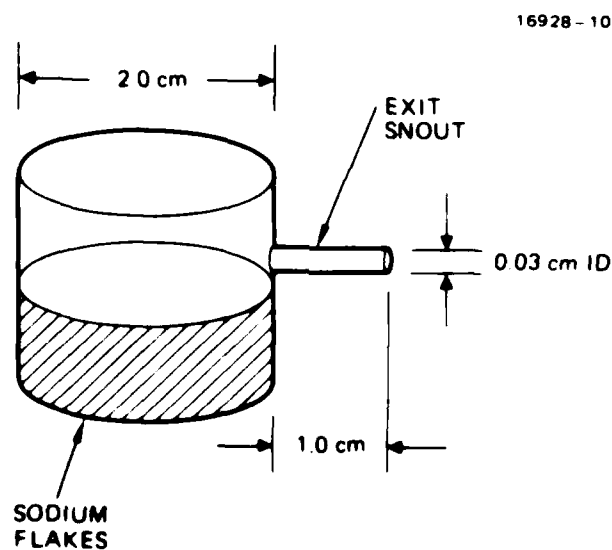


Figure 13. Sodium oven block diagram.

Since we were using the beam spatial profile to infer the beam momentum distribution, it was important that the longitudinal velocities of the atoms be uniform. We used the technique of Steel and McFarlane,¹¹ which is illustrated in Figure 14, to prepare the beam so that those atoms in the $F=2$ ground state were within a narrow velocity group. Figure 15 is a diagram of the hyperfine energy levels in the sodium D_2 line at 589 nm. We initially pumped the atoms with light that was resonant with the transition from the $F=2$ ground state to the $F=2$ excited state shown in the figure (beam "A"). The laser beam was oriented 90° to the beam, ensuring a zero Doppler shift. The atoms in the $F=2$ excited state could spontaneously decay to either the $F=1$ or $F=2$ ground states. Since atoms in the $F=1$ ground state would no longer be resonant with the laser, the number of atoms in the $F=2$ state would eventually be negligible.

The second step of the velocity selection process is to pass the atoms through a laser beam at an angle of approximately 45° to the atomic beam (laser beam "B" in the figure). If the atomic wave vector is k and the atomic velocity v , the laser frequency is Doppler shifted by an amount $-k \cdot v$ in the frame of each atom. The laser frequency was chosen to interact with a group of atoms having a particular velocity so that the Doppler-shifted light would be resonant with the $F=1 \rightarrow F=2$ transition of the sodium D_2 line. These excited atoms could spontaneously decay to either the $F=1$ or $F=2$ ground state. At the end of this two-step process, the only atoms left in the $F=2$ ground state were those atoms whose velocities were within the narrow band, permitting them to be resonant with the 45° laser beam. We were able to achieve a longitudinal velocity homogeneity for these atoms of $\Delta v/v = 0.06$. The rest of the experiment was done with light that was resonant with the $F=2$ to $F=3$ transition, prohibiting dipole decay to the $F=1$ ground state and hence optical pumping. Atoms with the "wrong" velocity will not be resonant with the light, and won't participate in subsequent measurements.

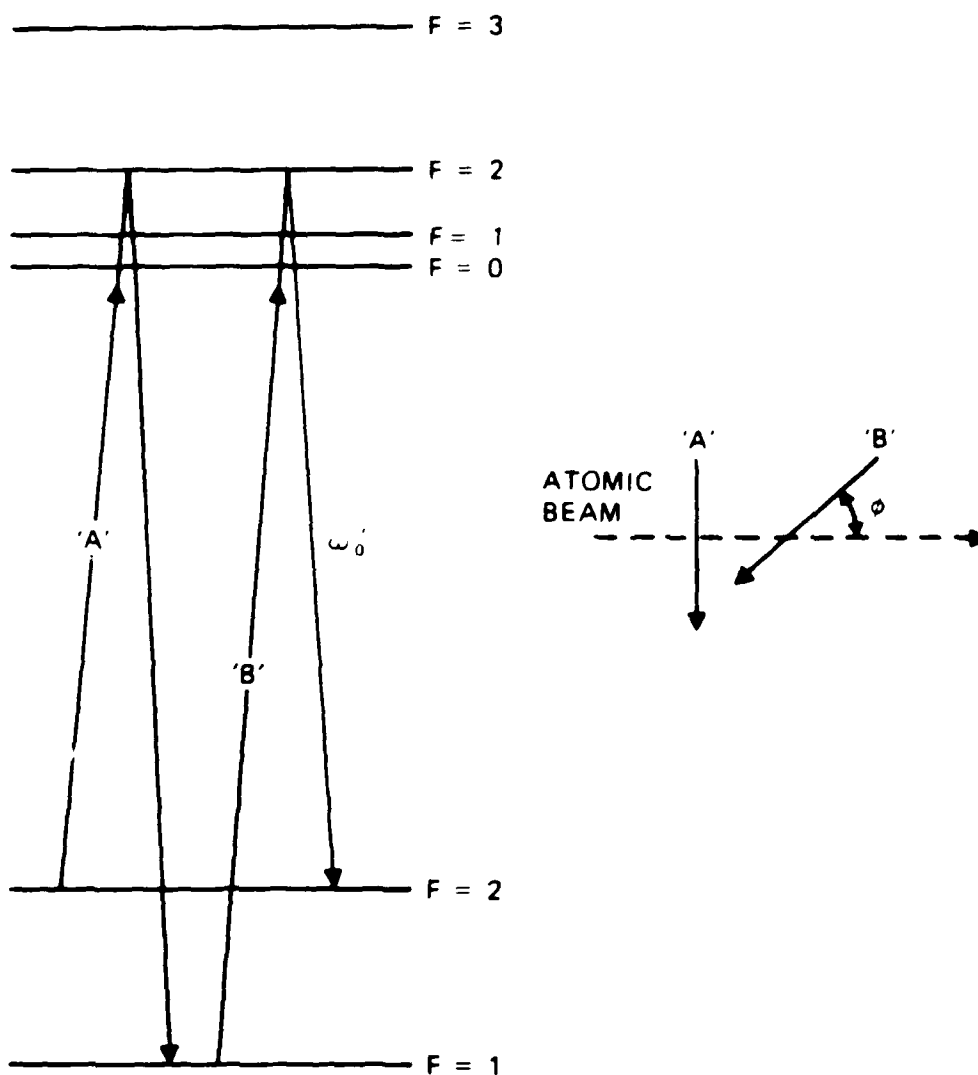


Figure 14. Sodium velocity selection scheme. Left, atomic energy level scheme showing the optical pumping sequence for velocity selection. Right, geometry for the optical pumping laser beam and the velocity selection laser beam.

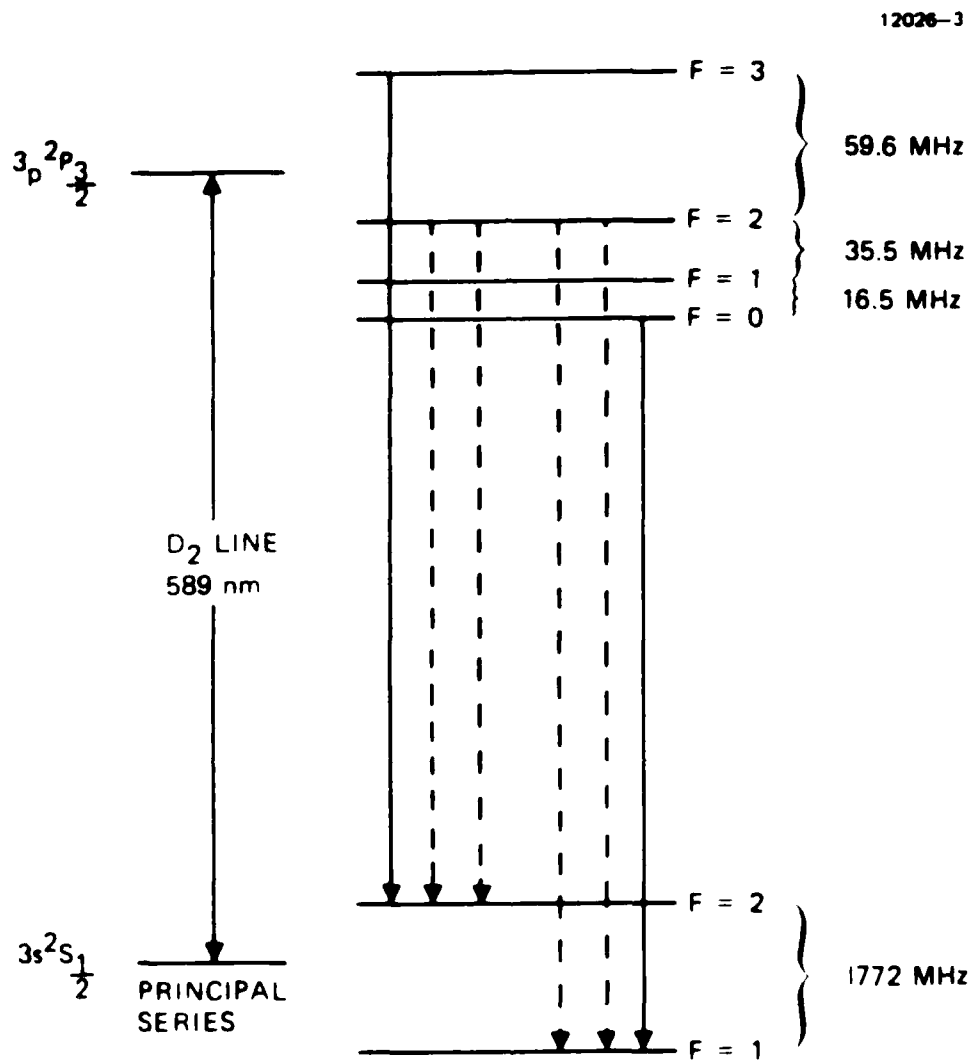


Figure 15. Energy level diagram for the D_2 line of atomic sodium at 589 nm, showing the hyperfine splitting.

The next stage in the atomic state preparation was to experimentally realize a strictly two level system, which was done by pumping the atoms with circularly polarized light resonant with the $F=2$ to $F=3$ transition. A small magnetic field of 1 to 3 gauss was applied to maintain the direction of the induced atomic dipole, without seriously removing the degeneracy of the magnetic substates. The selection rule for excitation is $\Delta m_F = +1$, and for spontaneous decay, $\Delta m_F = \pm 1, 0$. Thus all the atoms traveling into the interaction region are left in the $m_F = +2$ ground state. Light in the standing wave region was also circularly polarized, making the only allowed transition one from the $F=2$, $m_F = +2$ ground state to the $F=3$, $m_F = +3$ excited state. This process is illustrated in Figure 16.

The OKDE takes place in the standing wave region shown in Figure 17. As mentioned in the preceding paragraph, the standing wave is prepared with circularly polarized light so that the strictly two-level characteristic of the system can be preserved. The precise standing wave alignment is verified by monitoring the frequency dependence of the atomic fluorescence as a retro-reflecting mirror is adjusted to reflect the initial forward traveling wave back onto itself. For gross misalignments of the two beams, as the laser frequency is tuned, a double-peaked pattern is seen in the fluorescence spectrum corresponding to the fluorescence from each of the two beams. The center frequencies are shifted relative to each other because of the slightly different angles (and hence Doppler shifts) that the two optical beams make with the atomic beam. The retro-reflected beam angle is then adjusted so that the two fluorescence peaks exactly overlap each other in frequency. The $\lambda/4$ plate and polarizer, shown in Figure 17, provide for circular polarization of the light and for optical isolation of the retro-reflected laser beam from the dye laser. With careful alignment, we were able to obtain focused beam spot sizes of $7\mu\text{m}$ FWHM. This small spot size

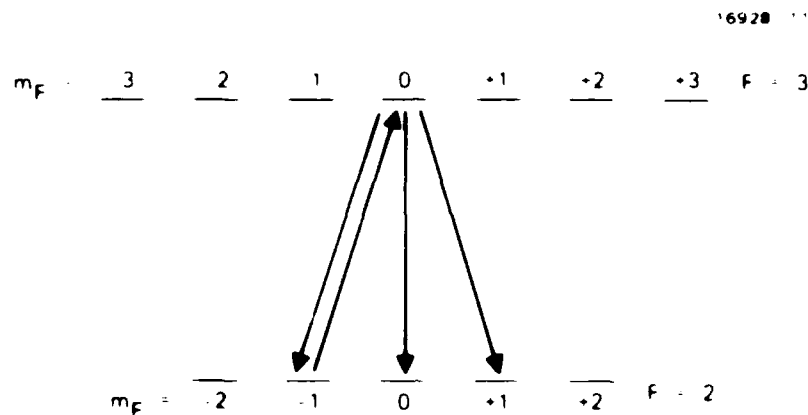


Figure 16. Optical pumping mechanism between the $F=2$ ground state and $F=3$ excited state in the D_2 transition in atomic sodium. In the transition shown in the figure, atoms in the $m_F = -1$ state are promoted to the $m_F = 0$ excited state by a photon with circular polarization. The atom can then decay to any of the $m_F = -1, 0, +1$ ground states. Eventually, this mechanism will result in all of the atoms being in the $m_F = +2$ ground state.

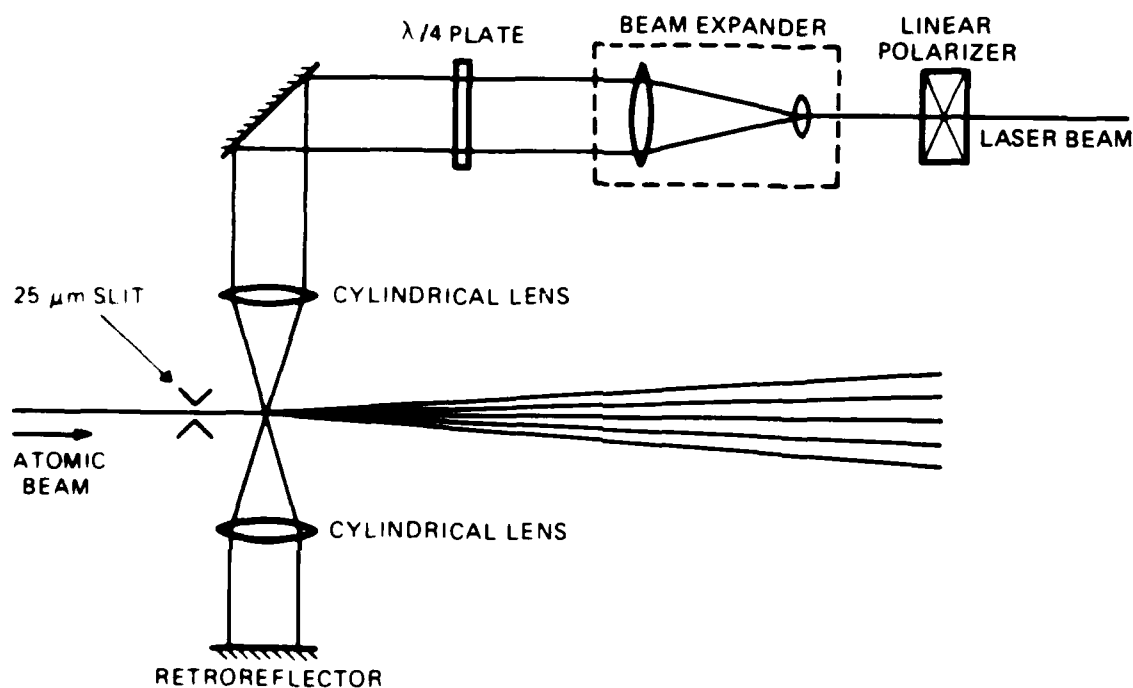


Figure 17. OKDE interaction region. Retroreflected light is blocked from returning to the laser because of the 90° rotation of the light by double passing the $\lambda/4$ plate. The return light is then blocked by the linear polarizer.

ensures that atoms will traverse the OKDE interaction region in less than one spontaneous decay lifetime. Spontaneous decay would have introduced a diffusive effect on the spatial, distribution which would have obscured the diffractive OKDE effect we were studying.

The transverse velocity distribution produced by the OKDE results in a spatial distribution if the atomic beam is detected sufficiently downstream from the interaction region. The apparatus we developed for monitoring the spatial profile of the beam is illustrated in Figure 18. The detector is essentially a fluorescence monitor tuned to the $F=2$ to $F=3$ transition so that it is sensitive only to the atoms within the velocity group of interest. The monitor consists of a laser beam that is reflected off a mirror mounted on a galvanometer. The galvanometer is located at the focus of a cylindrical lens that focuses the beam to a $23\text{ }\mu\text{m}$ spot. The accuracy of the galvo-drive circuit is sufficient to reproducibly position the spot to within $50\text{ }\mu\text{m}$. Thus, the beam effects are limited more by the $175\text{ }\mu\text{m}$ width of the atomic beam than by the precision of the spatial profile monitor.

Figure 19 is the spatial profile of an atomic beam before and after passing through the standing wave region. The original beam has a single peak that is split into two peaks that are characteristic of the theoretical distributions shown in Figure 6. The experimental resolution was insufficient to resolve the recoil due to single photons, which would have produced the comb effect seen in the fully quantum mechanical calculation.

Our analysis of the OKDE data has been enhanced by the development of two computer programs that run on the HRL VAX computers. The first program calculates the expected spatial beam profile monitor intensity as a function of position, standing wave intensity, standing wave spot size, and atomic

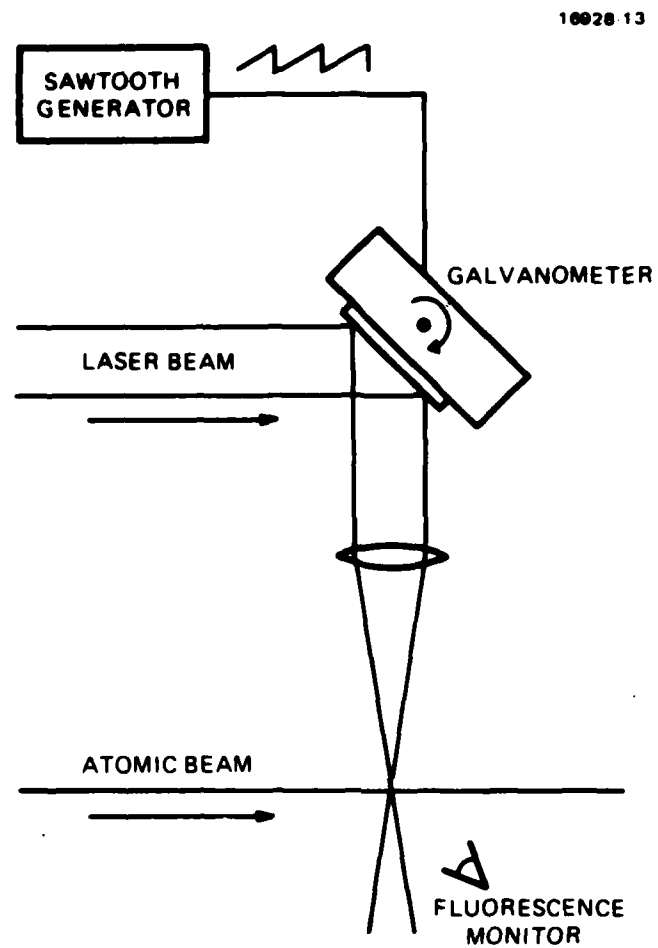


Figure 18. Spatial beam profile monitor.

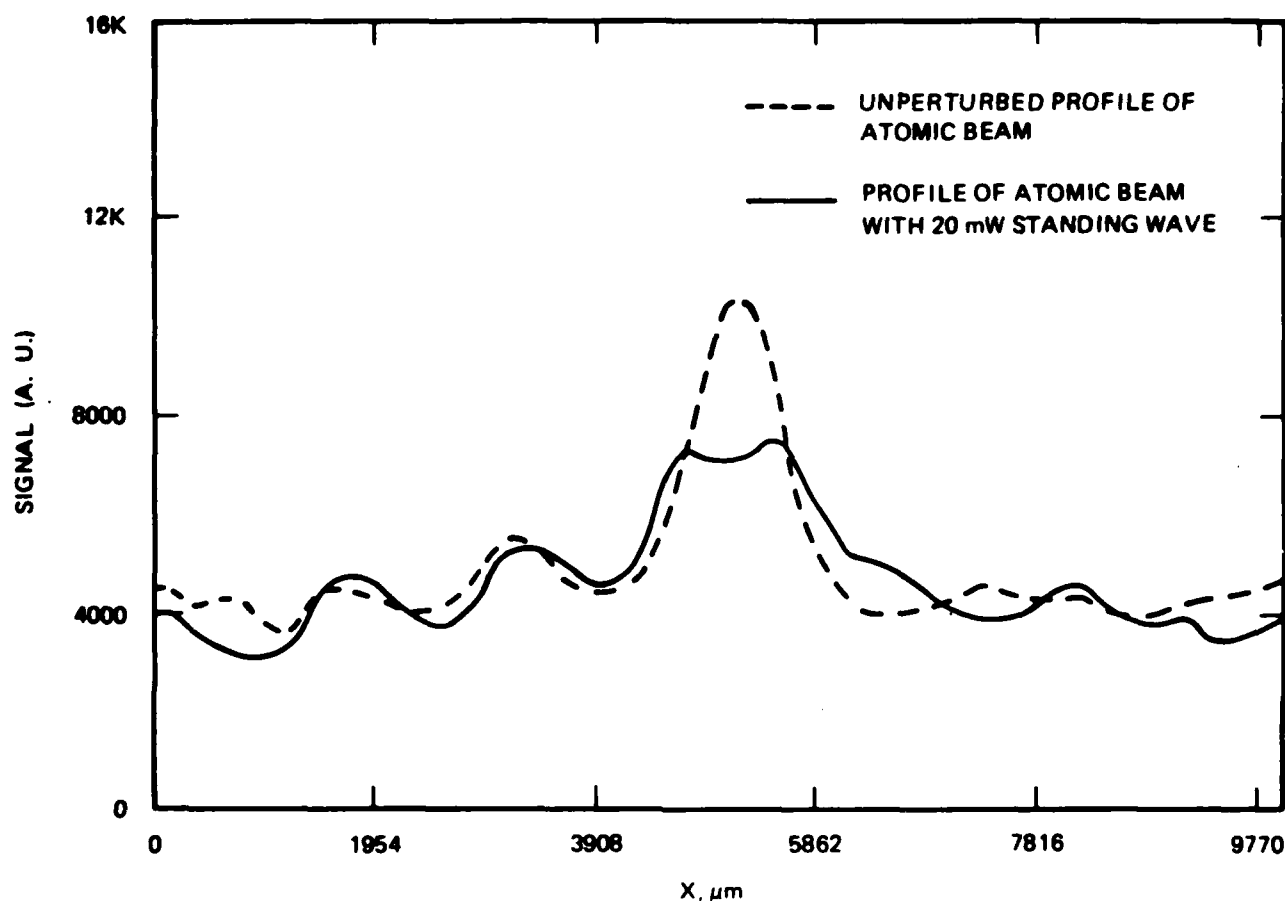


Figure 19. Experimental data showing the effect of the internal standing wave on the spatial profile of the atomic beam. The noise in the data and residual bumps is the result of a sodium oven malfunction during the experiment.

beam size. This program has been very useful in understanding the fundamental limits of the measurement system, in discovering how different misalignments affect the results, and in determining what kinds of signals we should be looking for.

The second program is used for analyzing the data from our TN-1710 signal averager on the VAX. This program can find peaks and widths of arbitrary line shapes, calculate statistical uncertainties and correlations of fit parameters, and generate graphical displays of the data and fits on a number of CRT and hard copy output units.

SECTION 4

ATOMIC HYDROGEN TWO-PHOTON IONIZATION

A. INTRODUCTION

One of the factors that could limit the maximum cooling rate of an atomic hydrogen beam is the maximum laser beam intensity possible before a significant number of hydrogen atoms are ionized by the cooling beam. We have undertaken experimental and theoretical studies to calculate and measure the magnitude and the features of this effect.

B. THEORETICAL STUDIES

Multiphoton ionization of hydrogenic systems is concerned with the dynamics involved in the coupling of external radiation fields with bound quantum systems leading to the production of free electrons and ions. As such, multiphoton ionization has been the subject of intense investigation during the past decade. One of the simplest and most fundamental problems concerns the ionization process when the input radiation fields induce a resonant two-photon transition into the continuum from the ground state of a hydrogenic system. In this case there are two regimes. If the radiation is not resonant with a bound-bound transition, the ionization rate can be computed by perturbation theory, and the results indicate that rate is proportional to the square of the input intensity. However, if the radiation is resonant with a bound-bound transition, saturation processes in the population difference yield an expression for the ionization rate that exhibits saturation behavior, as will be shown below.

Because of the importance of using Lyman- α radiation in the cooling and trapping of atomic hydrogen, we undertook a detailed description of the role of ionization of hydrogen atoms. The objective of this work was to present a self-consistent

calculation of the effects of resonance radiation on the two-photon ionization process in hydrogen atoms. The results showed that two-photon ionization of hydrogen remains negligible for intensities up to one kw/cm^2 .

Above $10 \text{ kW}/\text{cm}^2$, significant ionization will take place. The generation of such a plasma environment will necessarily increase the emittance of the beam, possibly leading to a catastrophic breakup as it propagates in space.

1. Formulation of the Problem

The starting point in our analysis was the formulation of a set of density matrix equations that describe the model shown in Figure 20. The bound states are labeled by $|i\rangle$ ($i=1,2$), and the continuum by the set $\{|k\rangle\}$. The resonance radiation oscillates at frequency ω_L . The spontaneous decay rate is given by γ . In order to derive a set of equations describing the evolution of each energy level via the density matrix formulation, it is important to understand the coherent coupling between state $|2\rangle$ and the continuum $|k\rangle$. This understanding comes from examining the temporal evolution of the probability amplitude in state $|2\rangle$.

Consider the Schroedinger equation

$$i\hbar \partial|\Psi\rangle/\partial t = (H_0 - \mu E) |\Psi\rangle, \quad (4.1)$$

and write the state vector $|\Psi\rangle$ as a coherent linear superposition of the eigenstates of H_0 ,

$$|\Psi\rangle = c_1(t) |1\rangle \exp(-i\omega_L t) + c_2(t) |2\rangle \exp(-i\omega_L t) + \int dk c(k,t) |k\rangle \exp(-i\omega_k t) \quad (4.2)$$

Using expression (4.2) in Eq. (4.1), we find that the amplitudes c_2 and $c(k,t)$ satisfy the following equations of motion;

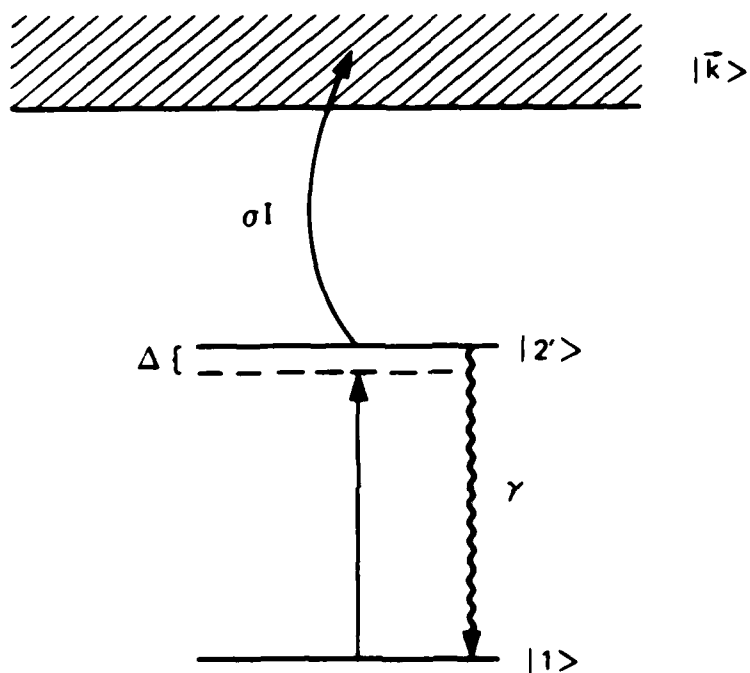


Figure 20. Model used in two-photon ionization calculations. The two bound atomic states are labeled $|1\rangle$ and $|2\rangle$. The continuum states are labeled $|k\rangle$. The laser is detuned from the resonance energy $E_2 - E_1$ by an amount Δ . The spontaneous decay rate from $|2\rangle$ to $|1\rangle$ is γ .

$$i\hbar \partial c_2(t)/\partial t = -\mu_{21} E c_1(t) \exp(i\omega_{21}t) - \int dk \mu_{2k} E c(k,t) \exp(-i\omega_{k2}t) \quad (4.3)$$

$$i\hbar \partial c(k,t)/\partial t = -\mu_{k2} E c_2(t) \exp(i\omega_{k2}t) \quad , \quad (4.4)$$

where $\mu_{\alpha\beta}$ and $\omega_{\alpha\beta}$ are the electric dipole matrix element and frequency separation between states $|\alpha\rangle$ and $|\beta\rangle$, respectively. We assume that the coupling among continuum states is negligible and that the off-resonant two-photon transition between the ground state and the continuum has a small contribution in comparison with the resonant transition.

Equations (4.3) and (4.4) can be reduced further by formally integrating Eq. (4.4) and using the result in Eq. (4.3). This procedure leads to the following expression for $c_2(t)$:

$$i\hbar \partial c_2(t)/\partial t = -\mu_{21} E c_1(t) \exp(i\omega_{21}t) + (i\hbar)^{-1} \int dk \int dt' \mu_{2k} E(t) \mu_{k2} E(t') \times \exp[-i\omega_{k2}(t-t')] c_2(t') \quad (4.5)$$

The evolution of $c_2(t)$ in the presence of the continuum can be deduced in a simple manner. The excitation of an electron from state $|2\rangle$ by the radiation field can only take place if $t' = t$. This simultaneity requirement implies that the second term in Eq. (4.5) can be reduced to a simple decay term of the form $-\Gamma c_2(t)$. $\Gamma = \sigma I$ is the intensity-dependent ionization rate from the excited state $|2\rangle$, and σ is the single-photon ionization cross section.

In light of this derivation for the temporal evolution of $c_2(t)$, the density matrix equations can be written as

$$\partial \rho_{11} / \partial t = \gamma \rho_{22} + i R_0 \rho_{21} - i R_0^* \rho_{12} \quad (4.6)$$

$$\partial \rho_{22} / \partial t = -(\gamma + \sigma I) \rho_{22} + i R_0^* \rho_{12} - i R_0 \rho_{21} \quad (4.7)$$

$$\partial \rho_{12} / \partial t = i(\omega_{21} + i\gamma/2) \rho_{12} + i R_0 (\rho_{22} - \rho_{11}) , \quad (4.8)$$

where R_0 is the on-resonance Rabi frequency. The set of Eqs. (4.6) through (4.8) describes the evolution of the bound system in the presence of the radiation fields.

2. Exact Analytical Solutions

Equations (4.6) through (4.8) have an exact analytical solution if the following assumptions are made:

- (1) The radiation field has a pulse duration longer than the response time of the medium (long pulse approximation).
- (2) The population difference between the bound states is slowly varying compared to the smaller of the natural linewidth and laser detuning from intermediate state resonance (rate equation approximation).
- (3) The laser detuning from resonance is small enough so that one can neglect the Bloch-Siegert shifts (rotating wave approximation).

The use of these assumptions in the formal integration of Eq. (4.8) gives the following expression for the optical coherence:

$$\rho_{12} = i R_0 L_{12} (\rho_{22} - \rho_{11}) , \quad (4.9)$$

where $L_{12} = \{ i\Delta + \gamma/2 \}$ is the complex Lorentzian factor. Using Eq. (4.9) in Eqs. (4.6) and (4.7), we obtain a closed system of equations for the population of each energy level:

$$\partial \rho_{11} / \partial t = \gamma \rho_{22} + |R_0|^2 (\rho_{22} - \rho_{11}) \text{Im}(L_{12}) \quad (4.10)$$

$$\partial \rho_{22} / \partial t = -(\gamma + \sigma I) \rho_{22} - |R_0|^2 (\rho_{22} - \rho_{11}) \text{Im}(L_{12}) , \quad (4.11)$$

where $\text{Im}(L_{12})$ denotes the imaginary part of L_{12} . We shall assume that the initial conditions of the problem are such that

$$\rho_{11}(t=-\infty) = N_0$$

and

$$\rho_{22}(t=-\infty) = 0.$$

N_0 is the initial density of the atoms in the ground state.

The reduced set of Eqs. (4.10) and (4.11) has the following exact analytical solutions:

$$\rho_{22} = \{N_0 K / \lambda_2\} \exp[-0.5(\gamma + \sigma I + K)t] \sinh(\lambda_2 t) \quad (4.12)$$

$$\rho_{11} = N_0 - \rho_{22} - \sigma I \int dt' \rho_{22}(t') , \quad (4.13)$$

where $K = |R_0|^2 \text{Im}(L_{12})$ and $\lambda_2 = \{(\gamma + \sigma I + K)^2 - 4\sigma I K\}^{1/2}$.

Equations (4.12) and (4.13) constitute the main result of this section and they are valid in the regime where the three fundamental assumptions (long pulse, rate equation, and rotating wave approximations) are valid.

3. Discussion

Consider hydrogen atoms excited by Lyman- α radiation tuned to the 1s-2p transition. We will assume a cross section of the order of 10^{-16} cm^2 for the ionization of an electron located in the 2p state. Figures 1 and 2 are plots of the temporal evolution of the total density of atoms (i.e., $\rho_{11} + \rho_{22}$).

Figure 21 corresponds to the case where the Lyman- α radiation is tuned on resonance to the 1s-2p transition, and shows that negligible ionization takes place for a radiation intensity of 1 kW/cm² over a period corresponding to 100 times the spontaneous decay lifetime (1.6 ns). As the intensity is increased to 500 kW/cm², significant ionization takes place, leading to the possible deterioration of the beam quality. Figure 22 shows the temporal evolution of the total density of atoms for fixed intensity as a function of the radiation detuning from line center. Again, for zero detuning, significant ionization occurs. However, as the detuning is set to 10 γ , ionization is reduced significantly. This behavior is easily explained. If the Lyman- α is on resonance, then there is significant excitation of the 2p state, leading to a stepwise resonantly enhanced ionization path. However, if the laser is tuned off resonance, negligible excited state population is achieved. Hence, the ionization process proceeds along a non-resonant pathway. This explanation is illustrated in Figure 23, where the excited state population is plotted as a function of time. As is shown the excited state population decreases with increasing detuning from resonance.

A quantity of interest in the measurement of the two-photon ionization cross section is the two-photon ionization rate, defined by,

$$r = - \{ \partial(\rho_{11} + \rho_{22}) / \partial t \} / (\rho_{11} + \rho_{22}) \quad (4.14)$$

Using the exact analytical expressions for ρ_{11} and ρ_{22} , the resonant two-photon ionization rate is given by,

$$r = (\sigma IK / \lambda_2) / \{ \coth(\lambda_2 t) + (\gamma + \sigma I + K) / 2\lambda_2 \} \quad (4.15)$$

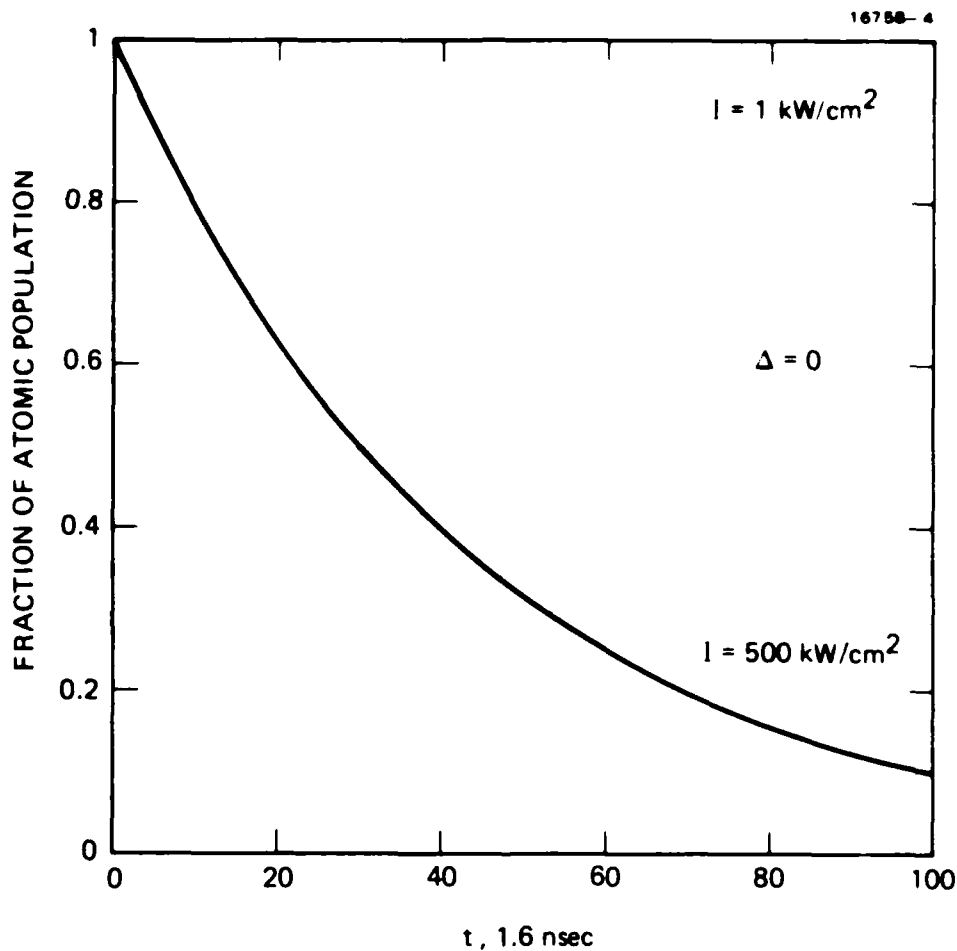


Figure 21. Fraction of remaining atoms during resonant photoionization. The detuning in this curve is zero. The upper curve is for an intensity of 1 kW/cm^2 . Even after 100 spontaneous decay lifetimes, no significant ionization has taken place. The lower curve is for an intensity of 500 kW/cm^2 . In this case, 90% of the atoms have been ionized after 100 spontaneous decay lifetimes. The x axis is time in units of the spontaneous decay lifetime (1.6 ns).

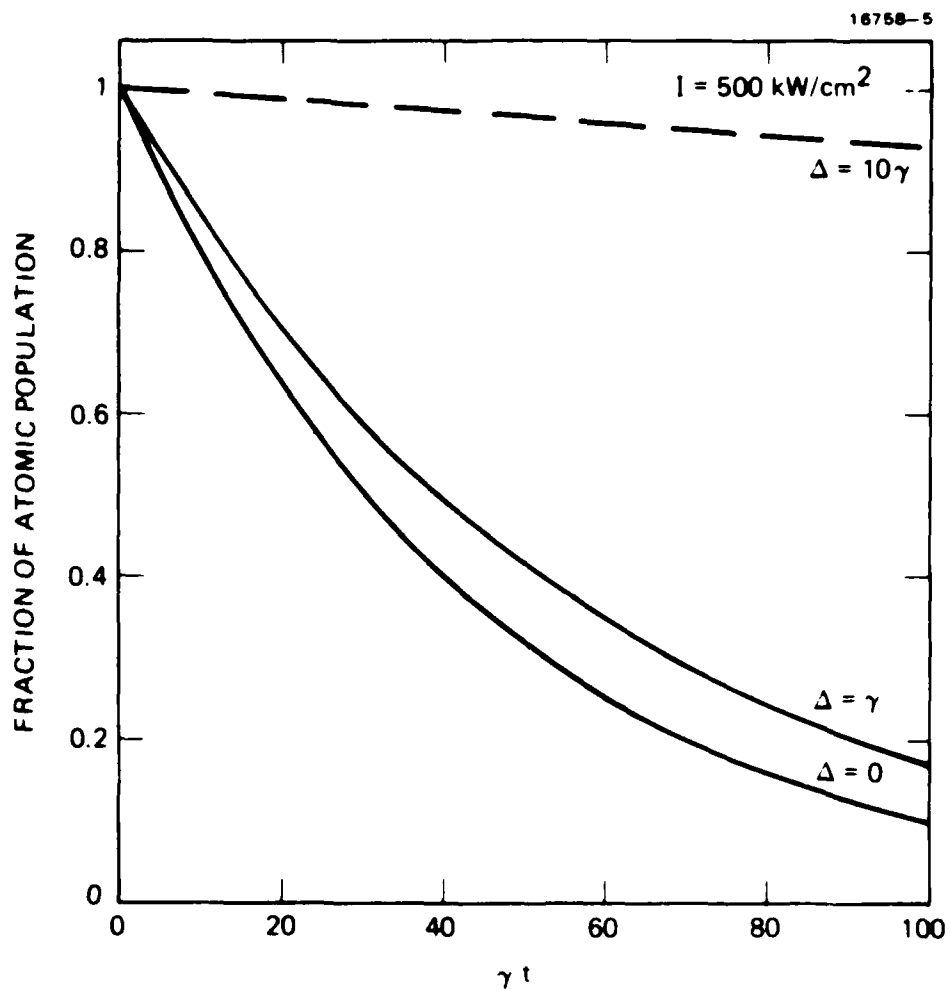


Figure 22. Fraction of remaining atoms during resonant photoionization. The intensity for all these curves is 500 kW/cm^2 . The three curves show detunings of ten times the natural line width, one natural line width, and zero.

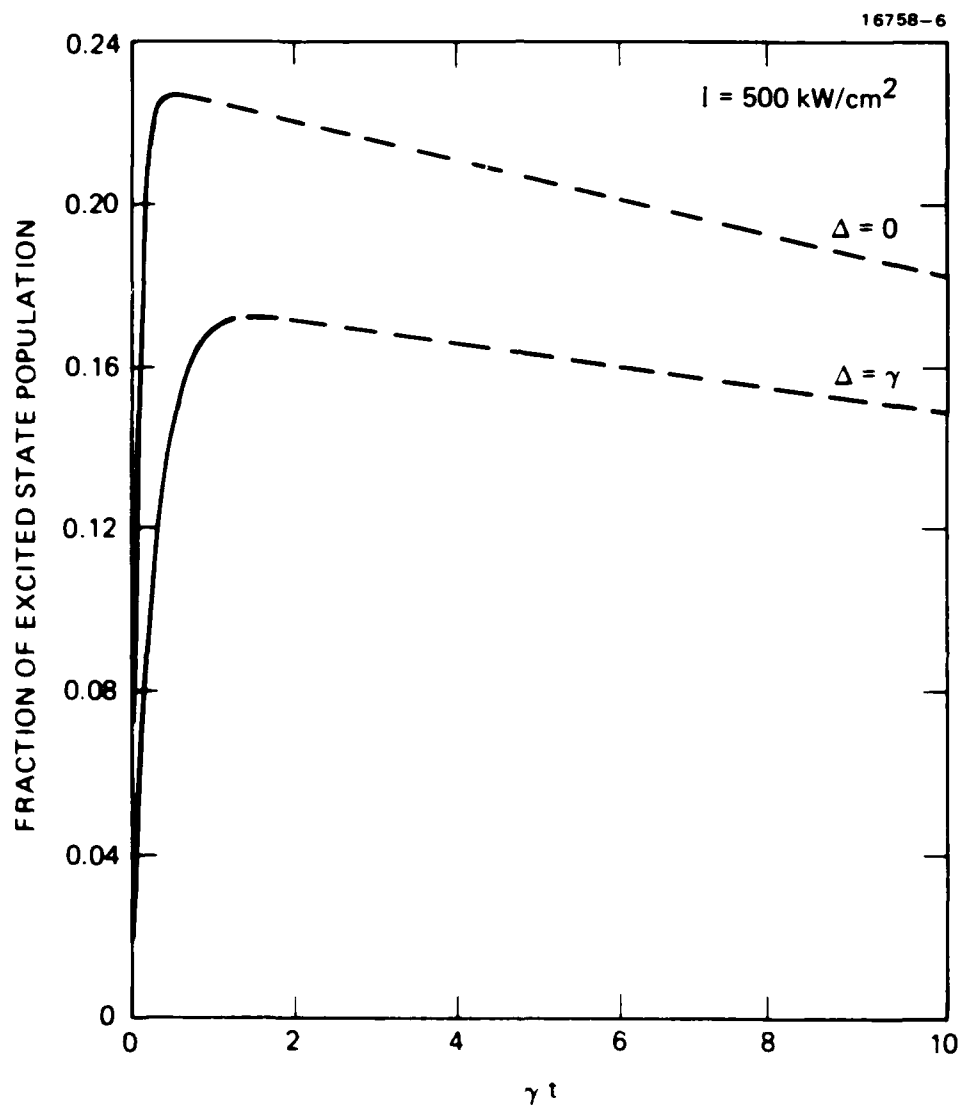


Figure 23. Fraction of excited atoms during resonant photoionization. The intensity for both curves is 500 kW/cm^2 . The upper curve is for no detuning. The lower curve is for a detuning of one natural line width.

It is interesting to note that the rate is time dependent, because the exact solutions describe the temporal behavior of the population density as a function of laser intensity and detuning from line center. The long-time behavior (as t tends to infinity) is given by,

$$r = 2 \sigma I K / (2\lambda_2 + \gamma + \sigma I + K) \quad , \quad (4.16)$$

which is a nonlinear function of the laser intensity. Equation (4.16) is the main result of this section; it reduces to the perturbation solution (proportional to I^2) in the low intensity regime, and exhibits saturation behavior when the single-photon ionization rate σI is of the same order of magnitude as the spontaneous decay rate γ .

4. Summary

We have presented a theory of resonant two-photon ionization of hydrogen atoms. We have obtained exact analytical results for the total density of the atoms, and for the ionization rate provided under the three assumptions of a long pulse, the rate equation, and the rotating wave approximation. Ionization of the hydrogen atoms can be avoided if the Lyman- α radiation intensity is restricted to less than 1 kW/cm^2 . The ionization rate was found to be a nonlinear function of the intensity resulting from saturation of the bound state transition. However, the ionization rate reduces to the result obtained from perturbation theory in the low intensity regime.

C. EXPERIMENTAL STUDIES

An experimental measurement of the Lyman- α two-photon ionization cross section of atomic hydrogen requires development and integration of both a tunable narrow-band coherent photon source and a high current, low divergence atomic hydrogen beam. We have developed the hydrogen beam needed for the experiment and have nearly completed the optimization of the Lyman- α beam source. Details of the two developments are given below.

1. Lyman- α Production

Figure 24 is a block diagram of the Lyman- α source we have developed. This photon source consists of two narrow band oscillators that are amplified in pulsed-dye amplifiers pumped by the outputs of a dual-beam Nd-YAG laser. The outputs from the amplifiers are combined in a mercury cell to provide the desired Lyman- α pulses.

The challenge of the Lyman- α system operation is to get concurrent state-of-the-art performance from the many complicated components in the system. Much of our development time was spent improving the reliability of the commercial components that were used in the system.

The narrow-band oscillators consist of two Coherent 699-21 ring dye lasers pumped by two Coherent CR-18 argon ion lasers. The first oscillator delivers 500 to 1000 mW of cw light at 5454 Å. The Rhodamine 560 dye is pumped by an argon ion laser operating at 8 W. The second oscillator contains Kiton Red dye and delivers 300 to 500 mW of power at 6254 Å. The Kiton red dye must be pumped at 8 to 9 W.

We found that it was necessary to modify the Coherent pump module to improve the lifetime of the Rhodamine 560 dye. We also developed a procedure for shutting down the dye lasers, which resulted in an order of magnitude improvement in the day-to-day reproducibility of our dye laser outputs.

The outputs of the dye lasers pass through optical isolators consisting of a pair of prisms and a Faraday rotator. The beams then enter modified Quanta-Ray PDA-1 pulsed dye amplifiers (PDAs) that are pumped by the doubled (532 nm) outputs of a dual-beam Nd-YAG laser. Required modifications in the PDAs for this application included replacing or modifying of the internal telescoping optics, replacing the metal pin holes with diamond ones, and mechanically improving the pin hole mounts. After these modifications, we were able to get 10 ns gaussian pulses in the far field from both PDA's.

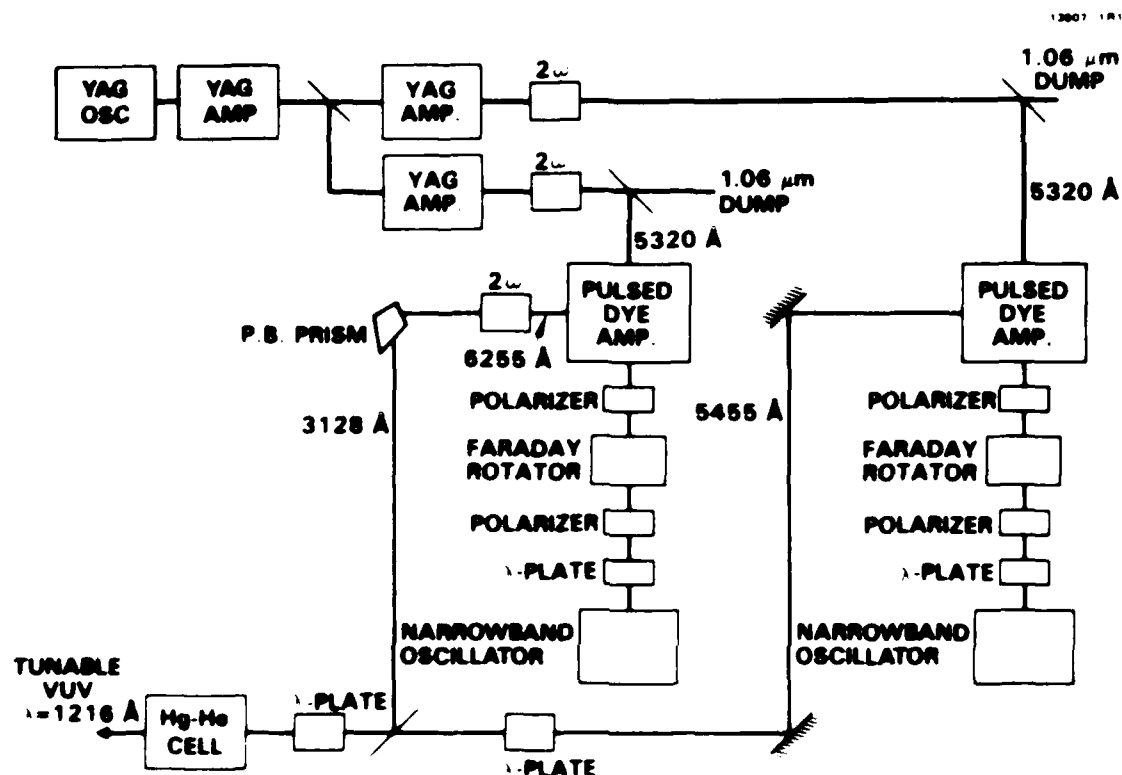


Figure 24 Experimental setup for generation of VUV Lyman- α radiation. The output from the dual beam Nd:YAG lasers are used as pumps to amplify the outputs of the two narrow-band oscillators. The photons at 6255 Å are doubled, yielding photons at 3128 Å. Light at 3128 Å and 5455 Å is combined in an Hg He cell to yield a sum frequency of 1216 Å.

The PDA manufacturer was unable to supply us with appropriate dye concentrations for our applications, so we also undertook a study to learn what combinations of available input power, pump power, and dye concentrations produced the best results. With optimum concentrations and input powers, we were able to achieve 20 mJ at 5454 Å, and 6.5 mJ at 6254 Å. The radiation at 6254 Å was doubled in a KDP crystal to produce 2.0 mJ of 3127-Å light.

The radiation at 3127 Å was combined with the 5454-Å pulses in the mercury cell illustrated in Figure 25. The cell consists of a center region that is heated to 150° to 200°C. Mercury from the wick evaporates and migrates towards the end regions of the cell, which are water cooled. The cooled buffer gas in the end regions condenses the mercury back onto the wicks. The mercury will then move back to the center of the cell where the evaporation/condensation cycle begins again. Our interaction region is approximately 10 cm long. We verified operation of the cell by measuring the absorption of light from the mercury lamp as a function of cell temperature. We measured an αL of 3.0 at a cell temperature of 177°C. After several weeks of operation, we had no accumulation of mercury on the cell windows.

The mixing process in the mercury cell is illustrated in Figure 26. Two photons at 3127 Å are resonant with the mercury transition from the $6s^2 \ ^1S_0$ ground state to the $6s7s \ ^1S_0$ state. The third photon at 5454 Å is non-resonant and can thus be tuned over a fairly broad range. The sum frequency generated by the addition of the three photons is at 1216 Å (Lyman- α). In our tight focusing geometry, the maximum signal is obtained by phase matching the sum of the wave vectors of the input and output waves so that $b\Delta k = -2,^{13}$ where b is the confocal beam parameter.

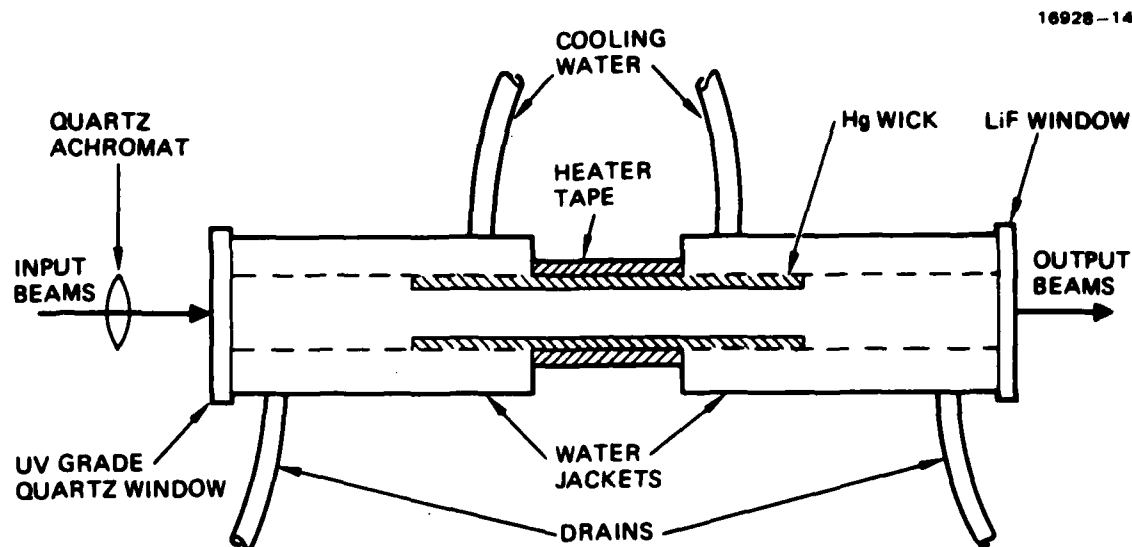


Figure 25. Mercury cell for VUV generation.

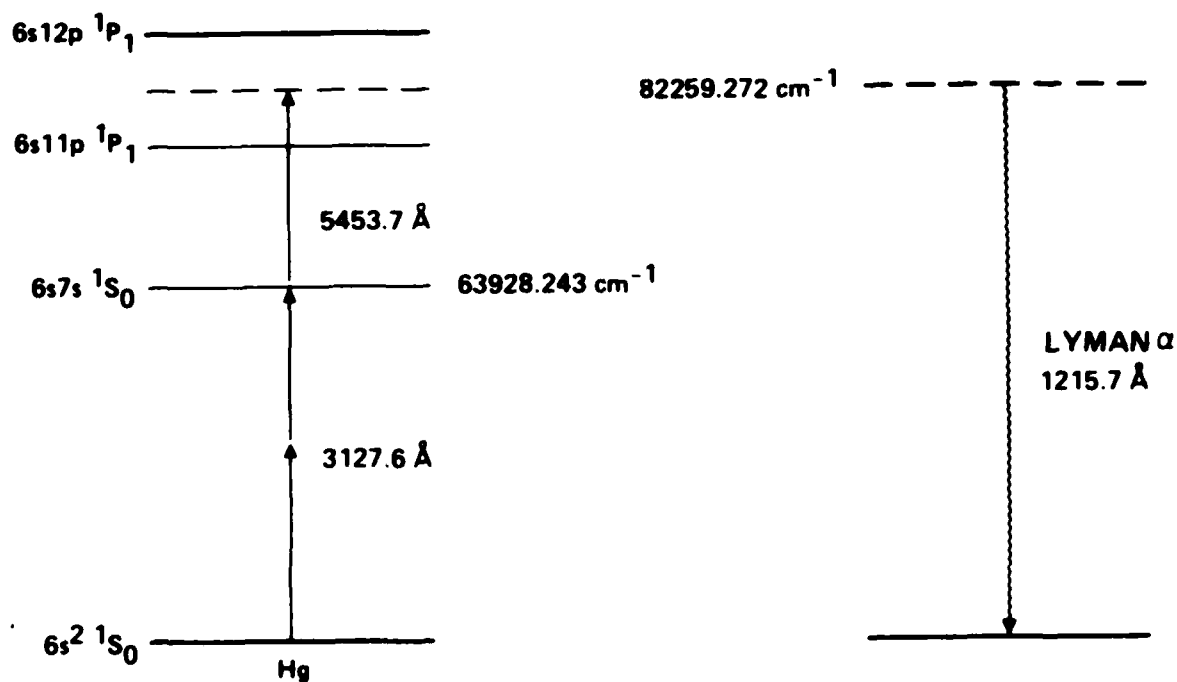


Figure 26. Four-wave mixing process used for generation of VUV Lyman- α radiation in mercury.

We have used two diagnostics to study the radiation exiting the mercury cell - a nitric oxide (NO) ionization chamber and a McPherson Model 225 one meter scanning VUV monochromator.

Figure 27 is a diagram of the NO ionization detector. The cell was filled with 3.0 Torr of NO gas, which ionizes with a high efficiency for radiation in the 102-nm to 135-nm wavelength range. With our geometry, we expected an efficiency of 50%.

With the NO detector attached to the cell, we saw a small ion signal when the 3127-Å light was introduced to the mercury cell. The signal was resonant with the two-photon resonance we were tuning for, but didn't show a strong dependence on the intensity of the 5454-Å light. Also, the tuning width was broader than we would have expected from either the natural line width of the mercury resonance or the Doppler broadening of the atoms in the mixing cell.

To better understand our results, we attached the mercury cell to the McPherson monochromator. The monochromator was first calibrated with a hydrogen Hinterreger light source at Lyman- α and with a number of lines from a mercury lamp. The radiation was detected with a solar blind photomultiplier tube. We have not yet been able to reproduce on the monochromator the VUV signals we saw in the NO detector.

2. Hydrogen Beam Production

Figure 28 is a diagram of our hydrogen beam production facility. Molecular hydrogen is dissociated by an rf field in a water cooled glass cell. A snout at the end of the cell is capped with an effuser plate consisting of a close packed array of 2.0- μ m-diameter, 3.0-mm-long capillaries. These capillaries provide a differential pressure between the rf discharge region and the high vacuum region, and they provide good beam collimation. With some experimentation, we were able to achieve a beam divergence of less than 1°. At this divergence, the natural line width of the hydrogen Lyman- α transition will be comparable to the Doppler line width.

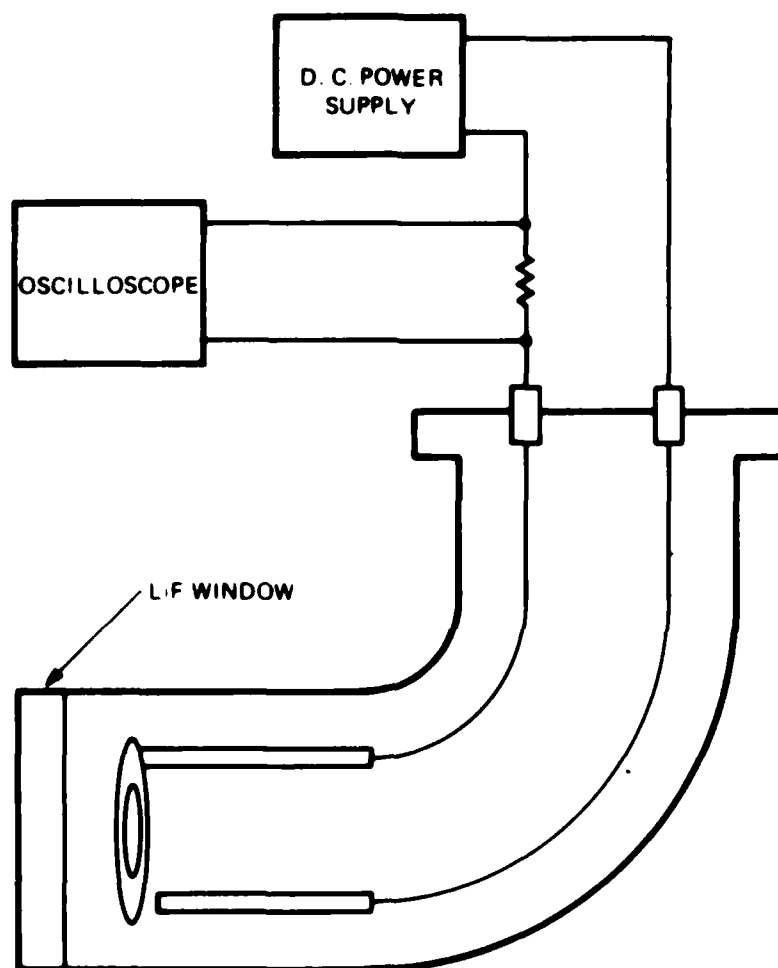


Figure 27. Nitric oxide ionization detector. Light passing through the LiF window ionizes the NO gas in the cell. The ions and electrons drift toward the two biased parallel plates, producing a signal on the oscilloscope.

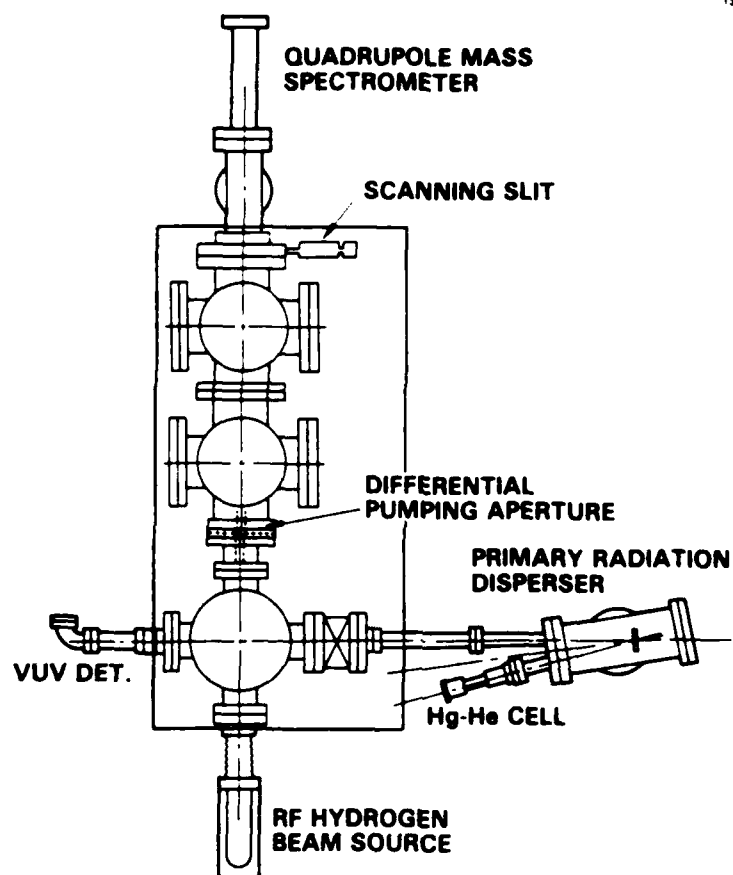


Figure 28. Hydrogen beam apparatus.

The hydrogen beam intersects the Lyman- α beam in the first chamber. Before intersecting the hydrogen beam, however, the photon beam is first dispersed by a diffraction grating to separate out photons (which also exit the mercury cell) with unwanted wavelengths. A hydrogen discharge cell is provided in the photon beam line to monitor the frequency of the radiation. Radiation flux is measured with an NO ionization detector.

The hydrogen flux can be monitored by two devices. The best absolute measurement is given by a bolometer, consisting of a platinum strip that intersects the entire hydrogen beam. Atomic hydrogen incident on the strip will recombine on the surface of the platinum and leave the surface as molecular hydrogen. The total energies of recombining hydrogen atoms will heat the strip, thus changing its resistance. After balancing a bridge circuit that has the platinum strip as one of its legs, the hydrogen beam is turned off and the platinum strip is electrically heated until its resistance matches that of the strip as it was being heated by the hydrogen beam. The product of the electrical current and voltage supplied to the strip gives the power that must also have been supplied by the recombining hydrogen atoms in the beam. Dividing this power by the energy of recombination of the hydrogen atoms yields the number of hydrogen molecules leaving the surface of the platinum, per second.

We also used a UTI mass spectrometer as a secondary monitor of the beam flux. Once calibrated against the platinum strip detector, this spectrometer provides a real-time measure of the hydrogen flux, which can be monitored continuously during data collection. We were able to generate atomic hydrogen beam currents of 6×10^{17} atoms/s.

SECTION 5

π -PULSE COOLING

A. INTRODUCTION

Experimental studies of laser modification of atomic velocities using the phenomenon of laser-induced fluorescence as proposed by Hänsch and Schawlow,¹⁴ have been quite extensive. Evidence of the slowing of an atomic beam by resonance radiation pressure was demonstrated by Bjorkholm et al.,¹⁵ Balykin et al.,¹⁶ Phillips and Metcalf,¹⁷ and Prodan et al.¹⁸ Recently, experiments by Prodan et al.¹⁹ and Ertmer et al.²⁰ demonstrated that an effusive atomic beam was stopped by laser light. These works were followed by the recent experimental demonstration of radiation trapping of atoms by Chu et al.²¹

In the Hänsch and Schawlow cooling procedure, the atoms are illuminated with counterpropagating laser beams that are tuned into the upper half of the Doppler contour of a resonance line, the laser frequency either covering the full upper half of the contour, or scanned toward line center as cooling progresses. Cooling results from the net momentum transfer from the laser photons to the atoms during resonance fluorescence events. The cooling rate is thus limited by the natural decay rate of the atoms from the spontaneous radiation; the maximum cooling rate occurs at laser power levels that saturate the transition.

The above limitation on the cooling rate could be lifted if it were possible to alternate the direction and detuning of the separate upward-stimulating and downward-stimulating photons. Then, a net momentum transfer to the atom could be made to occur at transition rates greater than the spontaneous decay rate. This goal can be achieved by using a train of alternately oppositely directed and oppositely detuned π pulses.

The concept of modifying the velocity of the atoms using π pulses was advanced by Kazantsev in 1974.²² A similar scheme was proposed by Nebenzahl and Szoke²³ in their studies of atomic-beam deflection using stimulated emission processes. Recently, Aspect et al.³ demonstrated the collimation of a cesium atomic beam using stimulated emission. A related application using π pulses to deflect an atomic beam for isotope separation was considered by Friedman and Wilson.²⁴

B. PHYSICAL PICTURE

The basic physics of π pulse cooling is described as follows: consider the interaction of a two-level atom with a pair of π pulses incident from opposite directions. First, a photon from the π pulse from the right is absorbed, exciting the atom to the upper state. An increment of momentum $-\hbar k$ has been transferred to the atom. Here k is the wavenumber and \hbar is Planck's constant divided by 2π . Next, the π pulse from the left stimulates the atom to emit a photon to the left, resulting in a recoil momentum transfer to the atom of $-\hbar k$. Hence the net momentum transferred to the atom from the interaction of both π pulses is $-2\hbar k$. Clearly, a train of n alternately counter-propagating π pulses sequentially incident upon the atom will result in a momentum transfer of $n\hbar k$ in the direction of propagation of the upward stimulating π pulses, provided that the duration of the pulse train remains short in comparison with the radiative lifetime of the transition. To retard the motion of the atom's the upward stimulating π pulses should be directed opposite to the motions of the atom and tuned above resonance, while the downward stimulating π pulses should be oppositely directed and tuned below resonance.

To cool a one-dimensional velocity distribution of atoms, a train of π pulses with a detuning sequence chosen to retard the motion of atoms moving in one direction must be followed by a train with the start of the detuning sequence shifted to the

oppositely directed beam in order to retard the motion of the atoms moving in the opposite direction. To ensure cooling of the distribution, each π -pulse train must effect a larger momentum transfer to atoms in the half of the distribution for which the motion is being retarded, than to the other half. This desired result will occur if the frequency of the π -pulse train is chosen to be resonant with atoms with Doppler shift of half the Doppler width of the distribution, since the excitation state of the atoms on that side of the distribution will remain in coherence with the π -pulse train for a larger number of π pulses than will atoms in the other side of the distribution. The two π -pulse trains must be separated by a few radiative lifetimes in order to reset the excitation state of all the atoms to the ground state before switching the detuning sequence.

This physical description of the cooling process achieved with the π -pulse technique is rigorously justified using quantum mechanical transport equations. The formulation of the equations is the core of the next section.

C. THE QUANTUM TRANSPORT EQUATIONS, INCLUDING ATOMIC RECOIL

The quantum transport equations were first derived by Kolchenko et al.²⁵ when they studied the spectral response of gaseous systems in saturated absorption spectroscopy. They observed that the origin of the symmetrical splitting of the Doppler-free absorption line was the atomic recoil experienced by the atom upon absorbing and emitting photons. The same equations have been rediscovered by numerous authors. This section presents a detailed derivation of the quantum transport equations, which take into account the effects of Doppler broadening, grating washout, and atomic recoil.

If R denotes the center-of-mass displacement vector and r the internal coordinates, then the space-time evolution of an atom is governed by the Schrodinger equation,

$$i\hbar \partial \Psi(R,r,t)/\partial t = [-\hbar^2 \nabla^2 / 2M + H_0 + V(R,t)] \Psi(R,r,t), \quad (5.1)$$

where the first term on the right hand side accounts for the translational motion of the atom, H_0 is the electronic Hamiltonian, and $V(R,t)$ is the interaction Hamiltonian. We will consider an interaction potential for the induced electric dipole moment of an atom interacting with the radiation field.

We begin by expanding the wavefunction Ψ as a linear superposition of eigenstates ϕ_m of H_0 :

$$\Psi(R,r,t) = \sum c_m(R,t) \phi_m \exp(-i\omega_m t), \quad (5.2)$$

where the probability amplitude c_m accounts for the translational motion of the atom in specific eigenstate ϕ_m . Using expression (5.2) in the Schrodinger equation (5.1), one finds the temporal evolution of c_n is described by

$$i\hbar \partial c_n / \partial t = -\hbar^2 \nabla^2 c_n / 2M + \sum \langle n|V|m \rangle \exp(i\omega_{mn}t) c_m \quad (5.3)$$

where $\langle n|V|m \rangle$ and ω_{nm} are the matrix element of V and frequency difference between eigenstates $|m\rangle$ and $|n\rangle$, respectively.

Our goal is to obtain an evolution equation for the observables of the problem in question. In this case, the observables are the population of each eigenstate and the optical coherence generated by the radiation field. Defining the Wigner distribution function as

$$f_{nm}(R,p,t) = (1/2\pi\hbar)^3 \int dR' \exp(-ip \cdot R' / \hbar) \rho_{nm}(R+R'/2, R-R'/2), \quad (5.4)$$

where ρ_{nm} is the observable, and using the Wigner distribution in expression (5.4), we find that the quantum mechanical transport equation is described by,

$$\begin{aligned}
& i\hbar(\partial/\partial t + \mathbf{p} \cdot \nabla/M) f_{nm}(\mathbf{R}, \mathbf{p}, t) \\
& = \int d\mathbf{k} [\langle n|V'|\alpha \rangle \exp(-i\mathbf{k} \cdot \mathbf{R}) f_{\alpha m}(\mathbf{R}, \mathbf{p} + \hbar\mathbf{k}/2, t) \exp(i\omega_{n\alpha} t) \\
& - f_{n\alpha}(\mathbf{R}, \mathbf{p} - \hbar\mathbf{k}/2, t) \langle \alpha|V'|\mathbf{m} \rangle \exp(-i\mathbf{k} \cdot \mathbf{R}) \exp(i\omega_{\alpha m} t)], \quad (5.5)
\end{aligned}$$

where the convective derivative $\mathbf{p} \cdot \nabla/M$ accounts for the translational motion of the atom and gives rise to Doppler broadening and grating washout. The quantity $\langle n|V'|\alpha \rangle$ is the spatial Fourier transform of $\langle n|V|\alpha \rangle$. Equation (5.5) is the main result of this section: it describes exactly the interaction of an atom with a classical radiation field, and takes into account the atomic recoil effect.

D. NUMERICAL SOLUTIONS

In essence, Eq. (5.5) is the quantum generalization of the classical Boltzmann equations. Applying it to the case of two level atoms, we can show that Eq. (5.5) reduces to equations describing the following distribution functions: $M(\mathbf{p}, t) = f_{22} + f_{11}$, the number density of atoms; $N(\mathbf{p}, t) = f_{22} - f_{11}$, the population difference between the two states; and $f_{12}(\mathbf{p}, t)$, the optical coherence. The quantum transport equations are

$$\partial N/\partial t = 4 \Omega F_i(\mathbf{p}, t) \quad (5.6)$$

$$\begin{aligned}
\partial M/\partial t &= 2 \Omega [F_i(\mathbf{p} + \hbar\mathbf{k}, t) - F_i(\mathbf{p}, t)] \\
(\partial/\partial t + i\Delta\omega - i\mathbf{p} \cdot \mathbf{k}) F(\mathbf{p}, t) & \quad (5.7)
\end{aligned}$$

$$= i \Omega N(\mathbf{p}, t) + i \Omega [M(\mathbf{p} + \hbar\mathbf{k}, t) - M(\mathbf{p}, t)], \quad (5.8)$$

where $\Omega = \mu E/\hbar$ is the on-resonance Rabi frequency, μ is the dipole moment of the transition, and E is the electric field amplitude. We have made the substitution: $F = f_{12} \exp(i\mathbf{k}x - i\Delta\omega t)$, where $\Delta\omega$ is the detuning from line center. F_i indicates the imaginary part of F .

We have carried out numerical solution of Eqs. (5.6) through (5.8), using a train of π pulses as the applied field, with alternate pulses oppositely directed and tuned on opposite sides of line center, as required for cooling. Hydrogen atoms were selected for the atomic system in question, and the wavelength of the radiation field was assumed to be tuned to the Lyman- α transition of hydrogen. The results of the simulation are detailed in Figure 29, which shows an initially Maxwellian momentum distribution, and the distribution after the application of 16 π -pulses tuned in the manner discussed above. Also shown are the plots of $|F|$ after the application of each of the π -pulse trains tuned to the opposite side of the distribution. We can see from these plots that coherence is maintained better on the side of the distribution that is being cooled than it is on the opposite side, as expected. As required, the phases of all of the atoms were reset to zero before the application of the second train of π -pulses. Also evident is an essentially symmetric distribution, $M(p)$, that is cooled, except at the wings of the distribution where some apparent heating of the distribution has occurred.

E. SUMMARY

In conclusion, we have examined radiation cooling of a distribution of two-level atoms in the coherent pulse regime. A train of oppositely directed and oppositely detuned π -pulses, with specific zero-field periods between the π -pulses, is required for optimal cooling. The cooling was demonstrated through numerical analysis of the quantum transport equations. The scheme proposed here provides an alternate method for cooling neutral particle beams.

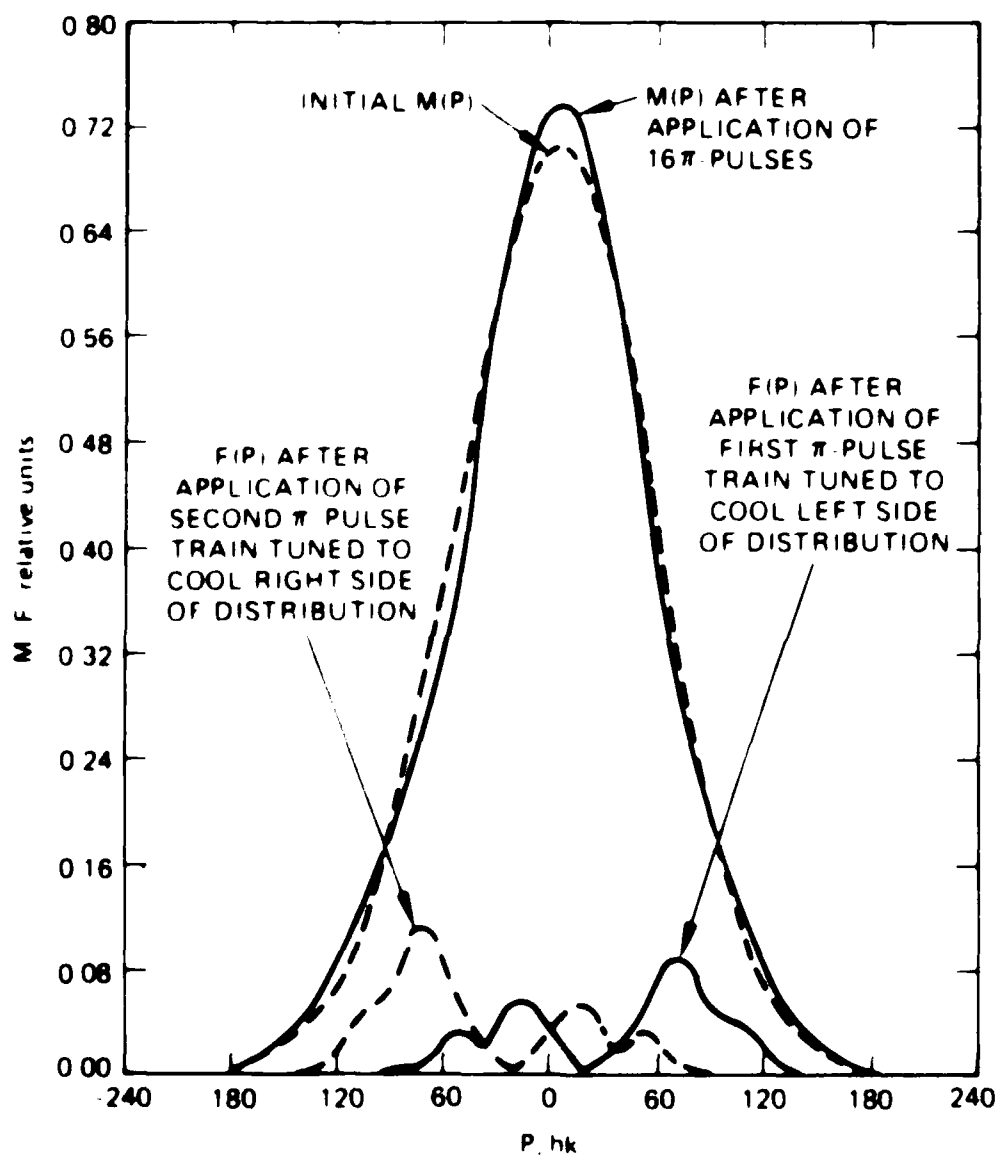


Figure 29 π -pulse cooling process.

SECTION 6

SUMMARY

In this report, we have summarized the work completed in three areas relevant to cooling and trapping of neutral atomic beams. We first provided a summary of ways in which radiation forces can be used to reduce the emittance or trap neutral atoms. This summary was followed by a brief review of the physics of atom/laser interactions. Finally, we reviewed our theoretical and experimental investigations in Optical Kapitza-Dirac Effect, hydrogen two-photon resonant ionization at Lyman- α , and π pulse cooling.

In our Optical Kapitza-Dirac work, we observed the diffraction effect predicted by theory. As a practical matter, the effect will not become significant in the time and intensity regimes expected for cooling relativistic atomic beams. Our theoretical studies of the effects of very intense beams on the OKDE were also presented. Our dressed state formalism provides a means of treating the effects of intense fields for large detunings and intensities above the saturation intensity.

The atomic two-photon ionization work also involved both experimental and theoretical investigations. Our calculations show that ionization will not be a problem in cooling a hydrogen beam, provided the intensity is kept below 1 kW/cm^2 . Since this figure is considerably larger than the Lyman- α saturation intensity, it is unlikely this limit will prove to be a serious one. The experimental efforts have resulted in development of a hydrogen beam source and a VUV source that should prove adequate to perform the indicated measurements. However, further work must be done on the VUV source before the measurements can be completed.

The theory of π pulse cooling was developed in Section 5. This technique appears to be a viable alternative to the more

traditional approach of cooling by spontaneous emission. A numerical simulation of cooling established the feasibility of this alternative.

In conclusion, laser cooling appears to be an attractive technique for cooling and trapping neutral atoms. The two limitations imposed by standing wave diffraction effects and photo-ionization are interesting and real, but aren't expected to seriously affect the performance of present cooling and trapping schemes. Alternative approaches to cooling appear to offer advantages over traditional cooling techniques that rely on spontaneous emission.

SECTION 7
PUBLICATIONS

1. D.G. Steel and R.A. McFarlane, Optics Letters 8, 33 (1983).
2. R.S. Turley, "H⁻ Photoneutralization," Brookhaven Neutralizer Conference, June 5-6, 1985.
3. Juan F. Lam, "A theory of resonant 2-photon induced ionization of hydrogenic systems," submitted to Phys. Rev. A (1987).
4. A.J. Palmer and J.F. Lam, "Radiation cooling using π pulses," JOSA B 3, 719 (1986).

REFERENCES

1. "Proceedings of the Cooling Condensation and Storage of Hydrogen Cluster Ions Workshop," Menlo Park, CA, January 8-9, 1987 (to be published).
 2. J.V. Prodan, A. Migdall, W.D. Phillips, I. So, H. Metcalf, and J. Dalibard, "Stopping atoms with laser light," *Phys. Rev. Lett.* **4**, 992 (1985).
 3. A. Aspect, J. Dalibard, A. Heidmann, C. Salomon, and C. Cohen-Tannoudji, "Cooling atoms with stimulated emission", *Phys. Rev. Letters* **57**, 1688 (1986).
 4. J. Dalibard and C. Cohen-Tannoudji, "Dressed-atom approach to atomic motion in laser light: the dipole force revisited," *JOSA B2*, 1707 (1985).
 5. R.J. Cook and A.F. Bernhardt, "Deflection of atoms by a resonant standing electromagnetic wave," *Phys. Rev.* **A18**, 2533 (1978).
 6. A.F. Bernhardt and B.W. Shore, "Coherent atomic deflection by resonant standing waves," *Phys. Rev.* **A23**, 1290 (1981).
 7. E. Arimondo, A. Bambini, and S. Stenholm, "Quasiclassical theory of laser-induced atomic-beam dispersion," *Phys. Rev.* **A24**, 898 (1981).
 8. C. Tanguy, S. Reynaud, M. Matsuoka, and C. Cohen-Tannoudji, "Deflection profiles of a monoenergetic atomic beam crossing a standing light wave," *Optics Comm.* **44**, 249 (1983).
 9. C. Tanguy, S. Reynaud, and C. Cohen-Tannoudji, "Deflection of an atomic beam by a laser wave: transition between diffractive and diffusive regimes," *J. Phys. B, At. Mol. Phys.* **17**, 4623 (1984).
 10. Philip E. Moskowitz, Phillip L. Gould, Susan R. Atlas, and David E. Pritchard, "Diffraction of an atomic beam by standing-wave radiation," *Phys. Rev. Lett.* **51**, 370 (1983).
 11. C. Cohen-Tannoudji, "1975 Proc. 2nd Laser Spectroscopy Conf," ed S. Haroche, J.C. Pebay-Peyroula, T.W. Hansch, and S.H. Harris (Berlin: Springer), 324 (1975).
- C. Cohen-Tannoudji, "1976 Frontiers in Laser Spectroscopy, Les Houches Summer School," Session 27, ed. R. Balian, S. Haroche, and S. Liberman (Amsterdam: North-Holland), (1977).

- C. Cohen-Tannoudji and S. Reynaud, "Dressed-atom description of resonance fluorescence and absorption spectra of a multi-level atom in an intense laser beam," J. Phys. b10, 345 (1977).
12. D.G. Steel and R.A. McFarlane, "Velocity-specific atomic-state selection in an atomic beam by continuous-wave optical pumping," Optics Letters 8, 33 (1983).
 13. Gary C. Bjorklund, "Effects of focusing on third-order nonlinear processes in isotropic media," IEEE JQE QE-11, 287 (1975).
 14. T.W. Hänsch and A.L. Schawlow, "Cooling of gases by laser radiation," Opt. Commun. 13, 68 (1975).
 15. J.E. Bjorkholm, R.R. Freeman, A. Ashkin, and D.B. Pearson, "Observations of focusing of neutral atoms by the dipole forces of resonance radiation pressure," Phys. Rev. Lett. 41, 1361 (1978).
 16. V.I. Balykin, V.S. Letokhov, and V.I. Mishin, "Cooling of sodium atoms by resonant laser emission," Sov. Phys. JETP 51, 692 (1980).
- V.O. Balykin, V.S. Letokhov, and A.I. Sidorov, "Intense stationary flow of cold atoms formed by laser deceleration of atomic beam." Opt. Commun. 49, 596 (1982).
17. W.D. Phillips and H. Metcalf, "Laser deacceleration of an atomic beam." Phys. Rev. Lett. 48, 596 (1982).
 18. J.V. Prodan, W.D. Phillips, and H. Metcalf, "Laser production of a very slow monochromatic atomic beam," Phys. Rev. Lett. 49, 1149 (1982).
 19. J.V. Prodan, A. Migdall W.D. Phillips, I. So, H. Metcalf, and J. Dalibard, "Stopping atoms with laser light," Phys. Rev. Lett. 54, 992 (1985).
 20. W. Ertmer, R. Blatt, J.L. Hall, and M. Zhu, "Laser manipulation of atomic beam velocities: ?Demonstration of stopped atoms and velocity reversal," Phys. Rev. Lett. 54, 996 (1985).
 21. S. Chu, L. Hollberg, J.E. Bjorkholm, A. Cable, and A. Ashkin, "Three-dimensional viscous confinement and cooling of atoms by resonance radiation pressure," Phys. Rev. Lett. 55, 48 (1985).
 22. A.P. Kazantsev, "The acceleration of atoms by light," Sov. Phys. JETP 39, 784(1974).

23. I. Nebenzahl and A. Szoke, "Deflection of atomic beams by resonance radiation using stimulated emission," Appl. Phys. Lett. 25, 327 (1974).
24. H. Friedman and A.D. Wilson, "Isotope separation by radiation pressure of coherent π pulses," Appl. Phys. Lett. 28, 270 (1976).
25. A.P. Kolchenko, S.G. Rautian, and R.I. Sokolvskii, "Interaction of atoms with a strong electromagnetic field with the recoil effect taken into consideration," Sov. Phys. JETP 28, 986 (1969).

Radiation cooling with π pulses

A. Jay Palmer and Juan F. Lam

Hughes Research Laboratories, Malibu, California 90265

Received April 8, 1985; accepted December 2, 1985

The concept of radiation cooling with π pulses is presented and quantified with a theoretical analysis. Numerical analysis of π -pulse cooling on the hydrogen Lyman- α transition is presented as an example. The cooling rate and limiting temperature are discussed and compared with steady-state radiation cooling.

1. INTRODUCTION

The possibility of using light to modify the velocity distribution of an ensemble of atoms appears to have originated with the pioneering work of Kolchenko *et al.*,¹ who analyzed the effect of atomic recoil in the spectral line shape of an atom interacting with a resonance radiation field. At almost the same time, Ashkin² proposed the concept of resonantly enhanced radiation pressure in a gaseous system. These works stimulated the development of two important contributions in the area of laser cooling. First was the concept of laser-induced cooling of gases by Hänsch and Schawlow,³ which is the foundation of much of today's research in the area. Second was the concept of atomic-beam birefringence under the action of a strong radiation field by Kazantsev,⁴ which was the cornerstone of the so-called optical Stern-Gerlach effect. The latter was recently demonstrated by Moskowitz *et al.*,⁵ and the theoretical analysis of Kazantsev was confirmed by Cook and Bernhardt.⁶

Experimental studies of laser modification of atomic velocities that use the phenomenon of fluorescence have been quite extensive. Evidence of the slowing of an atomic beam by resonance radiation pressure was demonstrated by Bjorkholm *et al.*,⁷ Balykin *et al.*,⁸ Phillips and Metcalf,⁹ and Prodan *et al.*¹⁰ Recently, experiments by Prodan *et al.*¹¹ and Ertmer *et al.*¹² demonstrated that an effusive atomic beam was stopped by laser light. These works were followed by the recent experimental demonstration of radiation trapping of atoms by Chu *et al.*¹³

In the Hänsch-Schawlow radiation cooling procedure, the atoms are illuminated with counterpropagating laser beams that are tuned into the upper half of the Doppler contour of a resonance line, the laser frequency either covering the full upper half of the contour or scanned toward line center as cooling progresses. Cooling results from the net momentum transfer to the atoms from the laser photons during resonance fluorescence events. The cooling rate is thus limited by the natural decay rate of the atom due to spontaneous radiation, the maximum cooling rate occurring at laser power levels that saturate the transition. An increase of laser power above saturation does not increase the cooling rate since absorption followed by stimulated emission from the same beams does not transfer any net momentum to the atom.

The above limitation on the cooling rate could be lifted if it were possible to alternate the direction and detuning of

the separate upward-stimulating and downward-stimulating photons. Then, a net momentum transfer to the atom could be made to occur at transition rates greater than the spontaneous decay rate. As will be illustrated below, this can be accomplished with the use of a train of alternately oppositely directed and oppositely detuned π pulses. The concept of modifying the velocity of atoms using π pulses was advanced by Kazantsev¹⁴ in 1974. A similar scheme was proposed by Nebenzahl and Szoke¹⁵ in their studies of atomic-beam deflection using stimulated-emission processes. A related application of using π pulses to deflect an atomic beam for the purpose of isotope separation was considered by Friedman and Wilson.¹⁶

The objective of this paper is to identify the critical issues associated with π -pulse cooling of a distribution of atomic velocities, to estimate the cooling rate and limiting temperature, and to compare these performance figures with those for steady-state laser cooling.¹⁷ Below, Section 2 describes the physical picture of π -pulse cooling and the restrictions on the incoming train of π pulses due to Doppler dephasing. A rigorous theoretical foundation for π -pulse cooling that utilizes the Wigner distribution function is presented in Section 3. The results of a numerical integration of the quantum-mechanical transport equations applied to π -pulse cooling on the hydrogen Lyman- α transition appear in Section 4. Section 5 compares the cooling rates and required power levels for steady-state and π -pulse cooling, and Section 6 summarizes our results.

2. PHYSICAL PICTURE

The basic physics of π -pulse cooling is as follows: Consider the interaction of a two-level atom with a pair of π pulses incident from opposite directions. First, a photon from the π pulse from the right is absorbed, exciting the atom to the upper state. An increment of momentum $-(\hbar k)$ has been transferred to the atom. (Here k is the photon wave number and \hbar is Planck's constant divided by 2π .) Next, the π pulse from the left stimulates the atom to emit a photon to the left, resulting in a recoil momentum transfer to the atom of $-(\hbar k)$. The net momentum transferred to the atom due to the interaction with both π pulses is $-(2\hbar k)$. Clearly, a train of N alternately counterpropagating π pulses sequentially incident upon the atom will result in a momentum transfer of $N(\hbar k)$ to the atom in the direction of propagation of the upward-stimulating π pulses, provided that the duration of

the pulse train remains short in comparison with the radiative lifetime of the transition. To retard the atom's motion, the upward-stimulating π pulses should thus be directed opposite to the atom's motion and tuned above resonance, while the downward-stimulating pulses should be oppositely directed and tuned below resonance.

To cool a one-dimensional velocity distribution of atoms, a train of π pulses with a detuning sequence chosen to retard the motion of atoms moving in one direction must be followed by a train with the start of the detuning sequence shifted to the oppositely directed beam in order to retard the motion of the atoms moving in the opposite direction. To ensure cooling of the distribution, each π -pulse train must, of course, effect a larger momentum transfer to atoms in the half of the distribution for which the motion is being retarded than to the other half. This will occur if the frequency of the π -pulse train is chosen to be resonant with atoms with a Doppler shift of, say, half the Doppler width of the distribution, since the excitation state of the atoms in that side of the distribution will remain in coherence with the π -pulse train for a larger number of π pulses than will atoms in the other side of the distribution. The two π -pulse trains must be separated by a few radiative lifetimes in order to reset the excitation state of all the atoms to the ground state before switching the detuning sequence.

It is interesting to inquire where the entropy of the atom motion goes in the case of cooling with a train of π pulses. In the case of steady-state laser cooling, the entropy is carried away by the spontaneously emitted photons. During cooling with a train of π pulses, spontaneous emission is assumed not to occur. However, the entropy generation still appears in the radiated photons. Radiation from the atoms during illumination by a π -pulse train is accounted for by the induced transition dipole moment, which is proportional to the off-diagonal terms in the density matrix, $F(t)$ (see below). The generated entropy comes from nonresonant atoms' emitting photons into a larger number of temporal modes than do the resonant atoms. As discussed above, the more randomized phase of $F(t)$ for the nonresonant atoms also accounts for the loss of phase sequencing with the π -pulse train necessary for adjacent π pulses to produce equally directed forces on the atom. Since $F(t)$ is cycling much faster than the spontaneous emission rate, the rate of entropy generation can be larger than in the case of steady-state laser cooling, thus permitting a faster cooling rate for π -pulse cooling.

The accumulated rate of phase error between the excitation state and the π -pulse train that occurs for nonresonant atoms will determine the maximum number of π pulses that can be used in a given π -pulse train. Also, the greater the disparity of the accumulated phase error on the different sides of the distribution, the faster the cooling rate will be for a given π pulse. It turns out that the accumulated phase error can be minimized and the disparity of phase error maximized through the use of a specific zero-field period between the π pulses. This technique is best appreciated through reference to the density-matrix vector model for the evolution of the coherent excitation state of a two-level atom.^{18,19}

Figure 1 shows the density-matrix vector for one atomic velocity before the application of the first π pulse, after the zero-field period, and after the application of the second π

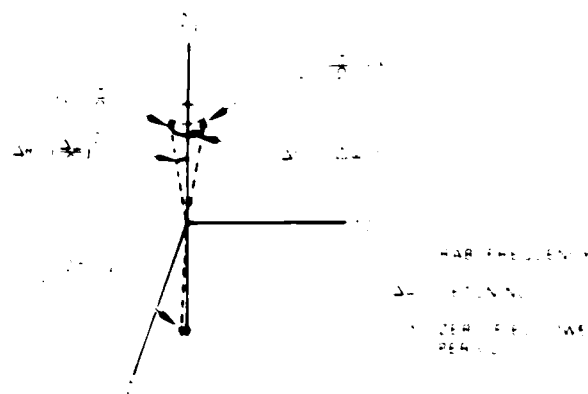


Fig. 1. Vector representation of the state of a two-level atom for one atomic velocity for time zero, after the first π pulse, after the zero-field period, and after the second π pulse.

pulse. The density-matrix vector rotates about the vector $\mathbf{B} = (\Omega\mathbf{e}_1 + \Delta\omega\mathbf{e}_3)$, where $\Omega = \mu E/\hbar$ is the Rabi frequency, μ is the transition dipole moment, E is the laser field, and $\Delta\omega$ is the detuning from resonance. It rotates about \mathbf{B} at an angular rate equal to $(\Omega^2 + \Delta\omega^2)^{1/2}$. When the vector points in the negative \mathbf{e}_3 direction the atom is in the ground state, when it points in the positive \mathbf{e}_3 direction the atom is in the upper state. All other directions represent the atom in a superposition of these two states.

It can be seen from this picture that if there is no field-off period between the π pulses, then the phase-error spread accumulates to $\sim\pi$ within $\sim(\Omega/\Delta\omega)$ pulses. However, during a zero-field interval between π pulses, the vector rotates about the \mathbf{e}_3 axis at a rate equal to the detuning. Thus, if we choose the duration of the off-field interval to be $\sim\pi/(\Delta\omega_0)$, where $\Delta\omega_0$ is the Doppler shift of the atom, then after each off-field period, the sign of the phase error with respect to the \mathbf{e}_3 axis will be reversed, and the subsequent π pulse will bring the phase error back to zero. The phase-error correction cannot be made exact for all atoms, of course, because of the spread in the precession rate about \mathbf{e}_3 caused by the finite velocity spread. The optimum zero-field period for minimizing the average phase error for that half of the distribution which is being cooled is roughly $\pi/(\Delta\omega_0/2)$, where $\Delta\omega_0$ is the Doppler width of the transition.

This phenomenon is similar to the phase-spread reduction that occurs in photon echoes. It is clear that for a given number of π pulses, the net accumulated phase error and the difference in the accumulated phase error between one side of the distribution and the other will be, respectively, less than and greater than their values for the case of no zero-field period. Thus the use of the zero-field period between π pulses will permit cooling over a broader velocity distribution.

We have carried out a theoretical analysis of the π -pulse cooling technique discussed above by utilizing the quantum transport equations. This analysis is described in the following two sections.

3. THEORETICAL FRAMEWORK: THE QUANTUM TRANSPORT EQUATIONS

For the purpose of completeness, we derive in this section the fundamental equations describing the quantum evolu-

tion of an ensemble of two-level atoms interacting with resonant radiation fields. The equations were first derived by Kolchenko *et al.* and have been rediscovered by several groups.²⁰ The equations include the effects of Doppler shift, grating washout, and atomic recoil. If \mathbf{R} denotes the center-of-mass displacement vector and \mathbf{r} the internal coordinates, then the space-time evolution of an atom is governed by the Schrodinger equation

$$i\hbar \partial_t \Psi(\mathbf{R}, \mathbf{r}, t) = [-\hbar^2 \nabla^2 / 2M + H_e + V(\mathbf{R}, \mathbf{r}, t)] \Psi(\mathbf{R}, \mathbf{r}, t) \quad (1)$$

where the first term on the right-hand side accounts for the translational motion of the atom, H_e is the electronic Hamiltonian, and $V(\mathbf{R}, \mathbf{r}, t)$ is the interaction potential. We shall consider an interaction potential for the case of the induced electric dipole moment of an atom interacting with the radiation field

We begin by expanding $\Psi(\mathbf{R}, \mathbf{r}, t)$ as a linear superposition of eigenstates $\Phi_n(\mathbf{r})$ of H_e

$$\Psi(\mathbf{R}, \mathbf{r}, t) = \sum_n c_n(\mathbf{R}, t) \Phi_n(\mathbf{r}) \exp(-iE_n t / \hbar) \quad (2)$$

where the probability amplitude $c_n(\mathbf{R}, t)$ accounts for the translational motion of the atom in a specific eigenstate $\Phi_n(\mathbf{r})$. Using expression (2) in the Schrodinger equation (1) one finds that the evolution of $c_n(\mathbf{R}, t)$ is described by

$$i\hbar \partial_t c_n = -\hbar^2 \nabla^2 c_n / 2M + \sum_m \int d\mathbf{r} V_m(\mathbf{r}) \exp(-iE_m t / \hbar) c_m(\mathbf{R}, t) \quad (3)$$

where

$$V_m(\mathbf{r}) = \int d\mathbf{R} \Phi_m^*(\mathbf{r}) V(\mathbf{R}, \mathbf{r}, t) \Phi_n(\mathbf{r}) \quad (4)$$

and $\nabla^2 = \nabla_{\mathbf{R}}^2 + \nabla_{\mathbf{r}}^2$.

We are interested in obtaining the evolution of bilinear combinations of probability amplitudes. Let

$$c_n(\mathbf{R}, t) c_m^*(\mathbf{R}, t) = c_{nm}(\mathbf{R}, t) \quad (5)$$

Then one can show that $c_{nm}(\mathbf{R}, t)$ evolves according to

$$i\hbar \partial_t c_{nm}(\mathbf{R}, t) = \hbar^2 \nabla_{\mathbf{R}}^2 c_{nm} / 2M + \sum_l \int d\mathbf{r} V_l(\mathbf{r}) c_{nl}(\mathbf{R}, t) \exp(-iE_l t / \hbar) \\ + \sum_l \int d\mathbf{r} V_l(\mathbf{r}) c_{lm}^*(\mathbf{R}, t) \exp(-iE_l t / \hbar) \quad (6)$$

where

$$V_l(\mathbf{r}) = \int d\mathbf{R} \Phi_l^*(\mathbf{r}) V(\mathbf{R}, \mathbf{r}, t) \Phi_n(\mathbf{r}) \quad (7)$$

Equation (6), though exact, does not show explicitly the effect of Doppler broadening and recoil shift. A useful technique that makes these effects explicit involves the use of the Wigner distribution function, which is defined as

$$W_{nm}(\mathbf{R}, \mathbf{p}, t) = (1/2\pi\hbar)^3 \int d\mathbf{R}' \\ \times \exp(-i\mathbf{p} \cdot \mathbf{R}') \hbar \partial_{\mathbf{R}'} c_{nm}(\mathbf{R} + \mathbf{R}', t) c_{nm}^*(\mathbf{R}, t) \quad (8)$$

where we identify $\mathbf{R} = \mathbf{R} + \mathbf{R}'/2$ and $\mathbf{R}' = \mathbf{R} - \mathbf{R}'/2$. Applying the same procedure, i.e., using expression (8) in Eq. (6), one finds that $W_{nm}(\mathbf{R}, \mathbf{p}, t)$ evolves according to

$$i\hbar \partial_t W_{nm}(\mathbf{R}, \mathbf{p}, t) = M \partial_{\mathbf{R}}^2 W_{nm}(\mathbf{R}, \mathbf{p}, t) \\ + \sum_l \int d\mathbf{k} \int d\mathbf{r} \exp(-i\mathbf{k} \cdot \mathbf{R}) \exp(-i\mathbf{k} \cdot \mathbf{R}') \\ \times \exp(-i\mathbf{p} \cdot \mathbf{R}') \\ \times \{ \mathbf{k} \cdot \mathbf{R}' W_{nm}(\mathbf{R}, \mathbf{p} - \hbar\mathbf{k}, t) + \hbar\mathbf{k} \cdot \mathbf{R} \\ \times \exp(-i\mathbf{k} \cdot \mathbf{R}) W_{nm}(\mathbf{R}, \mathbf{p} + \hbar\mathbf{k}, t) \\ - \mathbf{k} \cdot \mathbf{R} W_{nm}(\mathbf{R}, \mathbf{p} + \hbar\mathbf{k}, t) + \hbar\mathbf{k} \cdot \mathbf{R}' \\ \times \exp(-i\mathbf{k} \cdot \mathbf{R}') W_{nm}(\mathbf{R}, \mathbf{p} - \hbar\mathbf{k}, t) \} \quad (9)$$

where the convective derivative $\mathbf{p} \cdot \nabla / M$ accounts for the motion of the atom and gives rise to Doppler shift and motion washout. The quantity $\int d\mathbf{r} V_m(\mathbf{r})$ is the spatial Fourier transform of $V_m(\mathbf{r})$. Equation (9) is the quantum-mechanical transport equation describing the interaction of a two-level atom with near-resonant radiation fields. It is the difference aspect of these equations that gives rise to atomic recoil.

In essence, Eq. (9) is the quantum generalization of the classical Boltzmann equations. In the case of a two-level atom they govern the evolution of three distribution functions: $M(\mathbf{p}, t) = n/N$, the number of atoms, $N(\mathbf{p}, t) = n_1 - n_2$, the population difference between the two states, and

$\mathbf{p} = n_1 \mathbf{p}_1 - n_2 \mathbf{p}_2$, the optical coherence. For an assumed homogeneous distribution of atoms in one dimension interacting with a plane electromagnetic wave, the equations for these quantities reduce to

$$\partial_t N(\mathbf{p}, t) = -\partial_{\mathbf{p}} [2\hbar\mathbf{E} \cdot \mathbf{E}^* \mathbf{p} N(\mathbf{p}, t)] \\ + M(\mathbf{p}, t) \partial_{\mathbf{p}} [2\hbar\mathbf{E} \cdot \mathbf{E}^* \mathbf{p} + \hbar\mathbf{k} \cdot \mathbf{p}] \\ \times \{ \exp(-i\mathbf{k} \cdot \mathbf{R}) - \exp(-i\mathbf{k} \cdot \mathbf{R}') \} \\ + \partial_{\mathbf{p}} [2\hbar\mathbf{E} \cdot \mathbf{E}^* \mathbf{p} N(\mathbf{p}, t) + 2\hbar\mathbf{E} \cdot \mathbf{E}^* M(\mathbf{p}, t) + \hbar\mathbf{k} \cdot \mathbf{p} \\ \times M(\mathbf{p}, t)] \quad (10)$$

where the interaction potential with a plane wave is taken as $V_m(\mathbf{r}) = 2\hbar\mathbf{E} \cdot \exp(-i\mathbf{k} \cdot \mathbf{r})$, \mathbf{E} is the transition dipole moment, and \mathbf{k} is the wave vector of the incident plane wave. We have made the distribution $c_m(\mathbf{R}, t) = \exp(-i\mathbf{k} \cdot \mathbf{R})$, where $\mathbf{k} = \mathbf{k}_0 + \mathbf{k}'$, \mathbf{k}_0 is the wave vector of the center of gravity, and \mathbf{k}' indicates the imaginary part of \mathbf{k} .

4. NUMERICAL SOLUTIONS

We have carried out numerical integrations of Eqs. (10) using as the applied field a train of pulses with alternate pulses opposite in retarded and time origin, i.e., \mathbf{k}' is the center as required for focusing. As discussed in Section 3, optimal rephasing of the π pulses with respect to the path length of Doppler shifts will occur when a perfect π refocusing field is used between π pulses whose duration is $\tau = 2\Delta\omega^{-1}$. The results of our numerical analysis confirm that selective rephasing occurs as expected when the π refocusing period is implemented and that a better focusing effect than is results when two separate π pulse trains are applied in the manner described in Section 3.

Results of the numerical analysis for a two-level system are presented in Fig. 3. Shown is n_1 and n_2 as a function of

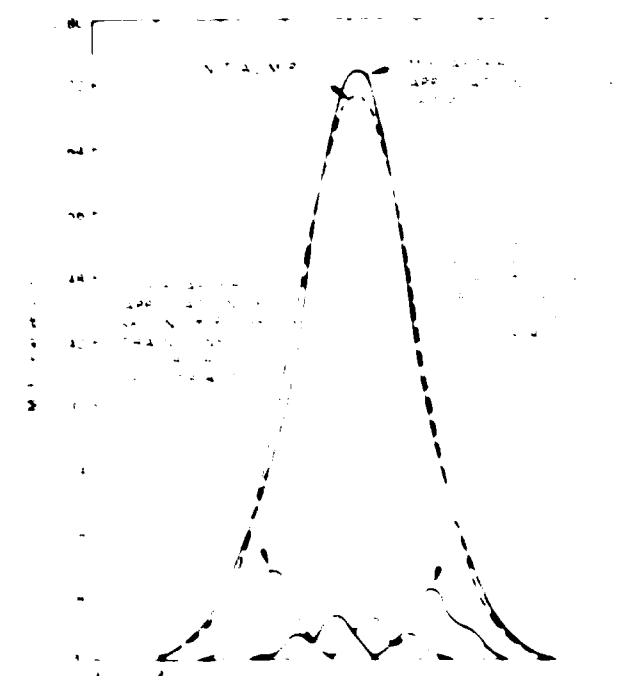


Fig. 1. Results of numerical integration of the momentum distribution of the tenfold atoms. M is equal to the peak momentum x of the pulse after pulse cooling.

momentum distribution and the distribution after the application of the π pulses tuned in the manner discussed above with the appropriate ten-field periods employed. As shown in the plots of Fig. 4, after the application of each of the π pulse trains the peaks in opposite sides of the distribution of the atoms from these pulses that coherence is maintained between the sides of the distribution that is being swept there is on the opposite side, as expected. As expected, the phases of the atoms were reversed after the application of the second π pulse train. An essential assumption in the use of M in Fig. 4 is that the coherence is maintained between wings of the distribution where some apparent heating of the distribution has occurred.

The inset of numerical integration in the integration could be prevented, the analysis is going with longer pulse trains. However, it was possible to extrapolate the results to obtain a characteristic cooling time that is greater than the distribution that experienced cooling. In the above example for pulse cooling in the hydrogen column, the extrapolated cooling time was estimated to be

$$\tau_{\text{cool}} = 1.5 \mu\text{s}.$$

This cooling time can be compared with the cooling time for steady-state cooling for the case when the natural linewidth is larger than the Doppler linewidth. The cooling time using the effective power broadening method is larger than the Doppler linewidth. This latter case is given by

$$\tau_{\text{cool}} = \frac{1}{\Gamma} \left(\frac{1 + \frac{1}{2} \frac{\Gamma}{\Delta} \frac{M}{\hbar k}}{1 - \frac{1}{2} \frac{\Gamma}{\Delta} \frac{M}{\hbar k}} \right)^2, \quad (10)$$

where k is the photon wave number. The atoms in the column are comparable in density to the atoms in the column of the hydrogen column. The atoms in the column have a similar mass to the atoms in the column of the hydrogen column.

Another interesting quantity associated with radiation cooling is the limiting temperature that can be reached. These limits have been discussed extensively for the steady-state case.¹¹ In the case of cooling with π pulses the cooling limit occurs when the Doppler width has been reduced to the natural linewidth since under this condition the zero-field periods have become comparable with the spontaneous decay time for the transition and coherence will be destroyed by the spontaneous decay process. Therefore the limiting temperature is given roughly by

$$T_{\text{lim}} = \frac{\hbar^2 k^2}{2m\Gamma}, \quad (11)$$

where Γ is the natural linewidth of the transition, k is the radiation wave number, and m is Boltzmann's constant.

5. SUMMARY

In conclusion, we have examined radiation cooling of a distribution of two-level atoms in the coherent pulse regime. Atoms with oppositely directed and oppositely detuned π pulses with specified ten-field periods between the pulses is required for optimal cooling. The cooling rate was found by numerical analysis of the quantum transport equations to be comparable with the rate for steady-state radiation cooling for the case when the Doppler linewidth is below the natural linewidth of the transition. The cooling temperature limit is defined by the Doppler width becoming comparable with the natural width of the transition.

For a wide range perspective on the parameters for radiation cooling compared with steady-state laser cooling, we illustrate qualitatively cooling of the temperature of a column of atoms in a column of atoms at a degree of freedom for hydrogen gas. For a column of atoms under the influence of laser cooling, the column of atoms is swept to the left, steady-state laser cooling of the Doppler width of this transition becomes comparable with the natural width at a temperature of 10^{-4} K. For steady-state laser cooling, the average atom momentum decreases through a linear width of the column. At this temperature, the laser frequency is less than the natural width of the transition, the laser frequency is swept to the left as cooling progresses, and the average atom momentum decreases through a linear width of the column that is less than the saturation power of the transition. Below this temperature, the frequency

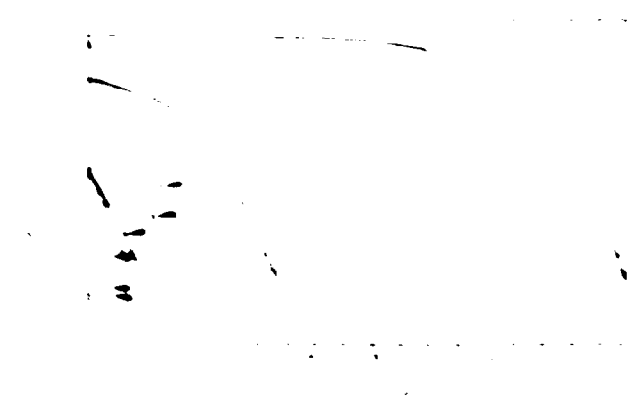


Fig. 2. Results of numerical integration of the momentum distribution of the tenfold atoms. M is equal to the peak momentum x of the pulse after pulse cooling.

need not be swept, and the cooling becomes exponential with time with the $(1/e)$ cooling time given by Eq. (14). The temperature limit most commonly assumed for the steady-state laser cooling is the so-called stochastic limit ($k_B T = \hbar \omega/2$).¹²

The dashed curves in Fig. 3 show the estimated exponential cooling for π pulses using the characteristic cooling time given by expression (13). The net cooling time is seen to be dramatically shorter for the larger initial temperatures but at the expense of considerable higher average power density. In this connection one must note that the Lyman- α photons are capable of photoionizing the upper state of the transition. The rate of energy released to electrons due to ionization is small compared with the cooling rates for the steady-state cooling power levels but is comparable with the cooling rates for the π -pulse average power levels and must be watched closely in further analysis of the practical application of π -pulse cooling. Photoionization of the upper level also gives rise to phase shifts not accounted for in the two-level treatment of π -pulse cooling given above, but these shifts can be expected to be small owing to the much smaller dipole matrix element between the upper state and the continuum compared with that of the Lyman- α transition.

ACKNOWLEDGMENTS

The authors wish to thank C. R. Giuliano for suggesting the use of π pulses for cooling and R. A. McFarlane, D. G. Steel, and C. R. Giuliano for technical discussions. This work was supported by the U. S. Air Force Office of Scientific Research under contract no. F49620-82-C-0004.

REFERENCES

1. A. F. Koichenko, S. G. Rautian, and R. I. Sokolyski, "Interaction of atoms with a strong electromagnetic field with the recoil taken into consideration," *Sov. Phys. JETP* **28**, 986 (1969).
2. A. Ashkin, "Atomic beam deflection by resonance radiation pressure," *Phys. Rev. Lett.* **25**, 1321 (1970).
3. T. W. Hansch and A. L. Schawlow, "Cooling of gases by laser radiation," *Opt. Commun.* **13**, 68 (1975).
4. A. F. Kazantsev, "Recoil effect in strong resonant field," *Sov. Phys. JETP* **40**, 825 (1974).
5. P. E. Moskowitz, P. L. Gould, S. R. Atlas, and D. E. Pritchard, "Diffraction of an atomic beam by standing wave laser radiation," *Phys. Rev. Lett.* **51**, 370 (1983).
6. R. J. Cook and A. F. Bernhardt, "Deflection of atoms by a resonant standing wave," *Phys. Rev. A* **18**, 2533 (1978).
7. J. E. Bjorkholm, R. R. Freeman, A. Ashkin, and D. B. Pearson, "Observations of focusing of neutral atoms by the dipole forces of resonance radiation pressure," *Phys. Rev. Lett.* **41**, 1361 (1978).
8. V. I. Balykin, V. S. Letokhov, and V. I. Mishin, "Cooling of sodium atoms by resonant laser emission," *Sov. Phys. JETP* **51**, 692 (1980); V. O. Balykin, V. S. Letokhov, and A. I. Sidorov, "Intense stationary flow of cold atoms formed by laser deceleration of atomic beam," *Opt. Commun.* **49**, 248 (1984).
9. W. D. Phillips and H. Metcalf, "Laser deceleration of an atomic beam," *Phys. Rev. Lett.* **48**, 596 (1982).
10. J. V. Prodan, W. D. Phillips, and H. Metcalf, "Laser production of a very slow monochromatic atomic beam," *Phys. Rev. Lett.* **49**, 1149 (1982).
11. J. V. Prodan, A. Migdall, W. D. Phillips, I. So, H. Metcalf, and J. Dalibard, "Stopping atoms with laser light," *Phys. Rev. Lett.* **54**, 992 (1985).
12. W. Ertmer, R. Blatt, J. L. Hall, and M. Zhu, "Laser manipulation of atomic beam velocities: Demonstration of stopped atoms and velocity reversal," *Phys. Rev. Lett.* **54**, 996 (1985).
13. S. Chu, L. Hollberg, J. E. Bjorkholm, A. Cable, and A. Ashkin, "Three-dimensional viscous confinement and cooling of atoms by resonance radiation pressure," *Phys. Rev. Lett.* **55**, 48 (1985).
14. A. P. Kazantsev, "The acceleration of atoms by light," *Sov. Phys. JETP* **39**, 784 (1974).
15. I. Nebenzahl and A. Szoke, "Deflection of atomic beams by resonance radiation using stimulated emission," *Appl. Phys. Lett.* **25**, 327 (1974).
16. H. Friedman and A. D. Wilson, "Isotope separation by radiation pressure of coherent π pulses," *Appl. Phys. Lett.* **28**, 270 (1976).
17. A. J. Palmer and J. F. Lam, "Radiation cooling using π pulses," *J. Opt. Soc. Am. A* **1**, 1251 (A) (1984).
18. R. P. Feynman, F. L. Vernon, and R. W. Hellwarth, "Geometrical representation of the Schrödinger equation for solving maser problems," *J. Appl. Phys.* **28**, 49 (1957).
19. M. Sargent, M. O. Scully, and W. E. Lamb, *Laser Physics* (Addison-Wesley, Reading, Mass., 1974), Sec. 7-5.
20. E. V. Baklanov and B. Ya. Dubetskii, "Fokker-Planck equation for gas atoms resonantly interacting with a light wave," *Opt. Spectrosc. (USSR)* **41**, 1 (1976); V. G. Minogin, "Kinetic equation for atoms interacting with laser radiation," *Sov. Phys. JETP* **52**, 1032 (1980); J. Javansian and S. Stenholm, "Broad-band resonant light pressure," *Appl. Phys.* **21**, 283 (1980); R. J. Cook, "Theory of resonance-radiation pressure," *Phys. Rev. A* **22**, 1078 (1980); C. Tanguy, S. Reynaud, and C. Cohen-Tannoudji, "Deflection of an atomic beam by a laser wave: transition between diffractive and diffusive regimes," *J. Phys. B* **17**, 4623 (1984).
21. See, for example, D. J. Wineland and W. M. Itano, "Laser cooling of atoms," *Phys. Rev. A* **20**, 1521 (1979).

APPENDIX B

A THEORY OF RESONANT 2-PHOTON INDUCED
IONIZATION OF HYDROGENIC SYSTEMS*

Juan F. Lam

Hughes Research Laboratories

Malibu , California 90265

ABSTRACT

A time-dependent theory of 2-photon induced ionization is presented. Exact analytical expressions are obtained for the total population of hydrogenic-like systems and the population of the intermediate resonant state as a function of the input intensity and detuning of the radiation field. The temporal behavior of the ionization rate is calculated.

* supported by AFOSR under Contract F49620-82-C-0004

Submitted to the Physical Review A (1987)

I. INTRODUCTION

Multiphoton ionization of hydrogenic systems is concerned with the dynamics involved in the coupling of external radiation fields with bound quantum systems, leading to the production of free electrons and ions. As such, the subject of multiphoton ionization has been the subject of intense investigation during the past decade¹. One of the simplest but most fundamental problem is the study of the ionization process when the input radiation field induces a resonant two-photon transition into the continuum from the ground state of a hydrogenic-like atom. In this case, there are two distinct regimes. First, if the input radiation is not in resonance with the bound-bound transition; the ionization rate can be computed by using perturbation theory². The results show that the rate for the production of electron is proportional to the square of the input radiation intensity. However in the case in which the input radiation is in resonance with the bound-bound transition, a simple intensity dependent ionization rate can not, in general, be derived³. The effect of saturation of the bound state population difference in the presence of the resonance radiation prevents a simple interpretation of the ionization process. The objective of this work is to present a self-consistent calculation of the effects of resonance radiation on the two-photon ionization process. The approach we shall take is to use

of the density matrix equations in the computation of the temporal evolution of the atomic density in the presence of radiation fields. Section II presents a detailed discussion and derivation of the density matrix approach which takes into account the ensemble of atoms passing through radiation field. We show in Section III that in the adiabatic regime, exact time dependent analytical solutions can be found for the total population of the atoms as well as for the ionization rate. The long time behavior of the ionization rate shows a rather simple, but not the square dependence, of the input intensity. As an example, we shall apply our results to the case of ionization of a H beam using Ly_{α} radiation. And finally in Section IV we summarize the main results of our work.

II. FORMULATION OF THE PROBLEM

The starting point in our analysis is the formulation of a set of density matrix equations which describes the model shown in Fig. 1. The bound states are labelled by $|1\rangle$ and $|2\rangle$, while the continuum is labelled by the set $\{|k\rangle\}$. The resonance radiation oscillates at frequency Ω . The spontaneous decay rate from the state $|2\rangle$ to the ground state $|1\rangle$ is given by γ . In order to derive a set of equations describing the evolution of each level via the density matrix formalism, it is important to understand the behavior of the coherent coupling between state $|2\rangle$ and $\{|k\rangle\}$. This is accomplished, in a rather straightforward manner, by studying the temporal evolution of the wavefunction in state $|2\rangle$. Consider the Schroedinger equation

$$i\hbar \frac{d}{dt} |\Psi\rangle = (H_0 - \mu E) |\Psi\rangle \quad (1)$$

where the state vector $|\Psi\rangle$ is given by

$$|\Psi\rangle = C_1(t) |1\rangle \exp(-i\omega_1 t) + C_2(t) |2\rangle \exp(-i\omega_2 t) + \int dk C(k,t) |k\rangle \exp(-i\omega_k t) \quad (2)$$

such that $|1\rangle$, $|2\rangle$ and $|k\rangle$ are the eigenstates of the unperturbed Hamiltonian H_0 . The interaction between the atom and the

radiation field E is $-\mu E$. The near resonant coupling between state $|2\rangle$ and the continuum can be obtained by projecting the state vector $|\Psi\rangle$ into the respective space. They are

$$\begin{aligned}
 i\hbar \frac{d C_2(t)}{d t} &= -\mu_{21} E C_1 \exp(i\omega_{21}t) \\
 &\quad - \int dk \mu_{2k} E C(k,t) \exp(-i\omega_{k2}t)
 \end{aligned} \tag{3a}$$

$$i\hbar \frac{d C(k,t)}{d t} = -\mu_{k2} E C_2(t) \exp(i\omega_{k2}t) \tag{3b}$$

where $\mu_{\alpha\beta}$ and $\omega_{\alpha\beta}$ are the electric dipole matrix element and frequency separation between states $|\alpha\rangle$ and $|\beta\rangle$; respectively. In the derivation of Eqs.(3), we assume that the coupling among the continuum states is negligible and the off-resonant two-photon transition between the ground state and the continuum has a small contribution in comparison with the resonant transition.

Equations (3) can be reduced further by formally integrating Eq.(3b) and use the result in Eq.(3a). This procedure leads to the following expression for the evolution of $C_2(t)$

$$\begin{aligned}
ih \frac{d C_2(t)}{d t} &= - \mu_{21} E C_1(t) \exp(i\omega_{21}t) \\
&+ (ih)^{-1} \int dk \int dt' \mu_{2k} E(t) \mu_{k2} E(t') \\
&\times \exp(-i\omega_{k2}(t-t')) C_2(t')
\end{aligned} \tag{4}$$

Now consider the approximations involved in the further simplification of Eq.(4). First, we shall assume that the amplitude $C_2(t')$ is slowly varying on the time scale of the radiation intensity and $1/\omega_{k2}$. Then we can extract $C_2(t')$ out of the integral and replace it by $C_2(t)$. Hence the integral involves only the intensity of the radiation field and the medium parameter. This integral is complex and the expression can be written as the sum of a real and an imaginary part; i.e.

$$(ih)^{-1} \int dk \int dt' \mu_{2k} \cdot E(t) \mu_{k2} \cdot E(t') \exp(-i\omega_{k2}(t-t')) = -ih (\Gamma - i\Delta).$$

Hence the net effect of the coupling between state $|2\rangle$ and the continuum, in the adiabatic limit, is the appearance of an irreversible transfer of energy (intensity dependent) from the bound state to the continuum. Furthermore, there exists an intensity dependent level shift of $|2\rangle$. We shall write the intensity dependence of Γ and Δ as σI and δI ; respectively. This result provides the starting point in the derivation of the density matrix equations. However if the assumption that the amplitude C_2 is not slowly varying, then additional complications may arise which may lead to the existence of two-photon Rabi

flopping, even in the presence of the continuum. This fact was pointed out by Kumenov and Perel⁴ in their discussion of single-photon induced ionization. We have carried out similar calculations for the case of two-photon resonant ionization and we found that the ionization process can be eliminated for certain range of the radiation intensity.

Let ρ_{11} , ρ_{22} and ρ_{12} be the population of state $|1\rangle$, population of state $|2\rangle$ and the optical coherence between states $|1\rangle$ and $|2\rangle$; respectively. The equations of motion is given by

$$ih \frac{d \rho_{11}}{d t} = \gamma \rho_{22} - \mu_{12} E \rho_{21} + \rho_{12} \mu_{21} E \quad (5a)$$

$$ih \frac{d \rho_{22}}{d t} = -\gamma \rho_{22} - \sigma I \rho_{22} - \mu_{21} E \rho_{12} + \rho_{21} \mu_{12} E \quad (5b)$$

$$ih \frac{d \rho_{12}}{d t} = -h\omega_{21} \rho_{12} - ih \frac{\gamma}{2} \rho_{12} - \mu_{12} E (\rho_{22} - \rho_{11}) \quad (5c)$$

where $\omega_{21} = \omega_0 + \delta I$. The set of equations (5) describes the evolution of the bound systems in the presence of radiation fields. It is interesting to note that Eqs.(5) describe the dynamics of the model shown in Fig.2. Hence within the approximations stated above, the dynamics of two-photon

ionization process can be described in terms of the dynamics of an open two-level atom, i.e. the atom is coupled with the continuum which is treated as a reservoir. In the next section we shall solve these equations and obtain the probability that the atoms are ionized by means of the two-photon excitation.

III. SOLUTIONS

The set of density matrix equations have exact analytical solutions provided that the following assumptions are made concerning the temporal evolution of the radiation field, the population difference, $\rho_{22} - \rho_{11}$, and the optical coherence. First, the radiation field is assumed to have a pulse duration that is longer than any response time of the medium. For sake of understanding of the process of resonant two-photon ionization, the radiation field is assumed to be cw. Second, the population difference is assumed to be slowly varying in a time compared to the smaller of the natural linewidth or laser detuning from intermediate resonance. This is just the Rate Equation Approximation. And last, the laser detuning from resonance is assumed to be small enough so that one can neglect the Bloch-Siegert shifts. This last assumption entails making the Rotating Wave Approximation.

Taking these assumptions into account, let us write the electric field as $E = E_0 \cos \Omega t$ and the on-resonance Rabi flopping frequency as $R_0 = \mu_{12} E_0 / 2\hbar$. In the rotating wave approximation, the optical coherence ρ_{12} is given by $\rho_{12} = \rho_{12} \exp(i\Omega t)$. Then the density matrix equations become

$$\frac{d \rho_{11}}{d t} = \gamma \rho_{22} + i R_{\theta} \rho_{21} - i R_{\theta}^* \rho_{12} \quad (6a)$$

$$\frac{d \rho_{22}}{d t} = -\gamma \rho_{22} - \sigma I \rho_{22} + i R_{\theta}^* \rho_{12} - i R_{\theta} \rho_{21} \quad (6b)$$

$$\frac{d \rho_{12}}{d t} + [i\Delta + \gamma/2] \rho_{12} = i R_{\theta} (\rho_{22} - \rho_{11}) \quad (6c)$$

Integration of Eq.(6c) and using the Rate Equation and Rotating Wave Approximations yield the solution for ρ_{12} . The expression for ρ_{21} can be obtained by taking the complex conjugate of ρ_{12} . They are given by

$$\rho_{12} = i R_{\theta} L_{12} (\rho_{22} - \rho_{11}) \quad (7a)$$

$$\rho_{21} = -i R_{\theta}^* L_{12}^* (\rho_{22} - \rho_{11}) \quad (7b)$$

where $L_{12} = \{ i\Delta + \gamma/2 \}^{-1}$ is the complex Lorentzian lineshape factor.

Using Eqs. (7a) and (7b) in Eqs. (6a) and (6b) yields a close system of equations for ρ_{11} and ρ_{22} .

$$\frac{d \rho_{11}}{d t} = \gamma \rho_{22} + |R_0|^2 (\rho_{22} - \rho_{11}) \text{Im} (L_{12}) \quad (8a)$$

$$\frac{d \rho_{22}}{d t} = -(\gamma + \sigma I) \rho_{22} - |R_0|^2 (\rho_{22} - \rho_{11}) \text{Im} (L_{12}) \quad (8b)$$

where we shall assume that the initial conditions are such that $\rho_{11} (t=-\infty) = N_0$ and $\rho_{22} (t=-\infty) = 0$. N_0 is the initial density of the atoms in the ground state. $\text{Im} (L_{12})$ stands for the imaginary part of L_{12} .

The reduced set of equations (8) has the following exact analytical solutions

$$\rho_{22} = \frac{N_0 K}{\lambda_2} \exp[-5(\gamma + \sigma I + K)t] \sinh(\lambda_2 t) \quad (9a)$$

$$\rho_{11} = N_0 - \rho_{22} - \sigma I \int^t dt' \rho_{22}(t') \quad (9b)$$

where $K = |R_0|^2 \text{Im}(L_{12})$ and $\lambda_2 = \{(\gamma + \sigma I + K)^2 - 4\sigma IK\}^{1/2}$.

Eqs.(9) constitute one of the two main results of this work and they are valid in the regime where the three fundamental assumptions are satisfied. Figure 3 shows a plot of the temporal evolution of the excited state population density. It shows that the population of the excited state achieves a large value within a short period of time due to the Rabi flopping process. After that, the single photon ionization process takes place to deplete the excited state population. A nearly complete depletion occurs within few hundreds of the spontaneous emission time. Figure 4 shows the temporal behavior of the total population density and exhibits the predicted depletion due to the ionization process in the high intensity regime; i.e. 500 Kw/cm². However, if the intensity is restricted to 1 Kw/cm², negligible ionization takes place. Hence the integrity of the atomic beam is preserved. Figure 5 shows the behavior of the total population density for fixed intensity (500 Kw/cm²) as a function of detuning from line center. For large detuning the ionization process becomes small. This behavior is understood in terms of the nonresonant nature of the detuned laser action. These plots consider the case of hydrogen atoms that are being ionized by the action of a

coherent Ly_α source. The bound transitions are composed of the 1s and 2p states of hydrogen. The cross section for ionization from 2p to the continuum was assumed to be of the order of 10^{-16} cm².

A quantity of interest is the resonant two photon ionization rate. It was stressed that this quantity has an intuitive physical meaning provided that perturbation theory holds, i.e. the Fermi's golden rule is used in the discussion. If we were to approach such a quantity in the regime of saturation of the bound transition, then the ionization rate is defined as

$$R_{ion} = - \frac{1}{\rho_{11} + \rho_{22}} \frac{d(\rho_{11} + \rho_{22})}{dt} \quad (10)$$

Using the exact analytical expressions (9), the resonant two-photon ionization rate is given by

$$R_{ion} = \frac{\sigma I K}{\lambda_2} \frac{1}{\coth(\lambda_2 t) + (\gamma + \sigma I + K)/2\lambda_2} \quad (11)$$

It is interesting to note that the rate is time dependent due to the fact that the exact solutions describe the temporal behavior of the population density as a function of the laser intensity. The long time behavior, i.e. as t tends to infinity, is given by

$$R_{ion} = \frac{2 \sigma I K}{2\lambda_2 + \gamma + \sigma I + K} \quad (12)$$

which is a nonlinear function of the laser intensity, contrary to the results obtained via the perturbation regime. Eq.(12) is the second of the two main results of this work. It shows that the two-photon ionization rate reduces to the perturbation results in the limit of low intensity and zero detuning from the intermediate state resonance, i.e. the ionization rate is proportional to I^2 . While in the high intensity limit the rate becomes linear in intensity.

AD-A179 226

EXPERIMENTAL AND THEORETICAL STUDIES OF LASER COOLING
AND EMITTANCE CONTR. (U) HUGHES RESEARCH LABS MALIBU CA
J F LAM ET AL 31 JAN 87 HAC-REF-E9913 AFOSR-TR-87-0139
F49620-82-C-0004

2/2

UNCLASSIFIED

F/G 28/8

NL





Microcopy Resolution Test Chart

IV. SUMMARY

We presented a theory of resonant two-photon ionization of hydrogenic-like systems. The analysis shows that exact analytical results are obtained for the total population of the atoms and the ionization rate, provided that three fundamental approximations are satisfied. They are the slowly varying envelope, rate equation and rotating wave approximations. These approximations are valid for situations where the laser pulse duration is long compared to the characteristic times of the atom and that the laser is tuned near resonance to the bound-bound transition.

The ionization rate was found to be a nonlinear function of the laser intensity due to the saturation process of the bound state transition. It reduces to the result obtained from perturbation theory in the limit of low intensity. In the high intensity limit the rate becomes linear in the intensity, which reflects the fact that the saturation process plays an important role in determining the dynamics of the two-photon ionization process.

In the course of this work, we found that under certain specific conditions it is possible to change the continuum in such a manner that ionization does not take place. Preliminary work points to the criterion that the laser pulse must be short

enough that the adiabatic condition is no longer valid. In this case it is not possible to extract C_2 from the integral in Eq. (4). It can be shown that there exists a range of parameters (laser pulse duration and intensity) such that state $|2\rangle$ does not experience an irreversible energy transfer. This results implies that the radiation field has modified the continuum such that the ionization process does not take place. We shall expose this subject matter in full detail in another publication.

And last, a brief comment is in order concerning the role of ionization in the proposed laser cooling of a H beam. Assuming that it takes of the order of microsecond to achieve a divergence of the order of μrad and the $\text{Ly}\alpha$ laser is saturating the $1s$ to $2p$ transition (for optimum radiation cooling), then Fig. 2 shows that a significant fraction of atoms are ionized during the cooling process. This calculation uses a single-photon cross section of 10^{-16} cm^2 for the transition from the $2p$ to the continuum. A more careful analysis of the cross section must be done in order to assess correctly the role of two-photon induced ionization on the laser cooling process.

REFERENCES

1. P. Lambropoulos, in ADVANCES IN ATOMIC AND MOLECULAR PHYSICS, edited by D.R. Bates and B. Bederson, (Academic Press, New York 1976) Vol. 12, p.87
2. C. Cohen-Tannoudji, B. Diu and F. Laloe, QUANTUM MECHANICS (John Wiley and Sons, New York 1977) Vol. 2
3. P. Lambropoulos, Phys. Rev. A 9 , 1992 (1974)
4. S.E. Kumekov and V.I. Perel, Sov. Phys. JETP 54 , 899 (1981)
5. E. Karule, in MULTIPHOTON PROCESSES, J.H. Eberly and P. Lambropoulos, editors (John Wiley and Sons, New York 1978) p. 159

FIGURE CAPTIONS

Figure 1. The model used to discuss the dynamics of two-photon resonant ionization. Ω is the frequency of the input radiation field and γ is the spontaneous emission decay rate.

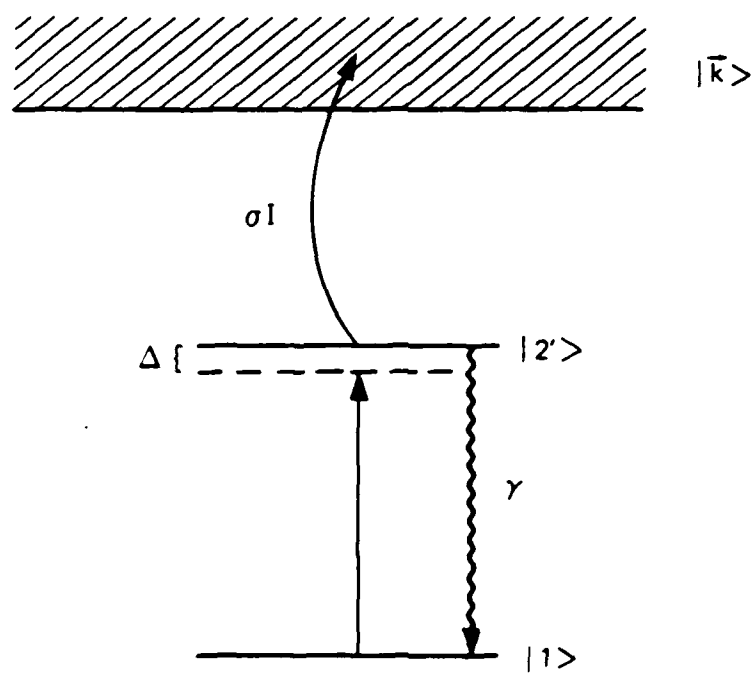
Figure 2. The reduced model showing that the net effect of the interaction between state $|2\rangle$ and the continuum is to introduce an incoherent decay rate σI and a shift in the energy level of the intermediate state.

Figure 3. Temporal evolution of the excited state population in the presence of two-photon induced ionization.

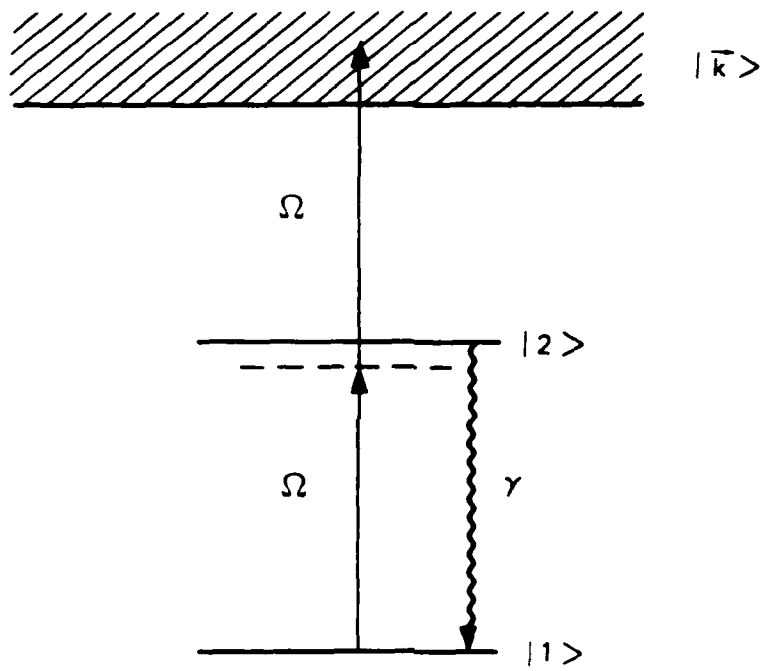
Figure 4. Temporal evolution of the total density of atoms in the presence of two-photon induced ionization
The Ly_{α} laser is tuned on-resonance.

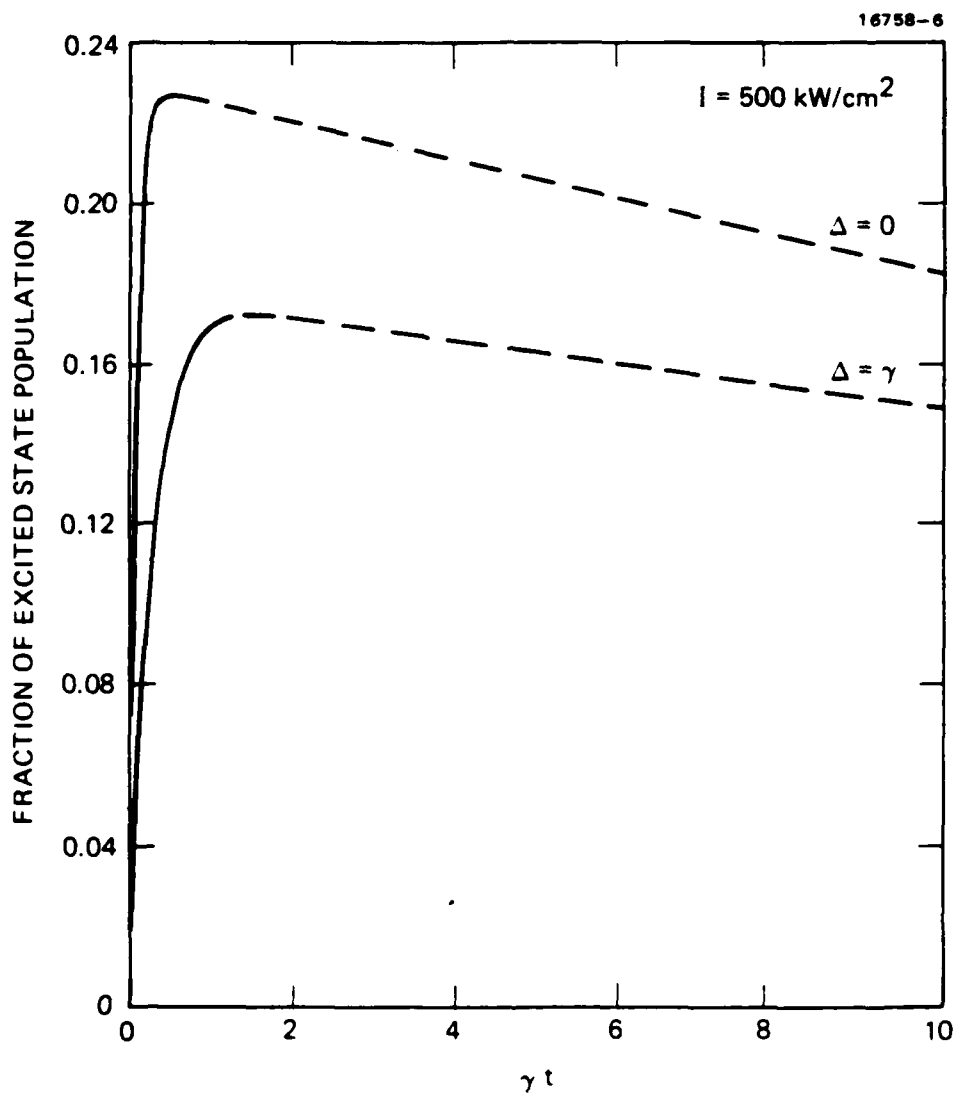
Figure 5. Temporal evolution of the total density of atoms in the presence of two-photon ionization, for fixed laser intensity. The Ly_{α} radiation intensity is set at 500 kW/cm^2 .

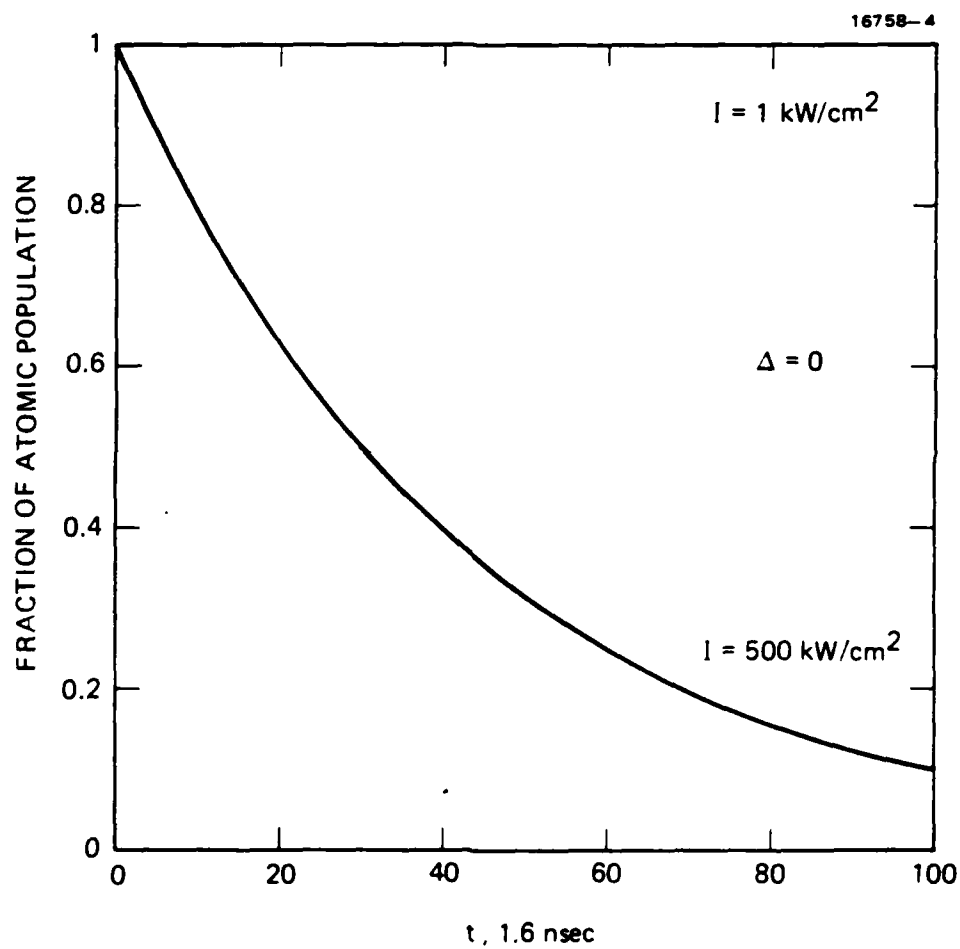
16758-1

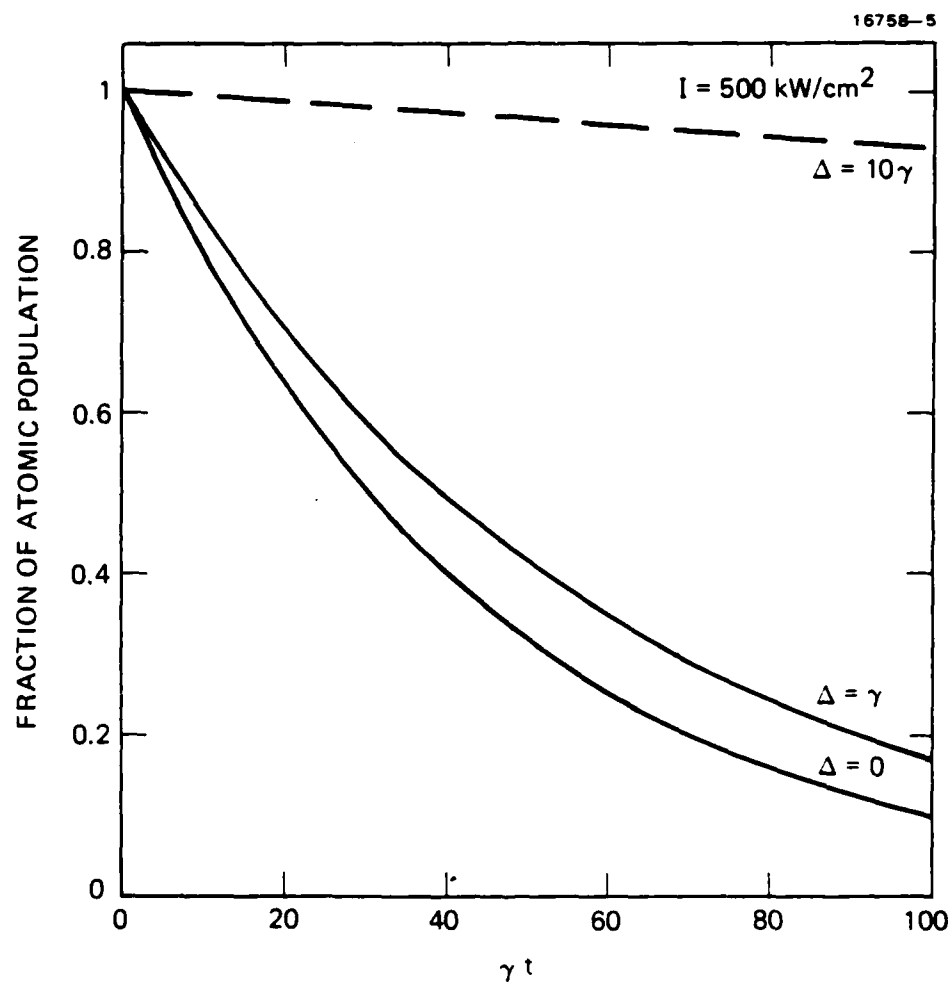


16758-2









APPENDIX C

Velocity-specific atomic-state selection in an atomic beam by continuous-wave optical pumping

D. G. Steel and R. A. McFarlane

Hughes Research Laboratories, 3011 Malibu Canyon Road, Malibu, California 90265

Received June 28, 1982

We present experimental results demonstrating strong velocity-distribution modification in a specific atomic state using optical pumping between hyperfine split levels. These results show that the velocity of a specific state can be defined within 6%, corresponding to a local temperature of 1 K. The velocity-specific-state selection is accomplished by using a nearly effusive atomic beam of sodium and a single frequency-stabilized dye laser.

In this Letter we describe experimental measurements demonstrating the use of optical pumping for generating an atomic beam with one of the ground states of the atomic species characterized by a nearly monochromatic longitudinal velocity distribution. Such a technique eliminates the complications associated with using a rotating-drum velocity selector.¹ The results show the significance of velocity-specific optical pumping and velocity-distribution modification, which characterize many nonlinear spectroscopy experiments.^{2,3}

The proposed basic approach was discussed earlier.⁴ We have implemented a slight modification to improve the original proposal, and, for the sake of completeness, we review the basic principles here. The technique is based on the optical-pumping properties of atomic states split by hyperfine interaction. In these experiments, we used the D_2 line of atomic sodium at 589 nm. An energy-level diagram of sodium is shown in Fig. 1, in which we have included only the $3s\ ^2S_{1/2}$ - $3p\ ^2P_{3/2}$ transition. The total angular-momentum quantum number F is the sum of the nuclear spin ($I = 3/2$ for ^{23}Na) and the particular J value for the given level. The various hyperfine splittings are shown in Fig. 1. For these transitions, the relevant dipole-selection rules are $\Delta F = 0, \pm 1$. Hence we see that an atom in the $3p\ ^2P_{3/2}(F = 3)$ state can decay by spontaneous emission only to the $3s\ ^2S_{1/2}(F = 2)$ state. Similarly, an atom in the $3p\ ^2P_{3/2}(F = 0)$ state can decay by spontaneous emission only to the $3s\ ^2S_{1/2}(F = 1)$ state. However, the $3p\ ^2P_{3/2}(F = 1)$ state and the $3p\ ^2P_{3/2}(F = 2)$ state can decay spontaneously to either of the $3s\ ^2S_{1/2}$ ground states. Therefore an atom initially in the $F = 2$ ground state that is excited to the $F = 2$ or $F = 1$ upper state can end up in the $F = 1$ ground state. Hence, by optical pumping, the entire atomic population can be transferred from the $F = 2$ ground state to the $F = 1$ ground state. In Fig. 1 the transitions that are not amenable to optical pumping are shown with solid lines, and the dotted lines show transitions that can be optically pumped. By an appropriate arrangement of optical frequencies and geometry, it is possible to convert the original broad velocity distribution of one of the ground states to a narrow velocity distribution. To see how this

is accomplished, we consider the optical-pumping scheme shown in Fig. 2. The energy-level spacing in the ground state is sufficiently small that one can assume that both ground states are thermally populated. We consider an optical-beam arrangement in which the atomic beam is sufficiently collimated that we need not consider any transverse velocity effects. We further assume that the initial longitudinal velocity distribution is thermal. The optical-pumping-induced velocity-distribution modification is a two-step process. The first step requires the frequency of a laser beam propagating perpendicular to the atomic beam (to avoid Doppler effects) to be resonant with the $3s\ ^2S_{1/2}(F = 2)$ - $3p\ ^2P_{3/2}(F = 2)$ [or $3p\ ^2P_{3/2}(F = 1)$] transition (e.g., transition A of Fig. 2). Assuming that the laser intensity is comparable with the transition-saturation intensity (given by $h\nu/\sigma T_1$, where σ is the absorption cross section and T_1 is the upper-state lifetime) and that the transit time is long compared with T_1 , the atoms in the $F = 2$ ground state will decay eventually to the $F = 1$ ground state, where they will no longer be resonant with the laser light (being out of resonance by some 1700 MHz). The second step in the velocity-distribution modification process is to pick a velocity class (i.e., a group of atoms moving within some velocity Δv about v) in the $F = 1$ ground state and transfer it to the $F = 2$ ground state. This is accomplished by taking ad-

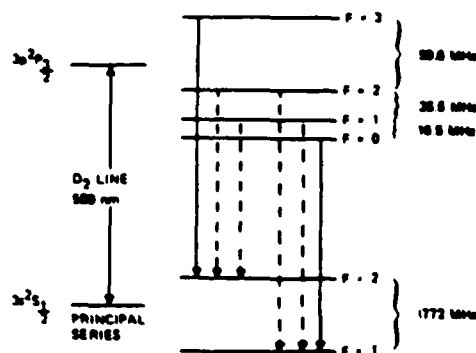


Fig. 1. Energy-level diagram for the D_2 line of atomic sodium at 589 nm showing the hyperfine splitting.

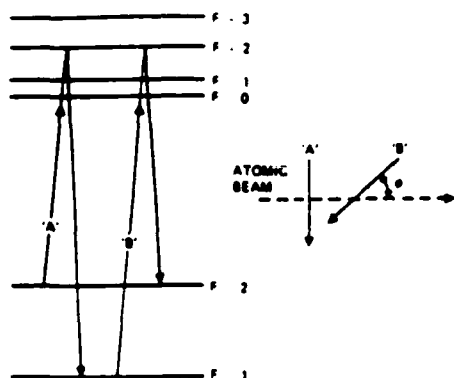


Fig. 2. Left, atomic-energy-level scheme showing the optical-pumping sequence for velocity selection. Right, geometry for the optical-pumping laser beam and the velocity-selection laser beam.

vantage of the longitudinal Doppler shift. A beam of light at frequency ω is directed at some angle ϕ with respect to the atomic beam. In this case, we want to choose a specific velocity group such that it is in resonance with the laser on the $3s\ ^2S_{1/2}(F=1)-3p\ ^2P_{3/2}(F=1)$ [or $3p\ ^2P_{3/2}(F=2)$] transition at ω_0' (or ω_0''). The resonance condition is given by $\omega - \omega_0 - \mathbf{K} \cdot \mathbf{v} = 0$, where \mathbf{K} is the \mathbf{K} vector of the laser beam, $\omega_0 = \omega_0'$ or ω_0'' , and \mathbf{v} is the atomic velocity of the velocity group we wish to excite. When ω satisfies this resonance condition, all atoms moving in the velocity group \mathbf{v} will be excited. Transition B of Fig. 2 shows an example when $\omega_0 = \omega_0''$. Assuming again that the laser intensity is comparable with the transition-saturation intensity, we find that those atoms excited will eventually decay back to the $F=2$ ground state, where they will be out of resonance again by some 1700 MHz. At this point, the velocity distribution of the $F=2$ ground state has been modified from a broad thermal distribution to a narrow distribution moving at velocity \mathbf{v} . An example of the geometry is shown in Fig. 2.

The width of the velocity distribution is limited in principle by the natural linewidth of the transition, i.e., the beam will pump all atoms whose velocity for a given ω and ω_0 satisfies the inequality $|\omega - \omega_0 - \mathbf{K} \cdot \mathbf{v}| \leq \gamma$, where 2γ is the transition linewidth (FWHM in radians). In this particular example, this limit cannot be realized because there are two optical-pumping transitions involving both the $F=1$ and $F=2$ levels in the upper state, yielding, in principle, a velocity doublet. If their frequency separation is given by δ , then the best longitudinal monochromaticity that can be realized is estimated by replacing γ with δ in the above inequality, showing that the beam monochromaticity should be of the order $\Delta v/v \sim \delta/(\omega - \omega_0)$, where δ is in radians. For these experiments in sodium we estimate that the minimum $\Delta v/v$ is of the order of 3% [for ω tuned to the $3s\ ^2S_{1/2}(F=2)-3p\ ^2P_{3/2}(F=3)$ transition].

The experimental configuration to demonstrate this behavior is shown in Fig. 3. The two-step process is accomplished with a single stabilized tunable dye laser tuned to 589 nm. This technique was developed not only to enable a single dye laser to accomplish the velocity-distribution modification but also to allow that

dye laser to be used as the radiation source for future experiments on the prepared monochromatic atomic beam. For those experiments, the dye laser is operated in resonance with the $3s\ ^2S_{1/2}(F=2)-3p\ ^2P_{3/2}(F=3)$ transition. Hence these experiments were performed with the laser tuned to that resonance. The frequency offset for adjusting the laser frequency to be in resonance with the $3s\ ^2S_{1/2}(F=2)-3p\ ^2P_{3/2}(F=2)$ transition was provided by an acousto-optic modulator tuned to 59.6 MHz. The downshifted optical beam was directed into the atomic beam at 90° to the direction of atomic-beam propagation. This beam transferred nearly all the population of the $F=2$ ground state into the $F=1$ ground state. The second step was accomplished by taking the original laser beam [tuned to the $3s\ ^2S_{1/2}(F=2)-3p\ ^2P_{3/2}(F=3)$ resonance] and directing it to intersect the atomic beam at 45° . Atoms moving at roughly 1.4×10^5 cm/sec will see this beam as being on resonance with the intermediate transition given by $3s\ ^2S_{1/2}(F=1)-3s\ ^2S_{1/2}(F=1)$ [or $3p\ ^2P_{3/2}(F=2)$]. These atoms will be pumped into the $F=2$ ground state. In this manner the atoms in the $F=2$ ground state are all moving at nearly the same longitudinal speed.

To verify the resultant velocity distribution experimentally, a second frequency-stabilized tunable dye laser was directed along the axis counterpropagating to the atomic beam, as shown in Fig. 3. A photomultiplier detected the scattered fluorescence from the second laser at a position downstream from the optical-pumping and velocity-selection region. In the absence of any optical pumping or velocity selection, we expect a double-humped fluorescence spectrum as the laser is tuned through the resonances. The data are shown in Fig. 4(a). The first peak is the Doppler-broadened spectrum corresponding to all transitions originating out of the $F=2$ ground state, and the second peak corresponds to the $F=1$ ground state. These peaks are separated by approximately 1700 MHz. Figure 4(b) shows the effect on the fluorescence spectrum as the optical-pumping beam is turned on. The peak corresponding to the $F=2$ transitions is reduced while the peak corresponding to the $F=1$ transitions is increased. Because of the geometry of the probing beam and the fact that the probe beam was larger than the optical-pumping beam, not all atoms that are probed have been pumped. Hence the $F=2$ level does not appear to be completely depleted in these data. However, a transverse probe beam (not shown in Fig. 4) is capable of measuring the remaining population (with the loss

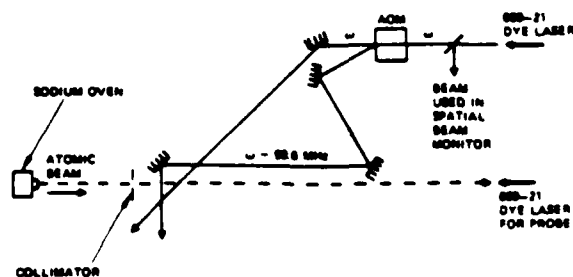


Fig. 3. Experimental configuration for optical pumping and velocity selection.

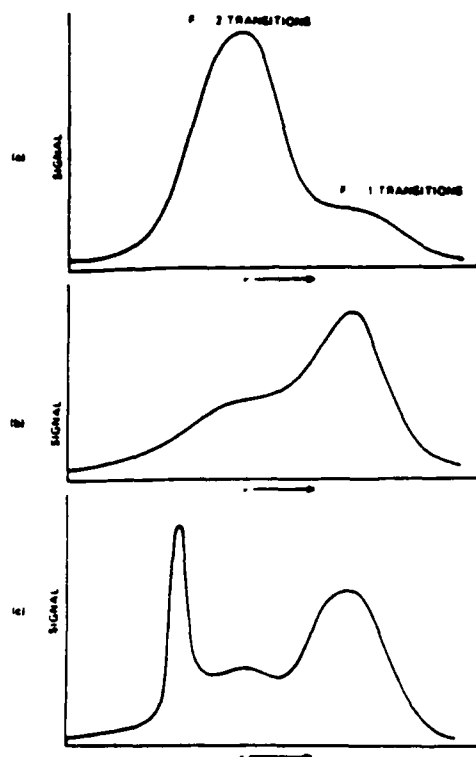


Fig. 4. Probe scan using the second dye laser to monitor the Doppler-broadened fluorescence spectrum. (a) The spectrum obtained with no optical-pumping beam or velocity-selection beam present. The double hump, separated by roughly 1700 MHz, is due to the hyperfine splitting in the ground state. (b) In the presence of optical-pumping beam A (see Fig. 2), we observe a depletion of the $F = 2$ ground state and an enhancement of the $F = 1$ state. (c) Fluorescence spectrum in the presence of both the optical-pumping beam and the velocity-selection beam. The spike on the low-frequency side shows the clear evidence of state-specific velocity selection. A high-resolution display of this peak shows a width of 90 MHz, corresponding to a velocity homogeneity of 5%.

of velocity resolution) and shows nearly complete transfer of population from level 2 to level 1. Figure 4(c) shows the effect on the velocity distribution when the velocity-selection beam is turned on at $\phi = 45^\circ$ with respect to the oncoming atomic beam. A strong peak is observed corresponding to atoms in the 1.4×10^5 cm/sec velocity group. A high-resolution display of this peak shows a width of 90 MHz, implying a velocity homogeneity of 6%, in good agreement with the estimates given above. The equivalent local temperature is of the order of 1 K. The velocity homogeneity was limited by power broadening and diffractive divergence of the velocity-selecting optical beam, thus eliminating the possibility of observing the velocity doublet.

The amplitude of the velocity peak is larger than expected based on the data of Fig. 4(a) because of optical pumping effects caused by the weak probe beam in collinear geometry.⁵ When a transverse probe is used, the increased signal amplitude is in agreement with that expected from the transferred population that is due to the velocity-selecting beam.

In these experiments we have demonstrated the effects of velocity-specific atomic-state selection by optical pumping. By incorporating an acousto-optic modulator, we have been able to accomplish the velocity selection while the laser is tuned to a nonoptically pumped transition. Hence additional experiments may be performed by using this atomic beam and the same laser with the laser directed toward the atomic beam at 90° . This eliminates the problem of using the laser tuned to an intermediate transition and then performing the experiments on the pumped transition by adjusting the angle of the beam away from 90° , as suggested by Stroud.⁴ This is important for experiments in which standing-wave effects occur, such as in the optical Stern-Gerlach effect,^{6,7} which we are now examining. The same laser can now be used to replace the classic hot-wire detector used to measure atomic-beam profiles. Since this laser is tuned to the $3s\ ^2S_{1/2}(F = 2) - 3p\ ^2P_{1/2}(F = 3)$ transition, it can be used as the atomic-beam detector downstream. In our experiments, the laser is focused to less than $30\ \mu\text{m}$ by using a cylindrical lens and is mechanically scanned to provide the transverse profile of the atomic beam. Because of the frequency resolution, it samples only atoms in the $F = 2$ state. A photomultiplier is then used to detect the side-scattered fluorescence. In this manner high-speed atomic-beam detection is accomplished with spatial resolution comparable with that obtained using a hot-wire detector with considerably increased bandwidth and none of the difficult technological problems associated with hot wires.

The authors would like to thank Concetto Giuliano for helpful suggestions and reading of the manuscript, J. Myer for the sodium oven design, and J. Shuler for his technical expertise. This research was supported in part by the U.S. Air Force Office of Scientific Research under contract F49620-82-C-0004.

References

1. R. C. Miller and P. Kusch, *Phys. Rev.* **99**, 1314 (1955).
2. M. S. Feld, M. M. Burns, T. U. Kuhl, P. G. Pappas, and D. E. Murnick, *Opt. Lett.* **5**, 79 (1980); P. G. Pappas, M. M. Burns, D. D. Hinschelwook, M. S. Feld, and D. E. Murnick, *Phys. Rev. A* **21**, 1955 (1980).
3. L. Julien, M. Pinard, and F. Laloe, *Phys. Rev. Lett.* **47**, 564 (1981); L. M. Humphrey, J. P. Gordon, and P. F. Liao, *Opt. Lett.* **5**, 56 (1980).
4. F. Schuda and C. R. Stroud, Jr., *Opt. Commun.* **9**, 12 (1973); J. A. Abate, *Opt. Commun.* **10**, 269 (1974).
5. Even though the probe intensity is less than I_{SAT} for D_2 transitions, strong optical pumping can still be induced since the effective saturation intensity is reduced by the ratio T_1/τ_T , where T_1 is the longitudinal relaxation rate and τ_T is the transit time through the beam. For the geometry above, that ratio is of the order of 10^{-5} . These optical-pumping effects are quite complicated and beyond the scope of this paper, but a detailed discussion is given by M. S. Feld *et al.* in *Opt. Lett.* **5**, 79 (1980); *Phys. Rev. A* **21**, 1955 (1980).
6. R. J. Cook and A. F. Bernhardt, *Phys. Rev. A* **18**, 2533 (1978).
7. E. Arimondo, A. Bambini, and S. Stenholm, *Phys. Rev. A* **24**, 898 (1981).

APPENDIX D

H⁻ PHOTONEUTRALIZATION

R. S. Turley
Hughes Research Laboratories

Brookhaven Neutralizer Conference
June 5-6, 1985

H⁻ Photoneutralization

Photoneutralization presents an attractive alternative for neutralization of H⁻ beams because of the possibility of drastically decreasing the divergence of the resultant neutral beam. Advances in laser technology make photoneutralization increasingly attractive from the point of view of space and power requirements as well. One of the traditional difficulties associated with weapons use of photoneutralization is the process's low cross section. This presentation presents some ideas for overcoming this limitation. Assessment of the technical feasibility of these techniques require experimental studies which should be initiated shortly.

The first possibility I will address for enhancing photoneutralization cross sections is to take advantage of two resonant structures in the cross section near the n=2 threshold of atomic hydrogen, a Feshbach and a shape resonance. The Feshbach resonance is located just below the n=2 threshold and has a cross section which is predicted to be about 300 times the background cross section at that energy. While it has been seen experimentally, previous experiments have insufficient resolution to determine details about its height and width.

The second resonance of interest is the shape resonance which peaks about 31 meV above the n=2 threshold. Although its cross section is predicted to be below that of the Feshbach resonance by about an order of magnitude, calculations indicate that this reaction strongly favors leaving the residual hydrogen atom in the n=2 state, giving the ejected electron a recoil energy of only 31 meV. Beam sensing is then possible at visible wavelengths via the 2p to n=3 transitions. Additionally, divergence due to the recoiling electron is extremely small.

A third technique which should be investigated is the possibility of electric and magnetic field induced resonances. When the hydrogen ions are placed in an external field, metastable excited states above the ionization threshold become possible. Since the transition becomes bound-bound rather than bound-free, the wave function overlap (and hence the cross section) is expected to increase substantially. Using an external magnetic field has a possible drawback of the fringing fields introducing a twisting motion in the beam which may add to beam divergence. This could be circumvented by using an electric field instead. Detailed study of electric field induced resonances needs to be done before more can be said about the details of this enhancement.

In conclusion, photoneutralization of H^- beams promises to be an attractive long-term alternative to other NPB neutralization techniques. This process presents the possibilities of lower contributions to beam divergence. The disadvantage of low cross sections which require large laser powers may be offset by successful utilization of resonant schemes which can enhance the cross section substantially. Detailed investigations of these processes should begin immediately so that the technology can be tested, understood, and developed if feasible.

OUTLINE

(1) RL Facilities

- High Power Narrow band tunable VUV source
- Hydrogen Beam Facility

(2) Resonant Photoneutralization

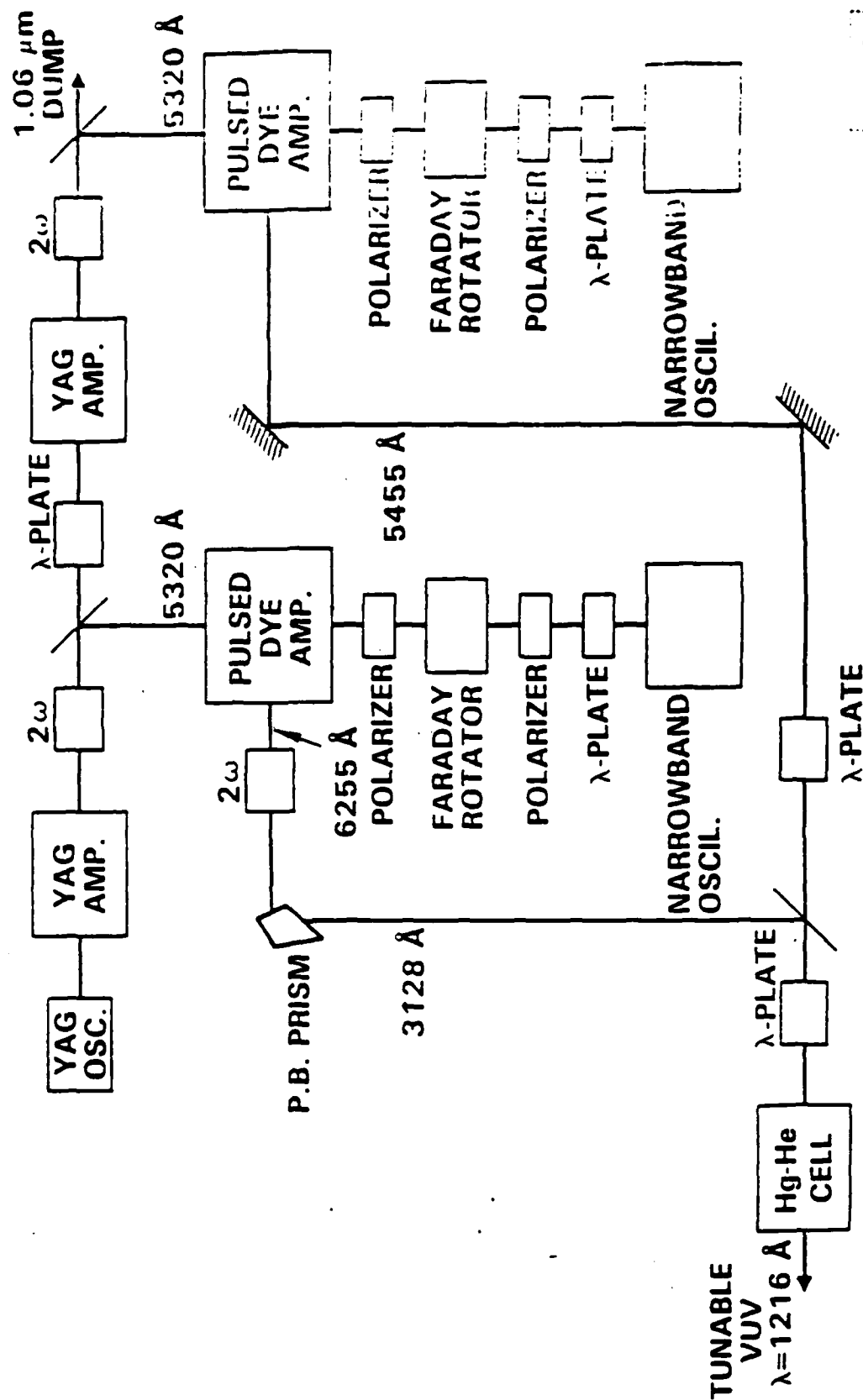
- Feshbach Resonance
- Shape Resonance

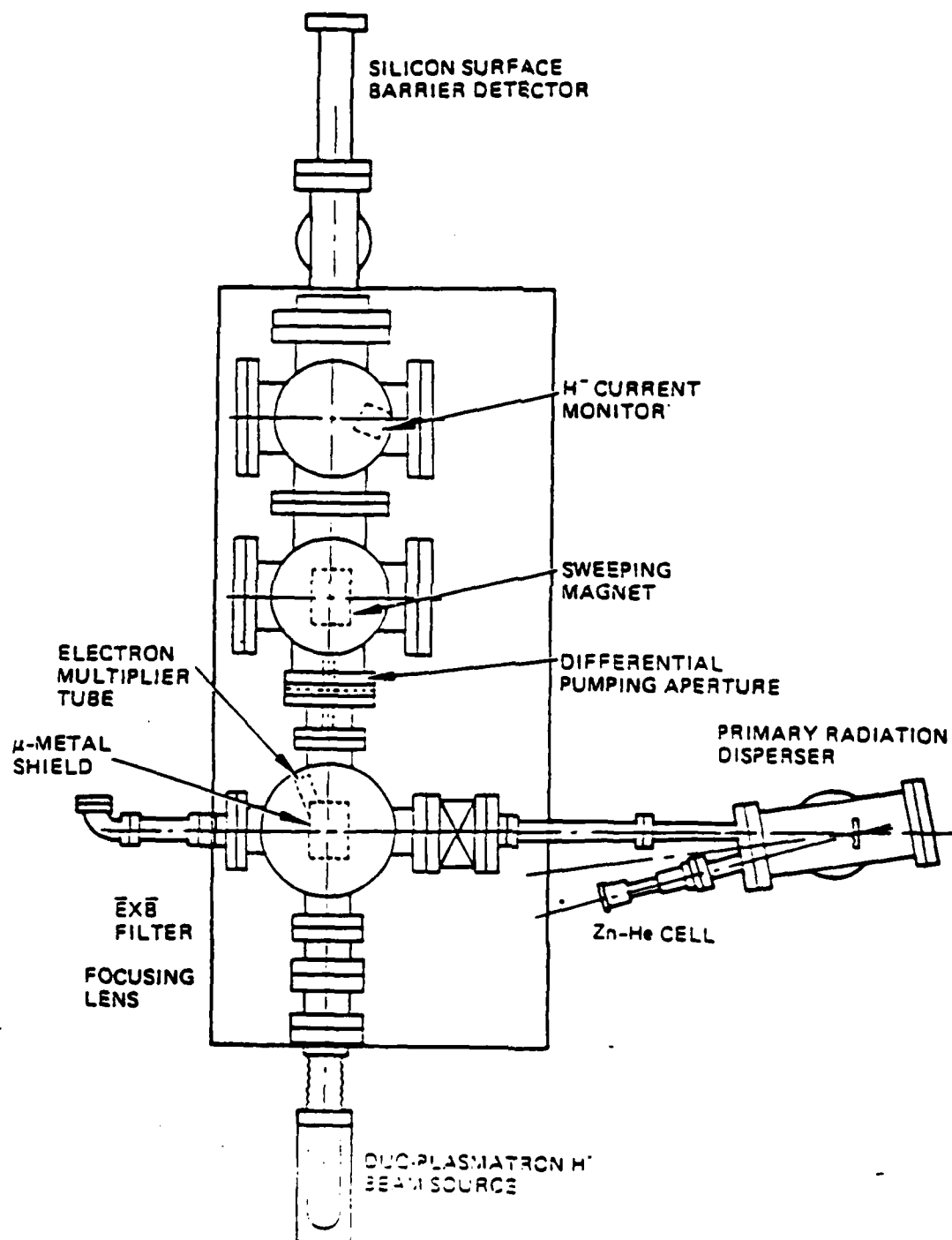
(3) Field Enhanced Photoneutralization

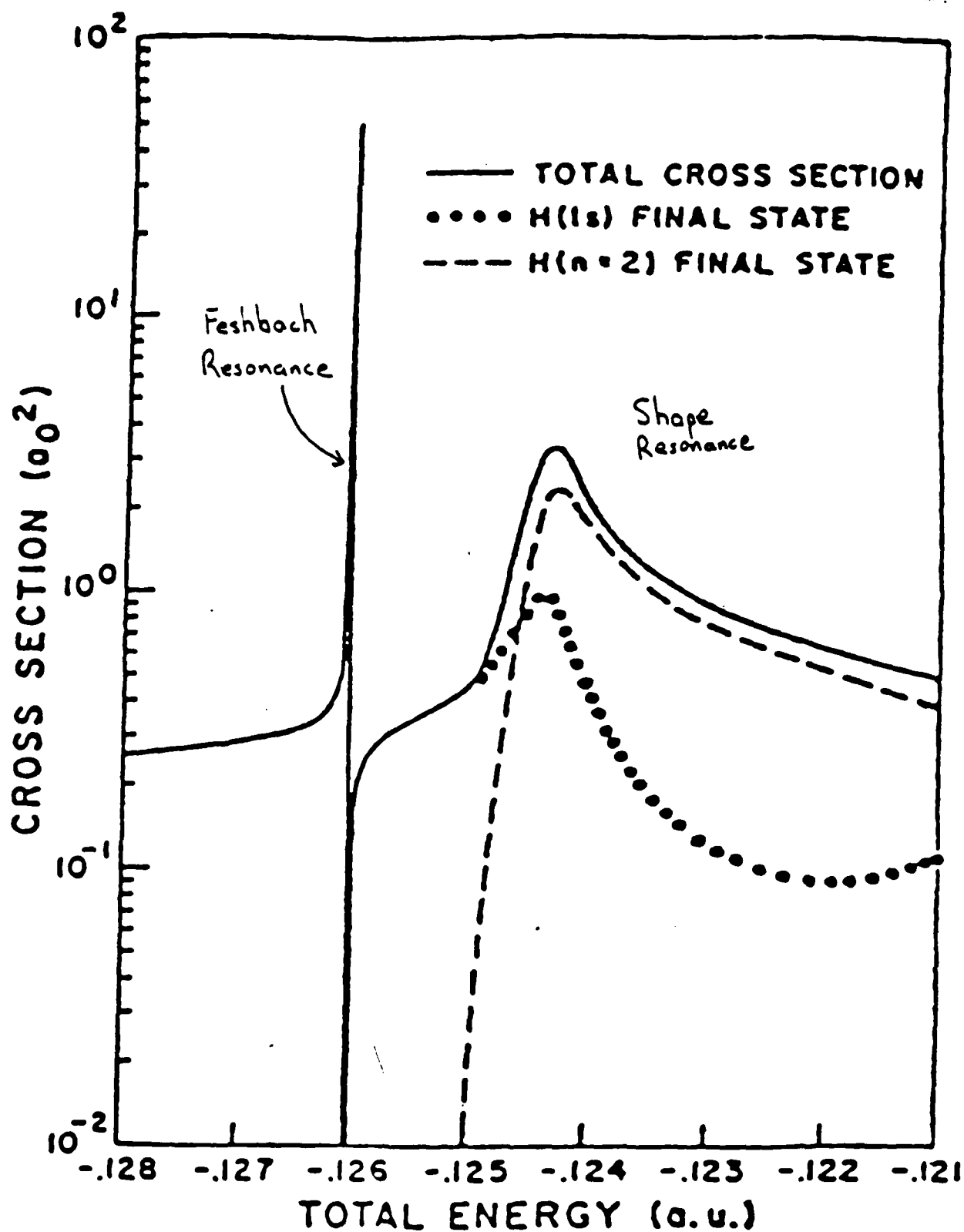
(4) Summary

TUNABLE TRANSFORM LIMITED BANDWIDTH VUV SOURCE

$$\lambda = 1216 \text{ \AA}$$







FESHBACH RESONANCE

--Relatively Large Cross Section

--1s Final State

10 eV e^- recoil produces $5\mu\text{rad}$ divergence in 200 MeV
beam

--Previous Work

electron scattering

LAMPF experiments

--Future Work

High Resolution studies

Resolve other states

SHAPE RESONANCE

--smaller cross section

--lower divergence

0.3 μ rad with a 200 MeV H^-

--previous work

Bryant, et al. (LAMPF)

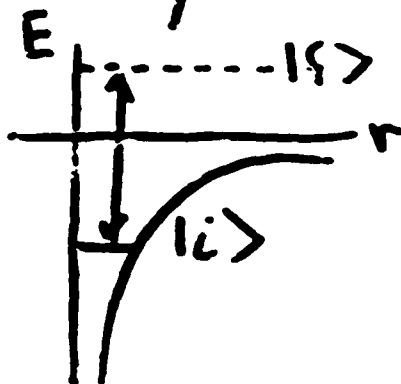
--need branching ratios

$n=2$ to $n=1$

$l=1$ to $l=0$ ($n=2$)

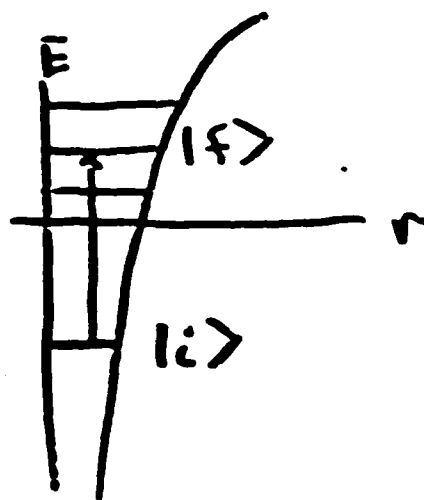
Field Enhanced Photo-neutralization

Ordinary P.I.



$\sigma_{\text{P.I.}} \propto |\langle f|r|i\rangle|^2$
small because of small
w.f. overlap
(bound - free)

Field Enhanced



overlap larger
(bound - bound)

SUMMARY

--Feshbach Resonance

High cross section / highest divergence

--Shape Resonance

Lower cross section / lower divergence

--Field Enhanced Photoneutralization

????

NOTE: studies can be done now on a benchtop with existing
laboratory equipment!

END

5-87

DTIC